Cell Reports

Resource

Definition of a High-Confidence Mitochondrial Proteome at Quantitative Scale

Graphical Abstract

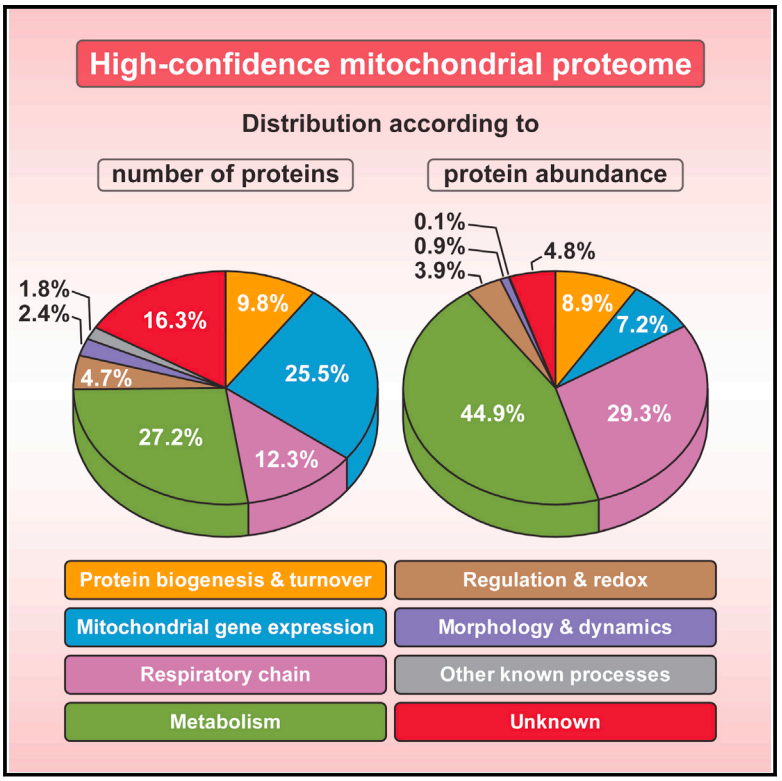

Highlights

- Classification of > 3,300 proteins of mitochondria and associated fractions
- High-confidence mitochondrial proteome with absolute quantification and topology
- Interactors of oxidative phosphorylation complexes and cristae organizing system
- Identification of system linking respiratory chain and AAA quality control

Authors

Marcel Morgenstern, Sebastian B. Stiller, Philipp Lübbert, ..., Nikolaus Pfanner, Nils Wiedemann, Bettina Warscheid

Correspondence

nils.wiedemann@biochemie.uni-freiburg.de (N.W.), bettina.warscheid@biologie.uni-freiburg.de (B.W.)

In Brief

Morgenstern et al. describe an integrative organelle proteomics analysis to define the mitochondrial proteome in baker's yeast. The study provides a quantitative footprint of the proteome and its dynamics under different conditions. The results expand the set of proteins assigned to the mitochondria and provide a resource for future mitochondrial research.

Accession Numbers

PXD006128
PXD006151
PXD006146
PXD006128
PXD006147

Morgenstern et al., 2017, Cell Reports *19*, 2836–2852
June 27, 2017
http://dx.doi.org/10.1016/j.celrep.2017.06.014

CellPress

OPEN ACCESS
CellPress

Cell Reports
Resource

Definition of a High-Confidence Mitochondrial Proteome at Quantitative Scale

Marcel Morgenstern,[1,7] Sebastian B. Stiller,[2,7] Philipp Lübbert,[2,3,7] Christian D. Peikert,[1,7] Stefan Dannenmaier,[1] Friedel Drepper,[1,6] Uri Weill,[4] Philipp Höß,[2,8] Reinhild Feuerstein,[2,9] Michael Gebert,[2,10] Maria Bohnert,[2,11] Martin van der Laan,[5] Maya Schuldiner,[4] Conny Schütze,[2] Silke Oeljeklaus,[1,6] Nikolaus Pfanner,[2,6] Nils Wiedemann,[2,6,*] and Bettina Warscheid[1,6,12,*]

[1]Institute of Biology II, Biochemistry and Functional Proteomics, Faculty of Biology, University of Freiburg, 79104 Freiburg, Germany
[2]Institute of Biochemistry and Molecular Biology, ZBMZ, Faculty of Medicine, University of Freiburg, 79104 Freiburg, Germany
[3]Faculty of Biology, University of Freiburg, 79104 Freiburg, Germany
[4]Department of Molecular Genetics, Weizmann Institute of Science, Rehovot 7610001, Israel
[5]Medical Biochemistry and Molecular Biology, Center for Molecular Signaling, PZMS, Saarland University, 66421 Homburg, Germany
[6]BIOSS Centre for Biological Signalling Studies, University of Freiburg, 79104 Freiburg, Germany
[7]These authors contributed equally
[8]Present address: Cell Biology and Biophysics Unit, European Molecular Biology Laboratory, 69117 Heidelberg, Germany
[9]Present address: Center for Chronic Immunodeficiency, Medical Center, University of Freiburg, 79106 Freiburg, Germany
[10]Present address: Baxter Deutschland GmbH, 72379 Hechingen, Germany
[11]Present address: Department of Molecular Genetics, Weizmann Institute of Science, Rehovot 7610001, Israel
[12]Lead Contact
*Correspondence: nils.wiedemann@biochemie.uni-freiburg.de (N.W.), bettina.warscheid@biologie.uni-freiburg.de (B.W.)
http://dx.doi.org/10.1016/j.celrep.2017.06.014

SUMMARY

Mitochondria perform central functions in cellular bioenergetics, metabolism, and signaling, and their dysfunction has been linked to numerous diseases. The available studies cover only part of the mitochondrial proteome, and a separation of core mitochondrial proteins from associated fractions has not been achieved. We developed an integrative experimental approach to define the proteome of east mitochondria. We classified > 3,300 proteins of mitochondria and mitochondria-associated fractions and defined 901 high-confidence mitochondrial proteins, expanding the set of mitochondrial proteins by 82. Our analysis includes protein abundance under fermentable and nonfermentable growth, submitochondrial localization, single-protein experiments, and subcellular classification of mitochondria-associated fractions. We identified mitochondrial interactors of respiratory chain supercomplexes, ATP synthase, AAA proteases, the mitochondrial contact site and cristae organizing system (MICOS), and the coenzyme Q biosynthesis cluster, as well as mitochondrial proteins with dual cellular localization. The integrative proteome provides a high-confidence source for the characterization of physiological and pathophysiological functions of mitochondria and their integration into the cellular environment.

INTRODUCTION

Mitochondria are essential for the viability of eukaryotic cells. They are crucial for numerous cellular functions, including oxidative phosphorylation, metabolism of amino acids and lipids, biosynthesis of heme and iron-sulfur (Fe/S) clusters, and programmed cell death (Nunnari and Suomalainen, 2012). Mitochondria are extensively connected with other cellular compartments. This includes the transport of numerous metabolites and ions between cytosol and mitochondria, the import of precursor proteins from the cytosol, the formation of contact sites with the endoplasmic reticulum (ER) and additional organelles, as well as the interaction of mitochondria with the cytoskeleton (Eisenberg-Bord et al., 2016; Klecker et al., 2014; Labbé et al., 2014; Neupert and Herrmann, 2007; Wiedemann and Pfanner, 2017).

Initial proteomic studies led to the identification of a considerable portion of the mitochondrial proteome (Mootha et al., 2003; Ohlmeier et al., 2004; Pflieger et al., 2002; Prokisch et al., 2004; Sickmann et al., 2003; Taylor et al., 2003). This led to a boost of studies on mitochondrial functions under physiological and pathophysiological conditions, including the identification and functional characterization of further mitochondrial protein import pathways, of machineries required for maintaining mitochondrial membrane architecture, of proteins involved in the biosynthesis of Fe/S clusters, and of enzymes required for lipid biosynthesis (Lill, 2009; Neupert and Herrmann, 2007; van der Laan et al., 2016; Wiedemann and Pfanner, 2017). The effective combination of genetic, cell biological, and biochemical methods in the yeast *Saccharomyces cerevisiae* provided powerful approaches for analyzing protein functions in vivo and in vitro. Further studies expanded the mitochondrial proteome of both yeast and mammals (Itzhak et al., 2016; Müller

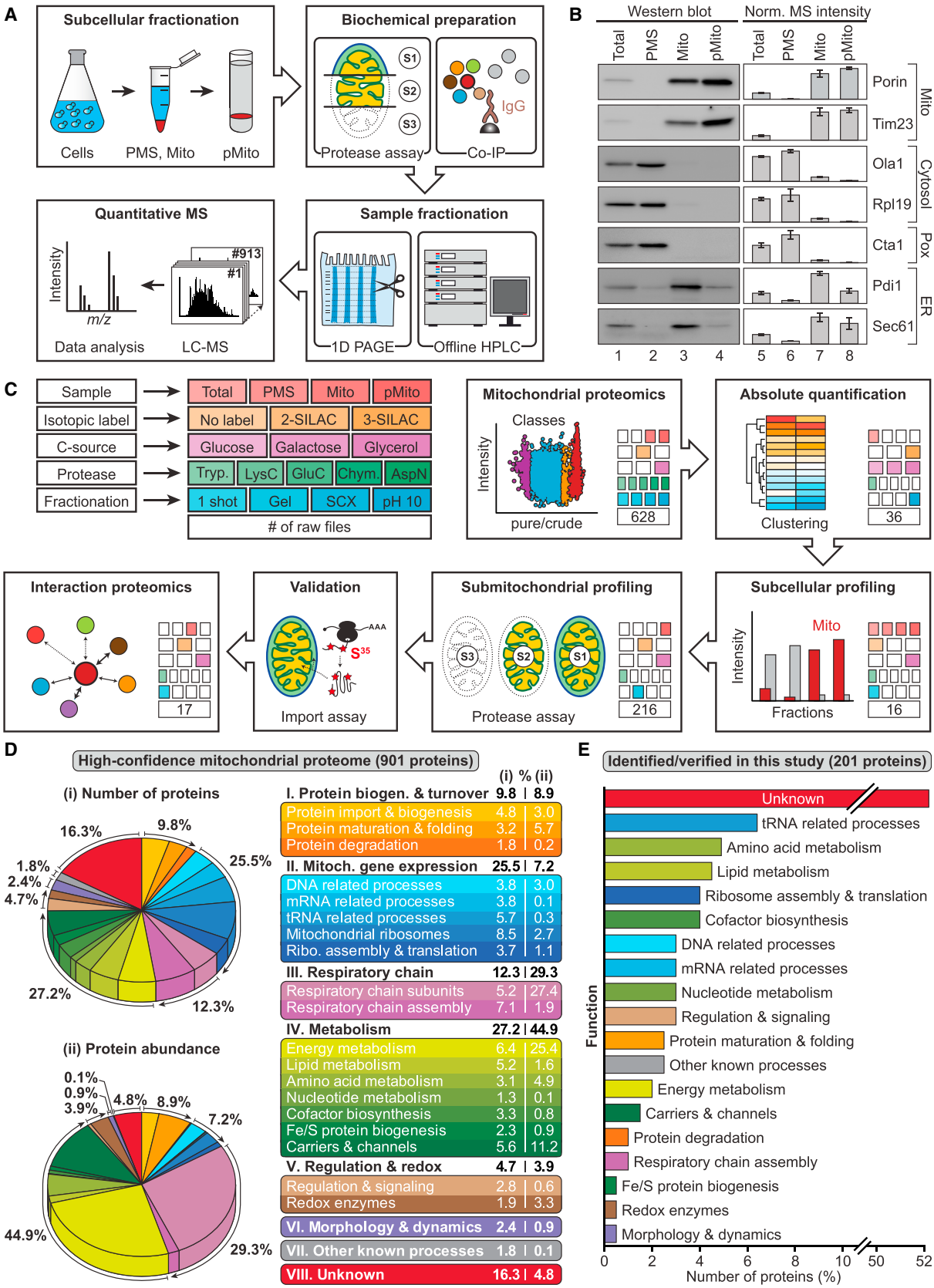

(legend on next page)

et al., 2016; Pagliarini et al., 2008; Rao et al., 2017; Reinders et al., 2006; Renvoisé et al., 2014; Stefely et al., 2016). In addition to direct proteomic studies of purified mitochondria (mentioned above) and mitochondrial subcompartments (Hung et al., 2014; Rhee et al., 2013; Vögtle et al., 2012; Zahedi et al., 2006), data mining, prediction programs for protein targeting, and literature entries were used to construct databases. Furthermore, numerous proteins were assigned to the mitochondrial compartment by genome-wide high-throughput localization studies using fluorescent tags (Kumar et al., 2002; Huh et al., 2003; Stadler et al., 2013; Yofe et al., 2016).

However, our knowledge about the mitochondrial proteome is far from being complete and the validity of mitochondrial entries in the widely used databases vary considerably for several reasons. (1) The high sensitivity of mass spectrometry (MS)-based approaches leads to the identification of even minor contaminations of organelle preparations, and thus the numerous lists of identified proteins contain a mixture of authentic mitochondrial proteins, loosely attached proteins, and contaminants. (2) High-throughput tagging studies yield important information about the global distribution of proteins but can lead to a misassignment of individual proteins to cellular compartments when they are not combined with single-protein analysis. (3) Prediction programs of protein targeting to distinct cell organelles and literature mining can provide important information, yet their use for databases without validating individual entries by experimental approaches can be misleading.

We developed an integrative experimental approach for organelle proteomics, generating a comprehensive proteome of mitochondria and associated fractions of baker's yeast. We combined high-sensitivity MS with quantitative analysis of protein abundance under different growth conditions, enrichment of proteins in distinct fractions, and subcellular classification of mitochondria-associated fractions. Many identified mitochondrial proteins were subjected to single-protein studies for in organello protein transport, interaction analysis, and subcellular and submitochondrial fractionation to define their localization and functional context, revealing partner proteins of key mitochondrial processes in respiration, quality control, and membrane architecture.

RESULTS

Experimental Approaches toward a Comprehensive Mitochondrial Proteome

To systematically explore the proteome of yeast mitochondria, we combined subcellular fractionation and biochemical methods with high-resolution proteomics and quantitative MS techniques (Figure 1A). We prepared highly purified mitochondria. The abundance of marker proteins was assessed by immunoblotting and MS (Figure 1B; Tables S1 and S2A). The purified mitochondria were virtually devoid of cytosolic and peroxisomal components, but still contained a fraction of ER proteins (Figure 1B, lanes 4 and 8). Figure 1C summarizes our multifaceted functional proteomic strategy. (1) Crude and purified mitochondria prepared from stable isotope labeling by amino acids in cell culture (SILAC)-yeast cells were analyzed by quantitative MS using a multi-protease digestion and orthogonal separation approach (Figures 1C and S1A). (2) Yeast cells grown under three different conditions were analyzed by MS to define an absolute quantitative blueprint of the mitochondrial proteome (Figures 1C and S1B). (3) We established the mitochondrial localization of identified and poorly characterized mitochondrial candidate proteins by subcellular protein profiling in a dual approach comprising label-free quantitative MS and epitope tagging combined with immunoblotting or microscopy (Figure 1C). (4) We studied submitochondrial protein localization using a gel-enhanced MS-based proteome profiling approach (Figure S1C) and mitochondrial import assays with radiolabeled precursor proteins (Figure 1C). (5) We delineated the functional protein interaction networks of identified mitochondrial proteins by SILAC-based quantitative affinity purification-MS (q-AP-MS) (Figure 1C). Altogether, we collected data of 913 liquid chromatography-tandem mass spectrometry (LC-MS/MS) runs with a total measurement time of 72 days. Overviews of the functional classification of the high-confidence mitochondrial proteome (901 proteins) and of the 201 mitochondrial proteins identified/verified in this study are shown in Figures 1D and 1E (see also Tables S3 and S4).

Classification of Mitochondria and Mitochondria-Associated Fractions

Our MS-based proteome profiling of crude and highly purified yeast mitochondria resulted in the identification of 3,512 proteins (SD, ±10) on average per biological replicate (n = 4), of which 1,024 (SD, ±1.4) were annotated as mitochondrial proteins in the *Saccharomyces* Genome Database (SGD) (Cherry et al., 2012) (Figure S2A; Tables S2B and S2C). To obtain a high coverage of protein sequences by identified peptides, we used five different proteases, leading to a 1.6-fold average increase of sequence coverage (1.5-fold for mitochondrial proteins) in comparison to the use of trypsin alone (Figure S2B; Table S2B; exemplified with the TIM23 presequence translocase of the inner membrane, Figure S2C). The overall sequence coverage for proteins with mitochondrial annotation was 64% compared to 45% for all identified proteins. Mitochondrial annotation of proteins in the SGD includes a broad range of approaches from detailed single-protein localization and functional studies to

Figure 1. Multi-dimensional MS Approach for Global Profiling and In-Depth Characterization of the Mitochondrial Proteome of *S. cerevisiae*

(A) Outline of experimental strategy. Total, cell lysate; PMS, post-mitochondrial supernatant; Mito, mitochondria; pMito, gradient-purified mitochondria.

(B) Western blot (lanes 1–4) and MS data (lanes 5–8) for selected subcellular marker proteins. Error bars indicate SEM for $n \geq 3$ and the range for n = 2.

(C) Overview of experimental approaches followed to define and characterize mitochondrial proteins.

(D) Overview of the functional classification of the high-confidence mitochondrial proteome. Relative protein quantification was based on the analysis of gradient-purified mitochondria from cells grown on glycerol.

(E) Overview of the functional classification of mitochondrial proteins identified or verified in this study.

See also Figure S1 and Tables S2A, S3, and S4.

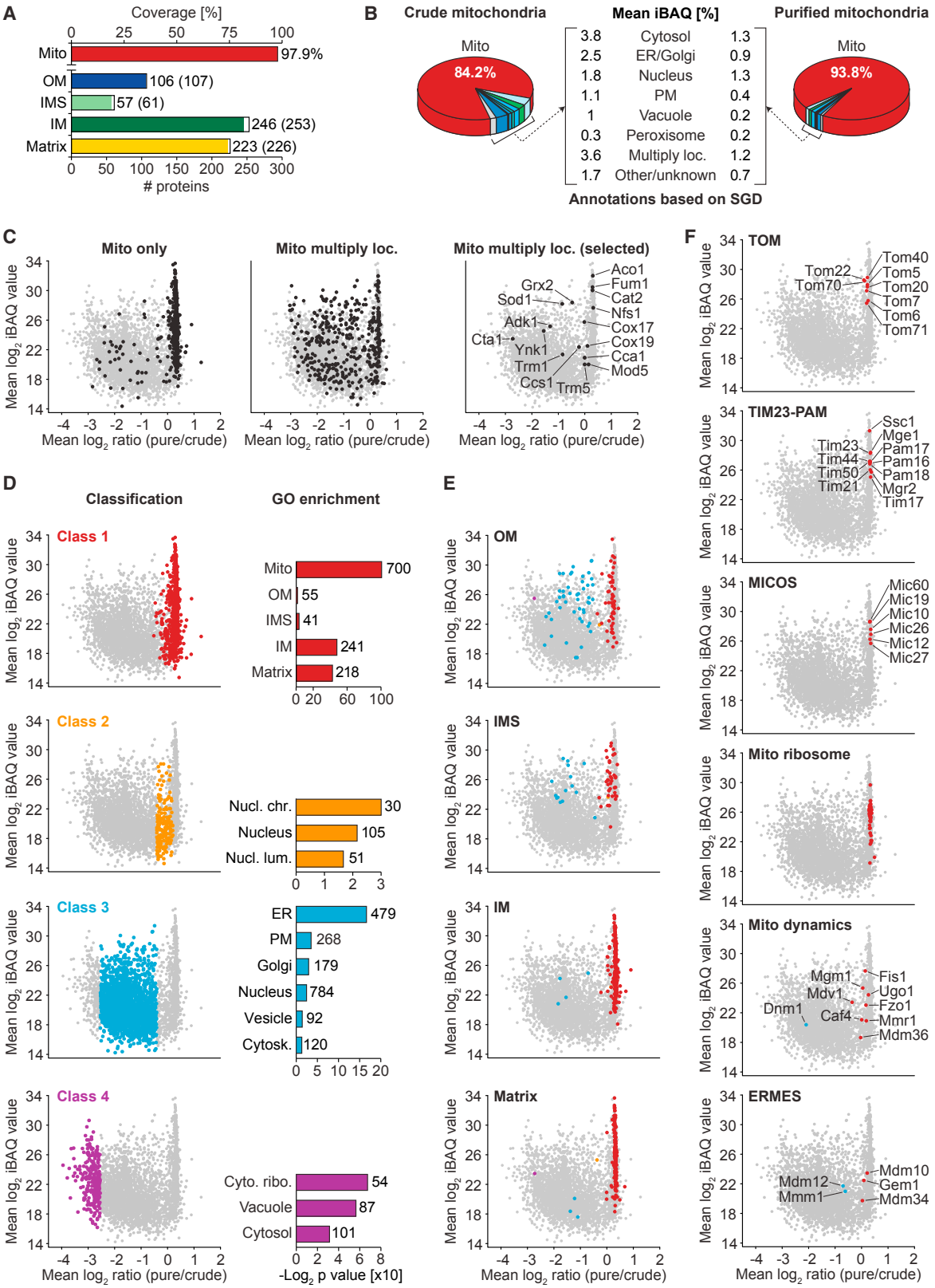

(legend on next page)

high-throughput analyses and putative mitochondrial assignments. To obtain a reference set of mitochondrial proteins, we used 583 mitochondrial proteins, for which a submitochondrial localization was reported in SGD (pointing toward single-protein studies); 520 proteins were assigned to a single submitochondrial compartment. We identified 98% of these reference set proteins (Figure 2A), indicating a high coverage of well-established mitochondrial proteins by our MS analysis.

With a number of 3,539 proteins identified in total across all replicates (based on 125,648 identified peptide sequences), this analysis considerably exceeds previous studies on the yeast mitochondrial proteome (Figures S2D and S2E; Tables S1 and S2B) (Ohlmeier et al., 2004; Prokisch et al., 2004; Reinders et al., 2006; Vögtle et al., 2012; Zahedi et al., 2006); however, due to the high sensitivity of MS, a large number of non-mitochondrial proteins were also identified. We thus searched for criteria to distinguish the core mitochondrial proteome from associated and contaminating proteins. Non-mitochondrial proteins were markedly decreased in abundance, but not in number of identified proteins, in purified mitochondria in comparison with crude mitochondria (Figure 2B; Tables S1 and S2B). For relative quantification, we calculated SILAC ratios of 3,453 proteins and established ratio-intensity plots of 3,365 proteins reliably quantified in all four biological replicates (Figures 2C, S2F, and S2G; Table S2B). Proteins with an exclusive mitochondrial localization exhibited a narrow distribution centered at a median $\log_2$ SILAC ratio of purified to crude mitochondria of 0.3 (Figures 2C, left plot, and S2H), whereas mitochondrial proteins with dual or multiple localizations (Yogev and Pines, 2011) displayed a broader distribution (Figure 2C, middle and right plots). Using a statistical approach, we classified proteins based on their mean $\log_2$ ratios, leading to a subdivision of the large dataset into four distinct classes (Figures 2D and S2H; Table S2B). All four classes contained mitochondrial proteins, but to a considerably different extent. Using gene ontology (GO) enrichment analysis (SGD), class 1 (864 proteins) contained a strong enrichment of the term mitochondrion including all four submitochondrial compartments, whereas this term was underrepresented in classes 2–4 (Table S5A). Class 2 features a set of nuclear proteins (105), whereas a larger population of nuclear proteins (784) are part of class 3 along with proteins of various subcellular compartments including the ER, Golgi, and the plasma membrane. GO enrichment analysis for class 4 showed that purified mitochondrial fractions are mostly devoid of vacuolar and cytosolic proteins including cytosolic ribosomes (Figure 2D; see also Figures 1B and 2B).

The proteins of the mitochondrial reference set with a defined submitochondrial localization were preferentially found in class 1 and to a lesser degree in class 3 (Figure 2E). As an example, the subunits of the TIM23 complex and the presequence translocase-associated motor (PAM), the mitochondrial contact site and cristae organizing system (MICOS), and the mitochondrial ribosome featured highly consistent mean $\log_2$ ratios centered at 0.3 within class 1 (Figure 2F). The translocase of the outer membrane (TOM) equally qualified for class 1 but is slightly shifted to lower mean $\log_2$ ratios compared to TIM23-PAM, MICOS, and the mitochondrial ribosome. The ER-mitochondria encounter structure (ERMES) revealed a remarkable separation with three subunits present in class 1 and two in class 3. This dual distribution is consistent with data from previous work showing that Mdm10, Mdm34, and Gem1 are anchored in the mitochondrial outer membrane, whereas Mmm1 localizes to the ER membrane and Mdm12 is bridging Mmm1 and Mdm34/Mdm10 at the cytosolic side (Ellenrieder et al., 2016; Kornmann et al., 2009). Various proteins controlling mitochondrial fusion and fission were also present in class 1, albeit with a broader distribution (Figure 2F). Dnm1 was considerably depleted in highly purified mitochondria in agreement with its distribution between cytosol and mitochondria (Labbé et al., 2014).

For the definition of a high-confidence mitochondrial proteome, we applied stringent criteria and included the following: class 1 proteins with a sequence coverage of > 20% (SD, < 0.75; Figure S2I); experimentally validated mitochondrial proteins via import of radiolabeled precursors into mitochondria, subcellular fractionation, or fluorescence microscopy; manually curated mitochondrial proteins from single-protein studies; and proteins of dual localization, for which a presence in the mitochondrial proteome was demonstrated by experimental analysis/manual curation as outlined below. In total, this stringent mitochondrial proteome contains 901 proteins (Figure 1D; Tables S1 and S3).

Assessment of Copy Numbers of Mitochondrial Proteins

At present, there is no consistent picture about the absolute copy numbers of mitochondrial and mitochondria-associated proteins. Several studies using glucose-grown yeast cells reported different cellular copy numbers for the same proteins (Tables S1 and S2D) (Chong et al., 2015; Ghaemmaghami

Figure 2. Quantitative Deep Proteome Analysis of Yeast Mitochondria by SILAC-MS

(A) Coverage of proteins of distinct submitochondrial localization. Proteins identified in pure/crude mitochondria were categorized as outer membrane (OM), intermembrane space (IMS), inner membrane (IM), or matrix protein based on GO annotations. Shown is the number of proteins assigned to a given term and (in parentheses) the total number of proteins with this annotation. Mito, sum of all proteins in OM, IMS, IM, and matrix.

(B) Protein composition of crude versus gradient-purified mitochondria. Shown are mean percentages of intensity-based absolute quantification (iBAQ) values (n = 4). Loc., localized; PM, plasma membrane; SGD, *Saccharomyces* Genome Database.

(C) Ratio-intensity plots of quantified proteins (n = 4). Proteins exclusively localized to mitochondria (left), to mitochondria and other organelles (middle), and selected proteins with multiple subcellular localization (right) are highlighted.

(D) Distribution of proteins grouped into distinct classes by statistical data analysis (left panel) and selected GO cellular component terms significantly enriched in each class (right panel) with the number of proteins assigned. Cyto. ribo., cytosolic ribosome; Cytosk., cytoskeleton; Nucl. chr./lum., nuclear chromosome/lumen.

(E and F) Ratio-intensity plots as shown in (D) highlighting mitochondrial subcompartment annotations (E) and subunits of the TOM, TIM23-PAM, MICOS, and ERMES complex as well as mitochondrial ribosomal proteins and proteins involved in mitochondrial dynamics (F). Coloring reflects the class a protein was assigned to.

See also Figure S2 and Tables S1, S2A, and S5A.

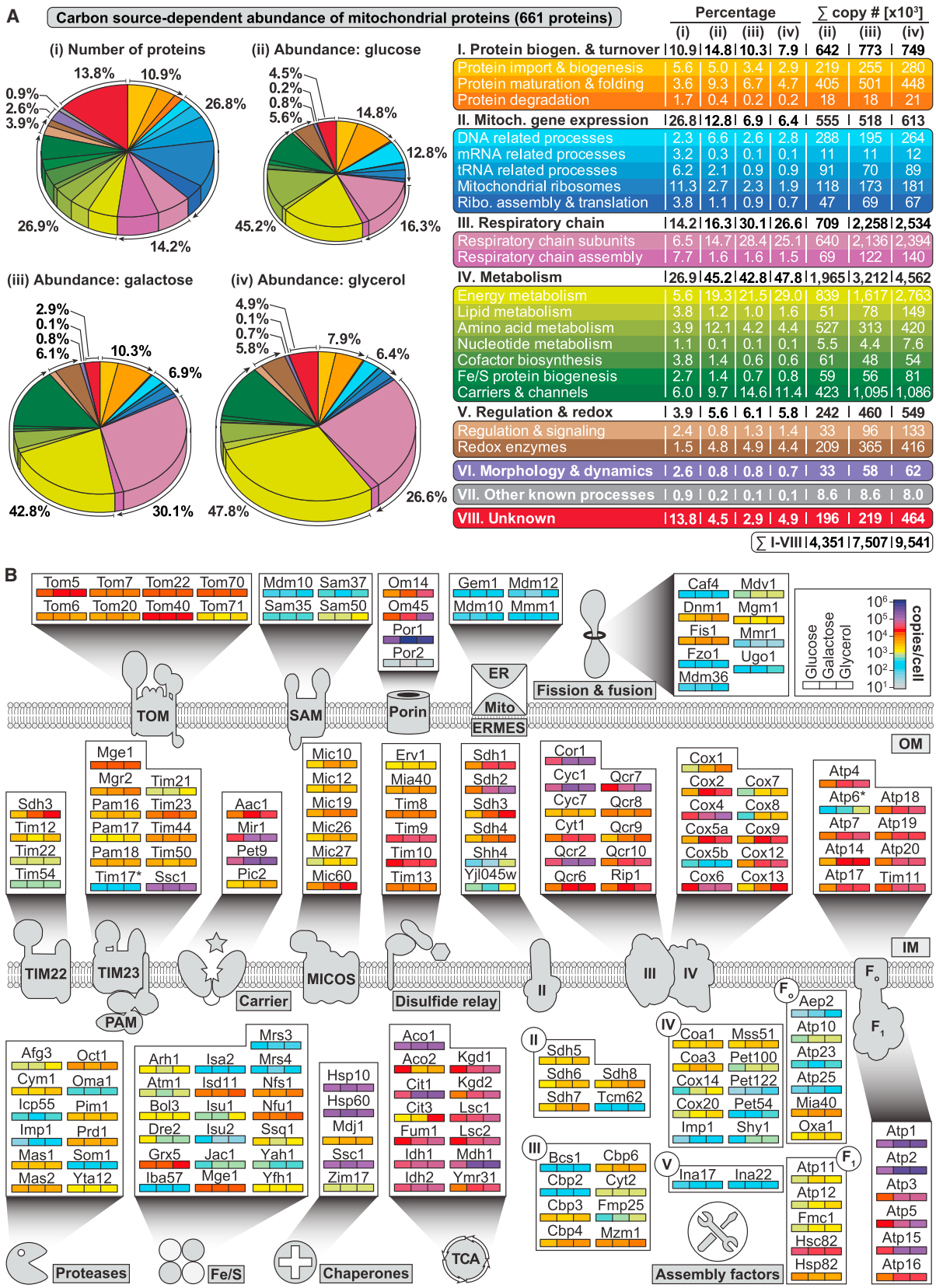

(legend on next page)

et al., 2003; Kulak et al., 2014). To obtain a quantitative understanding of the mitochondrial proteome and its changes under different growth conditions, we grew yeast cells on fermentable (glucose), alternative sugar (galactose), and non-fermentable (glycerol) carbon sources. For each condition, we analyzed biological triplicates using triple-SILAC labeling and high-pH reversed-phase peptide fractionation for proteome-wide quantification by MS. The calculated SILAC ratios of more than 4,000 proteins were reproducible between biological replicates and carbon sources with Pearson correlation coefficients between 0.78 and 0.9 (Figure S3A; Table S2E). We extracted MS intensities and used the proteomic ruler method (Wiśniewski et al., 2014) to estimate copy numbers. Altogether, we report 12,111 copy numbers for 4,039 yeast proteins and thus significantly expand absolute quantitative information on yeast proteins (Figure S3B; Table S2D). A comparison of our glucose-specific copy number data with reported copy numbers showed the best correlation with the MS approach of Kulak et al. (2014), whereas the correlation was lower with quantification data obtained by single-cell imaging (Chong et al., 2015) or a tagging approach (Ghaemmaghami et al., 2003). Our analysis was not biased against low abundant proteins. For both non-mitochondrial and mitochondrial proteins, we observed a large dynamic range of up to six orders of magnitude, varying from proteins with less than 10 to more than 1,000,000 copies per cell (Figure S3C). The majority of proteins (~70%) were present in the range of 100 to 10,000 copies per cell, whereas approximately the same number of proteins exhibit copy numbers below or above the main distribution. A total of 1,576 proteins exhibited a significant change in abundance (ANOVA, p value $\geq$ 0.05, n = 3) in yeast grown on galactose or glycerol in relation to glucose and were grouped to 14 clusters by k-means clustering (Figure S3D; Table S2D). We revealed a significant overrepresentation of mitochondrial terms in all three GO domains for proteins in cluster C02–C06 that were considerably more abundant in galactose- and glycerol-grown yeast (Figure S3E; Tables S5B–S5D). We independently corroborated carbon source-dependent effects on the expression levels of mitochondrial proteins by direct comparison of immunoblotting data using antibodies specifically directed against mitochondrial proteins and global MS-based copy number estimation (Figure S3F; Table S2F).

Our analysis leads to a three-carbon source-specific absolute quantitative blueprint of the yeast mitochondrial proteome (Figures 3A and S3G; Tables S1 and S2D); representative examples are shown in Figure 3B. The protein import machineries of the outer membrane (TOM, SAM), inner membrane (TIM23-PAM, TIM22), and intermembrane space (mitochondrial disulfide relay system Mia40-Erv1) (Neupert and Herrmann, 2007; Wiedemann and Pfanner, 2017) constitute a rather static part of the mitochondrial proteome. The TOM complex exhibited a high abundance, highlighting its role as main protein entry gate. Mitochondrial proteins with functions in Fe/S cluster biogenesis and iron homeostasis (Lill, 2009) were mostly low abundant and constant in expression, consistent with these functions being essential and steady functions of mitochondria under all conditions (Figures 3B and S3G). The carbon source-dependent (dynamic) part of the mitochondrial proteome largely consists of the highly abundant oxidative phosphorylation protein network (respiratory complexes II–IV, ATP synthase, and proteins of the tricarboxylic acid [TCA] cycle) (Murphy et al., 2015; Ohlmeier et al., 2004; Paulo et al., 2016); the metabolite channel Por1/VDAC and its interaction partners OM14 and OM45 (Lauffer et al., 2012), which are the most abundant proteins in the outer membrane (Zahedi et al., 2006); and the highly abundant carrier proteins of the inner membrane such as the phosphate carrier Mir1 and the adenine nucleotide translocators Pet9 and Aac1 (Palmieri et al., 2006). Por2, the paralog of Por1, was found to be five orders of magnitude lower expressed than Por1, and expression of Pic2 was two orders of magnitude lower than Mir1, to which it is functionally redundant. Mitochondrial ribosomes were of medium abundance yet showed a growth condition-dependent expression as expected (Figure S3G). The MICOS complex also exhibited a carbon source-dependent expression pattern in agreement with its dynamic role in the maintenance of inner membrane architecture (van der Laan et al., 2016).

Identification of Mitochondrial Proteins and Submitochondrial Localization

Our high-confidence mitochondrial proteome includes 82 proteins that were previously not demonstrated to localize to mitochondria (Table S4A). The proteome also includes 119 proteins, for which a mitochondrial annotation was inferred from high-throughput studies without further verification (Table S4B). In addition to the presence in class 1 using stringent criteria (Figures 4A and 4B), we employed distinct experimental assays to demonstrate a mitochondrial localization for this group. A total of 58 proteins was selected for this in-depth analysis (shown in bold in Table S4). (1) Precursor proteins were synthesized in a cell-free system, labeled with [^{35}S]methionine and imported into isolated mitochondria; proteolytic processing and/or translocation to a protease-protected location in dependence on the mitochondrial membrane potential ($\Delta\psi$) were taken as specific criteria for mitochondrial import. This includes the respiratory chain interactors Rci37 and Rci50, the coenzyme Q cluster protein Coq21, and the mitochondrial glutaredoxin-like protein Mgp12 (Figure 4C). (2) Proteins were tagged with a C-terminal green fluorescent protein (GFP), and the subcellular localization was analyzed by fluorescence microscopy. The GFP signal

Figure 3. Proteome-wide Absolute Quantification of Carbon Source-Dependent Protein Expression

(A) Overview of the functional classification of 661 high-confidence class 1 mitochondrial proteins according to copy numbers per cell determined for three different carbon sources. The areas of the pie charts (ii), (iii), and (iv) are directly proportional to the determined copy numbers of the mitochondrial proteins.

(B) Proteins of selected mitochondrial complexes, functions, or pathways and their carbon source-dependent copy numbers per cell. Colors indicate absolute mean copy numbers per cell and carbon source (n = 3). Asterisks, low sequence coverage or low quantification accuracy can lead to an underestimation of the copy number of components such as for Atp6 and Tim17. Fe/S, iron–sulfur cluster biosynthesis; F_oF_1, ATP synthase; TCA, tricarboxylic acid cycle; II/III/IV, complexes II/III/IV of the respiratory chain.

See also Figure S3 and Table S2D.

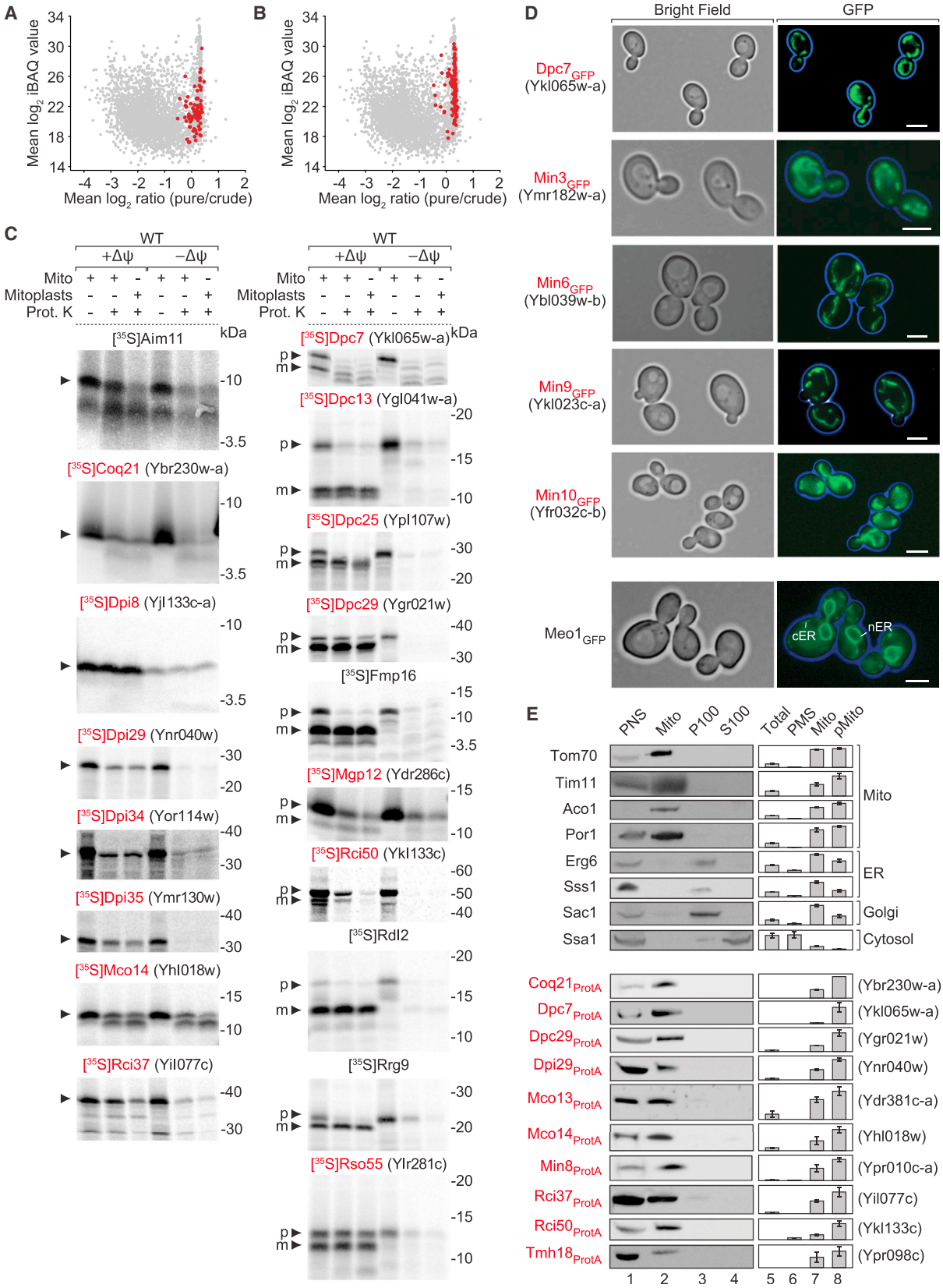

(legend on next page)

showed a typical elongated mitochondrial network for the selected proteins (Figure 4D). For comparison, we show the localization of the recently identified mini-ER open reading frame (ORF) Meo1 (Yofe et al., 2016). (3) We used N-terminal GFP tag libraries with native promoters (Figure S4A) or with constitutive promoter (Figures S4B and S4C; Tom5 as reference) (Yofe et al., 2016) to show mitochondrial localization, including the transmembrane protein (TMEM) family members Tmh11 and Tmh18 as well as Rci37 and Rci50. (4) We individually tagged 38 proteins with C-terminal protein A or hemagglutinin tags and performed biochemical subcellular fractionation (Figures 4E, S4D, and S4E). (5) Subcellular fractionations of untagged yeast cells were subjected to MS analysis, yielding an additional dataset to corroborate the high-confidence mitochondrial proteome (Figures 4E, S5A, and S5B; Table S2A). Our analysis included the mitochondrial localization of Rso55 (related to spastic paraplegia with optic atrophy and neuropathy SPG55) (Figures 4C, S4A, and S4D), a homolog of the human gene C12orf65 that was previously linked to spastic paraplegia SPG55 and associated with mitochondrial translation defects (Perocchi et al., 2006; Shimazaki et al., 2012).

To determine the suborganellar localization, we combined protease accessibility assays, in which gradient-purified mitochondria were differentially treated with detergents and proteases, with SILAC-MS (Figure S1C; Tables S2G and S2H). Incubation of intact mitochondria with proteinase K and trypsin (Figure 5A, sample 1 [S1]) leads to degradation of outer membrane proteins Tom22 and Tom20 (Figure 5B, lane 2), whereas proteins of the other mitochondrial subcompartments remain unaffected. Protease treatment of mitoplasts (Figure 5A, sample 2 [S2]), generated by rupturing the outer membrane with low concentrations of digitonin, leads to proteolytic degradation of intermembrane space-exposed proteins such as Pam18 and Mic12 (Figure 5B, lane 3). Matrix-exposed proteins like Mdm38 and Tim44 are only accessible to proteases upon lysis of both mitochondrial membranes by Triton X-100 (Figure 5A, sample 3 [S3]; Figure 5B, lane 4). SILAC-MS analysis of S1–S3 mixed with intact mitochondria (n = 3; Figure S6A) led to signature plots for proteins of different mitochondrial subcompartments (Figure 5B, lanes 5–7). Class 1 proteins were subjected to clustering analysis, revealing three clusters specific for outer membrane proteins, intermembrane space-exposed proteins, or matrix-exposed proteins (Figure 5C; Table S2G). Principal-component analysis of proteins in these clusters and further proteins meeting the criteria for the signature plots visualizes the data in a two-dimensional plot, showing the separation into three distinct clusters specific for individual subcompartments in good agreement with GO cellular component annotations (Figure 5D). Using the clustering analysis and signature plots, we established the submitochondrial localization of 219 proteins, for which the assignment to mitochondrial subcompartments had not been achieved previously. A total of 21 proteins were located at the outer membrane, 50 proteins were exposed to the intermembrane space, and 148 proteins were exposed to the matrix (Figure 5D, right plot; Tables S2G and S5E). To control the MS-based submitochondrial protein localization, we prepared mitochondria and mitoplasts from yeast strains expressing representative protein A-tagged class 1 proteins, treated both fractions with proteinase K, and analyzed them by immunoblotting. The biochemical data were in very good agreement with the MS data and confirmed the submitochondrial assignment of the selected proteins (Figures 5E, 5F, S6B, and S6C; Tables S2G and S6). Comparison of our suborganellar data with previous studies targeting the outer membrane and intermembrane space proteomes (Zahedi et al., 2006; Vögtle et al., 2012) showed substantial overlap with proteins of our high-confidence mitochondrial proteome (Figure S6D).

To gain insight into the membrane topology of authentic (untagged) mitochondrial proteins, we established peptide plots based on S/M SILAC ratios of the submitochondrial profiling analysis (Figures 5E and 5F). We first demonstrated the feasibility of the approach by analyzing two proteins with known topology. Tom70 contains a single transmembrane domain (TMD) near the N terminus (amino acids [aa] 12–29) (Li and Shore, 1992). A high S1/M ratio of the peptide N-terminal to the TMD indicated a protection from degradation when intact mitochondria were treated with proteases, whereas the low S1/M ratios of peptides C-terminal to the TMD confirmed that this part was accessible to the proteases and thus facing the cytosol (Figure 5E; Table S2I). Tim23 contains four TMDs and an N-terminal hydrophilic domain in the intermembrane space (Alder et al., 2008). When mitoplasts were subjected to protease treatment (S2), the peptides N-terminal to the first TMD and the peptide stretching across the fourth TMD exhibited low S2/M ratios, confirming that N and C termini were exposed to the intermembrane space (Figure 5E; Table S2I).

We then applied this approach to proteins with unknown topology, using TMHMM predictions to reveal putative TMDs (Figures 5E and 5F; Table S2I). Our analysis indicates that the single-spanning proteins Pth2, a peptidyl-tRNA hydrolase, and Tcd2, tRNA threonylcarbamoyladenosine dehydratase, are located in the outer membrane with a short N-terminal portion residing in the intermembrane space and the major C-terminal portion exposed to the cytosol. For Scm4, an outer membrane protein

Figure 4. Biochemical, Fluorescence Microscopy, and MS-Based Subcellular Localization Analysis of Mitochondrial Proteins

(A and B) Ratio-intensity plots, as shown in Figures 2C–2F, highlighting proteins from Tables S4A (A) and S4B (B).

(C) Protein import assays with radiolabeled mitochondrial precursor proteins. $+/-\Delta\psi$, mitochondria with or without membrane potential; Prot. K, proteinase K; p, precursor; m, mature form.

(D) Images of yeast cells expressing GFP-tagged proteins analyzed by fluorescence microscopy. cER/nER, cortical/nuclear ER. Scale bar, 5 μm.

(E) Subcellular protein profiling. Yeast strains were subjected to subcellular fractionation followed by SDS-PAGE and immunoblotting (lanes 1–4) or quantitative MS analysis (n = 4) (lanes 5–8). Shown are data for selected marker proteins (upper panel) and proteins that were only listed as ORF in the SGD and named in this study (shown in red, lower panel). Y axes of bar charts, mean of normalized MS intensities; error bars indicate SEM for $n \geq 3$ and the range for n = 2. PNS, post-nuclear supernatant; PMS, post-mitochondrial supernatant; pMito, gradient-purified mitochondria.

See also Figures S4 and S5, and Tables S1 and S2A.

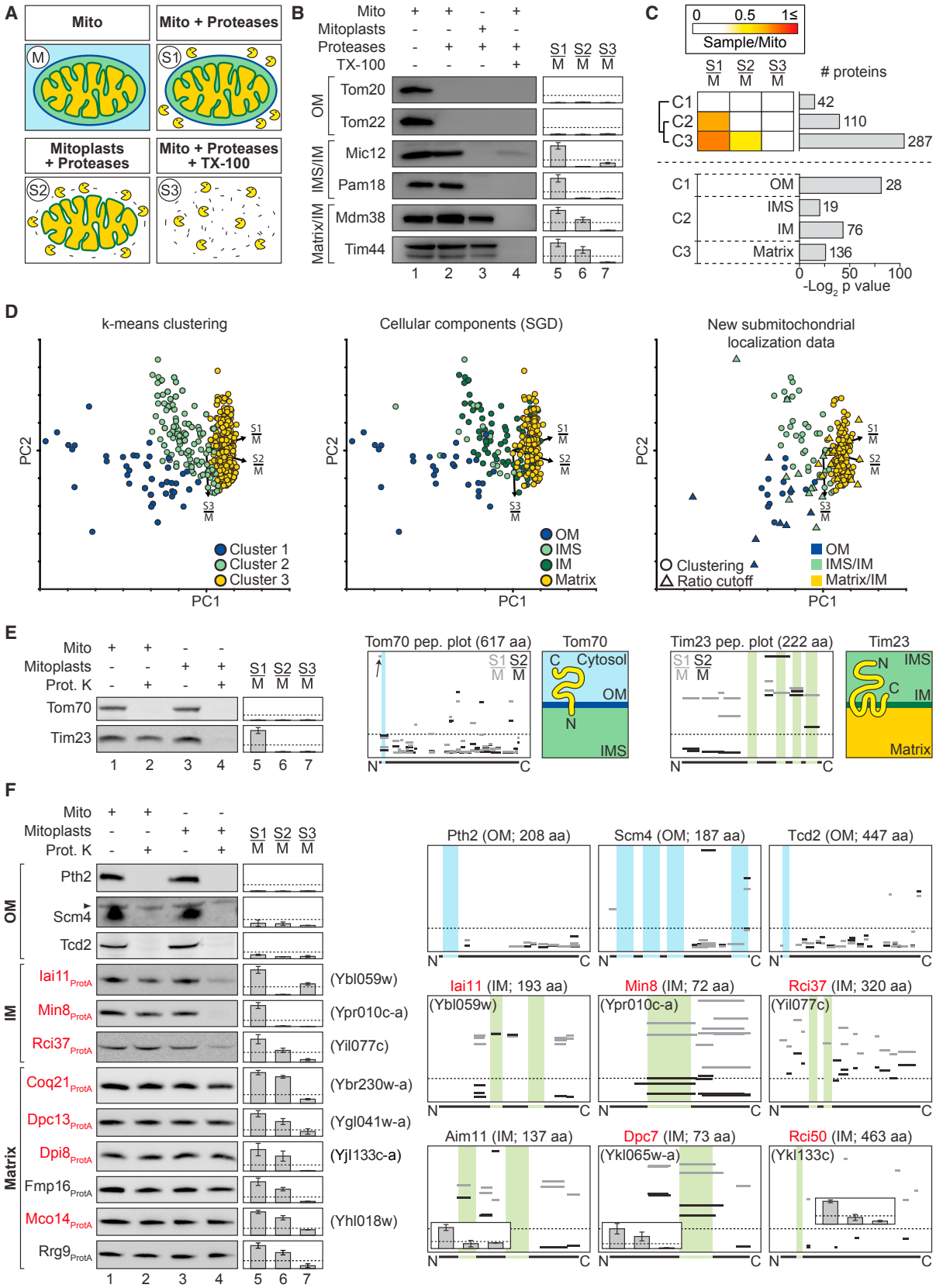

(legend on next page)

with four predicted TMDs (Becker et al., 2011), peptide ratios suggest that both protein termini are located in the cytosol. The inner membrane proteins Aim11, Iai11, and Rci37, all predicted to have two TMDs, project both termini into the intermembrane space, whereas the single-spanning proteins Min8, Rci50, and Dpc7 show a matrix-intermembrane space orientation of their N and C termini, respectively. Information about S/M peptide ratios determined for all proteins with TMHMM prediction identified in this experiment are provided in Table S2I.

Mitochondrial Proteins with Dual Localization

Studies by Pines and colleagues demonstrated a dual cellular localization of several yeast mitochondrial proteins (Yogev and Pines, 2011). To identify further dual-localized mitochondrial proteins, we analyzed the high-confidence class 1 mitochondrial proteome by stringent criteria outlined in Table S7, including the presence of significant amounts of a protein in both the post-mitochondrial supernatant (PMS/total ratio > 0.5) and the mitochondrial fraction in the cellular fractionation. These criteria led to a list of 57 proteins (Table S7).

We tested the validity of our selection approach by two means. (1) We performed a literature analysis: 30 of the 57 proteins were previously assigned to mitochondria by manual annotation (single-protein analysis). A total of 15 of these proteins was shown to possess a dual/multiple cellular localization (summarized in SGD): the copper chaperone Ccs1, which is located in the mitochondrial intermembrane space, cytosol, and nucleus; the cytosolic and mitochondrial glutathione oxidoreductase Glr1, the glycerol-3-phosphate dehydrogenase Gpd2, the protease Prd1, the flavohemoglobin protein Yhb1, the kynurenine aminotransferase Bna3, and Nif3, a protein of unknown function; the nuclear and mitochondrial DNA ligase Cdc9 and the 5′-flap endonuclease Rad27; and the cytosolic/nuclear mitochondrial tRNA metabolism-related proteins Dia4, Hts1, Mod5, Pus4, Trm5, and Vas1. (ii) We selected 11 of the further proteins from Table S7 for experimental analysis (Figures 6A and 6B). Eight candidates were previously annotated to the nucleus or cytosol, but not to mitochondria, including the tRNA metabolism-related enzymes Deg1, Smm1, and Sua5; Ymr087w, now named Pdl32 for protein of dual localization of 32 kDa; the glutathione transferase Ecm4; Meu1, which catalyzes the initial step in the methionine salvage pathway; the putative nitroreductase Hbn1; and acyl-protein thioesterase 1 (Ylr118c) (Duncan and Gilman, 2002), now named Tml25 for 25-kDa acyl-protein thioesterase with multiple localizations (Figure 6C, upper panel). Two candidates were previously localized to peroxisomes by single-protein studies and linked to mitochondria only by high-throughput analysis: the peroxisomal matrix protein Pxp2 and acyl-CoA thioesterase Tes1 (Jones et al., 1999; Nötzel et al., 2016). The thiouridine modification enzyme Tum1 was linked to the cytoplasm and to mitochondria by high-throughput analysis (Figure 6C, upper panel). For an experimental analysis, we individually tagged nine candidate proteins and controlled the proper subcellular fractionation of each resulting yeast strain manually, demonstrating a dual localization for each protein, including the presence of Pdl32 and Tml25 in both cytosol and mitochondria (Figure 6A). Seven candidate proteins were efficiently synthesized and labeled with [^{35}S]methionine in a cell-free system, and thus their $\Delta\psi$-dependent import into mitochondria could be analyzed: each protein was imported in a $\Delta\psi$-dependent manner, but not processed (Figure 6B). Submitochondrial analysis by swelling followed by protease treatment demonstrated that each of these hydrophilic proteins was translocated to the mitochondrial matrix (Figure 6B). Taken together, these experiments fully support a dual/multiple localization of the 11 candidate proteins (Figure 6C, lower panel).

We conclude that literature analysis and biochemical characterization demonstrate a dual localization of 26 proteins selected from the list of 57 putatively dual-localized mitochondrial proteins (Table S7), providing strong evidence for the validity of the approach.

Interaction Networks of Identified Proteins

To obtain functional information about identified or poorly characterized mitochondrial proteins (Tables S4A and S4B), we analyzed the organization of selected proteins in protein complexes and networks (summarized in Figures 7 and S7, and Table S2J). For an overview, mitochondria containing tagged proteins

Figure 5. Profiling of Suborganellar Localization and Membrane Topology of Mitochondrial Proteins

(A and B) Protease accessibility assay. Gradient-purified mitochondria (M, S1), mitoplasts (S2), and mitochondrial Triton X-100 (TX-100) lysates (S3) were treated with proteases (proteinase K and trypsin) as indicated. (B) Samples were analyzed by SDS-PAGE and immunoblotting using antisera against marker proteins of the mitochondrial outer membrane (OM), and intermembrane space (IMS)- and matrix-exposed proteins (lanes 1–4). For submitochondrial profiling, SILAC-labeled untreated mitochondria (M) and S1, S2, or S3 were mixed and analyzed by MS (n = 3) (lanes 5–7). Y axes, mean S/M protein ratios; error bars indicate SEM for n = 3 and the range for n = 2; dotted lines, S/M ratios of 0.25. IM, inner membrane.

(C) Top, k-means clustering performed based on S/M ratios of proteins (n = 3) with a ratio $\leq$1.1 that were present in class 1 in pure/crude experiments and showed decreasing ratios with increasing accessibility of the proteases (i.e., S1/M $\geq$ S2/M > S3/M). Bottom, selected GO terms significantly enriched in each cluster.

(D) Principal-component (PC) analysis of $\log_2$-transformed mean S/M ratios of the proteins present in the clusters depicted in (C) and further proteins meeting the criteria for signature plots. Shown are all proteins of C1–C3 (left), proteins with previous GO annotations (middle), and proteins without previous GO annotation that were assigned to mitochondrial subcompartments based on our experimental data (right). PC 1–3 account for 45.7%, 35.3%, and 19.0% of the variability in the data. Arrows point to the direction of increasing values for the different experimental conditions.

(E and F) Mitochondrial sublocalization and membrane protein topology. Intact mitochondria (lanes 1 and 2) or mitoplasts (lanes 3 and 4) were treated with proteinase K (Prot. K) where indicated. Marker proteins of the mitochondrial outer (Tom70) and inner membrane (Tim23) shown in (E) belong to the fractionation of $Mco8_{ProtA}$ (Figure S6). Bar charts (lanes 5–7) show the corresponding S/M protein ratios. Peptide plots illustrate the topology for Tom70, Tim23 (both summarized in adjacent cartoons), and selected proteins of the high-confidence mitochondrial proteome. Plotted are S/M ratios of tryptic peptides identified in submitochondrial profiling experiments. Transmembrane segments (TMHMM prediction or according to Alder et al. [2008] for Tim23) are indicated in blue (OM) or green (IM). Y axes of bar charts and peptide plots, mean S/M ratio; dotted lines indicate S/M ratios of 0.25; error bars indicate SEM for n = 3 and the range for n = 2. See also Figure S1C and Tables S1, S2G, and S5E.

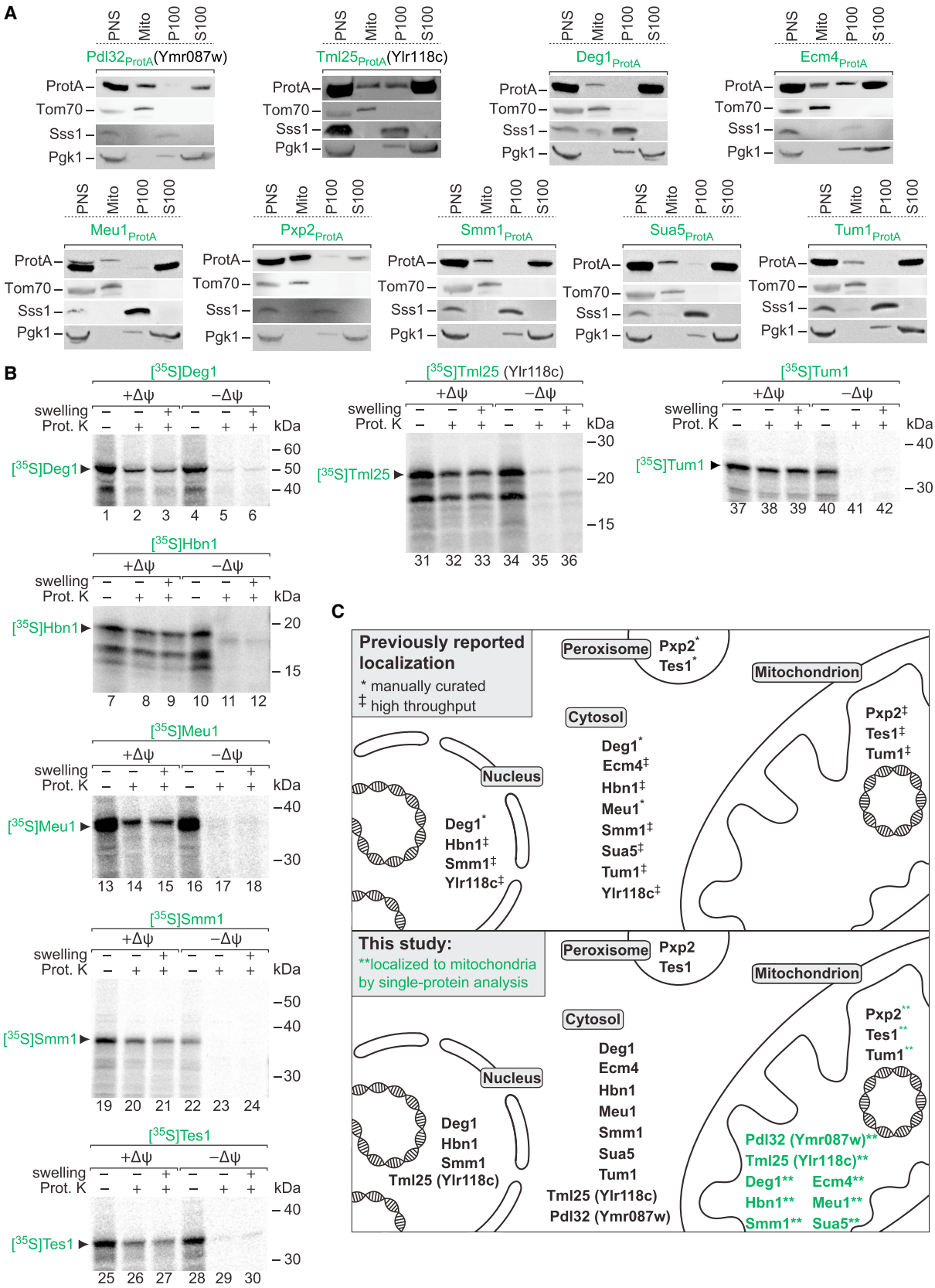

(legend on next page)

or imported ^{35}S-labeled proteins were lysed with digitonin and analyzed by blue native electrophoresis, revealing distinct high-molecular-weight complexes (Figures 7A and S7A). $\Delta\psi$-dependent formation of protein complexes demonstrates that the precursor proteins were translocated into or across the inner membrane to form a complex (shown here for Dpa10, Mco14, Dpi29, and Dpi34), whereas $\Delta\psi$-independent complex formation typically points to an outer membrane/intermembrane space location (Min6, in agreement with its localization to the outer membrane [Figure 5D; Table S6]).

To define interaction partners of the selected proteins, we performed SILAC labeling of wild-type yeast and yeast strains containing protein A-tagged proteins with a tobacco etch virus (TEV) cleavage site. After lysis with digitonin, interacting proteins were identified by q-AP-MS. In addition, interaction partners were analyzed by affinity purification and immunoblotting using specific antibodies. (1) Ybr230w-a, which was imported into the mitochondrial matrix in a $\Delta\psi$-dependent manner (Figure 4C), specifically co-purified the coenzyme Q biosynthesis enzymes Coq4, Coq5, Coq6, Coq9, Coq11, and Cat5/Coq7 (Figure 7B), and was thus named Coq21. (2) The mitochondrial class 1 protein of 10 kDa (Mco10) is an interaction partner of the F_1F_o-ATP synthase, revealed by the specific enrichment of ten ATP synthase subunits (Figure S7B). (3) Ybl059w interacted with the altered inheritance rate of mitochondria protein Aim11, the genetic interactor of prohibitins Gep7, and the high-confidence class 1 protein Mtc3 (Figure S7C, left panel). The reverse pulldown via Aim11 similarly co-purified Ybl059w, Gep7, and Mtc3 (Figure S7C, right panel). Both pulldowns led to the co-purification of three subunits of respiratory complex IV (Cox2, Cox6, Cox20), the mitochondrial peculiar membrane protein Mpm1, and numerous subunits of the F_1F_o-ATP synthase. Due to the specific interaction with Aim11, Ybl059w was named Iai11 (interactor of Aim11). The topology of Aim11 and Iai11 in the inner membrane was determined in Figure 5F. We conclude that Aim11 and Iai11 are core components of an inner membrane complex that interacts with a set of complex IV components and the F_1F_o-ATP synthase. (4) Tmh11 (TMEM14 homolog of 11 kDa) contains conserved GxxxG transmembrane segment interaction motifs in two of its predicted membrane anchors (Figure S7D, alignment). ^{35}S-labeled Tmh11 was imported into isolated mitochondria in a $\Delta\psi$-dependent manner and assembled into a high-molecular-weight complex in the megadalton range (Figure S7D, left panel). Tmh11 predominantly interacted with other GxxxG motif-containing mitochondrial inner membrane proteins such as the MICOS subunit Mic10, the F_1F_o-ATP synthase dimerization subunit e (Tim11), and Fmp10 (with unknown function) (Figure S7D, middle panel). The matrix-facing subunits Sdh1 and Cor1 of respiratory complexes II and III also interacted with Tmh11. Remarkably, Tmh11 only co-purified Mic10, but not other MICOS subunits (Figure S7D, right panel), suggesting that Tmh11 interacts with an inner membrane pool of Mic10 that is distinct from the MICOS complex. (5) During the preparation of this manuscript, Ybr255c-a was identified as Rcf3, a homolog of the respiratory supercomplex factor Rcf2 (Römpler et al., 2016). Our co-purification analysis agrees with the interaction of Rcf3 with Rcf1, Rcf2, and respiratory complexes III and IV (Römpler et al., 2016). In addition, we observed that Rcf3 co-purified all six subunits Mic10, Mic12, Mic19, Mic26, Mic27, and Mic60 of the MICOS complex (Figure 7C, SILAC and immunoblotting) (van der Laan et al., 2016). Rcf3 may thus function as mediator between respiratory chain III–IV supercomplexes and MICOS. (6) Yil077c assembled into large blue native gel complexes that are characteristic for III–IV supercomplexes (Figures 7A and 7D, right panel), in agreement with the co-purification of Yil077c with Rcf3 (Figure 7C) (Römpler et al., 2016). Tagged Yil077c, named Rci37 (respiratory chain interacting protein of 37 kDa), co-purified subunits of complexes III and IV and additionally the subunits Afg3 and Yta12 of the inner membrane m-AAA protease (Rugarli and Langer, 2012), followed by the prohibitin complex (Figure 7D). (7) Ykl133c co-purified subunits of respiratory complexes III and IV and was named Rci50 (respiratory chain interacting protein of 50 kDa). Rci50 shows sequence similarity to the i-AAA adaptor Mgr3 (Dunn et al., 2008). SILAC and immunoblotting analysis indeed revealed that Rci50 co-purified the i-AAA protease Yme1 (Figure 7E) (Rugarli and Langer, 2012). Thus, Rci37 and Rci50 are interaction partners of the two inner membrane AAA proteases: Rci37 of the matrix-exposed m-AAA protease and Rci50 of the intermembrane space-exposed i-AAA protease.

DISCUSSION

We developed an extensive protein resource of mitochondria and mitochondria-associated fractions in baker's yeast (Table S1). Approaches were established to classify > 3,300 proteins into a high-confidence mitochondrial proteome (Figure 1D; Table S3) and three distinct mitochondria-associated fractions. The resource includes the absolute copy numbers of yeast proteins under different growth conditions, substantially expanding previous studies on the absolute quantification of the mitochondrial proteome (Figures 3 and S3; Tables S1 and S2) (Chong et al., 2015; Ghaemmaghami et al., 2003; Kulak et al., 2014). We characterized the subcellular and submitochondrial localization of proteins, defined an assay for determining the membrane topology of mitochondrial proteins, and identified many mitochondrial

Figure 6. Mitochondrial Proteins with Dual Localization

(A) Yeast strains expressing proteins with a protein A tag previously reported to localize to the cytosol, nucleus, or peroxisome were subjected to subcellular fractionation as described in Figure 4E.

(B) ^{35}S-labeled proteins were incubated with isolated wild-type mitochondria in the presence (+$\Delta\psi$) or absence (−$\Delta\psi$) of a membrane potential. Where indicated, mitochondria were subjected to hypoosmotic swelling and/or proteinase K (Prot. K) treatment.

(C) Schematic representation of the previously reported subcellular localization of selected proteins (upper panel). In this study, all proteins were additionally found in mitochondria by quantitative MS (Tables S4A and S4B) and single-protein analysis (lower panel). ‡/*, subcellular localization reported from high-throughput studies/manual curation (SGD).

See also Tables S1, S2, and S7.

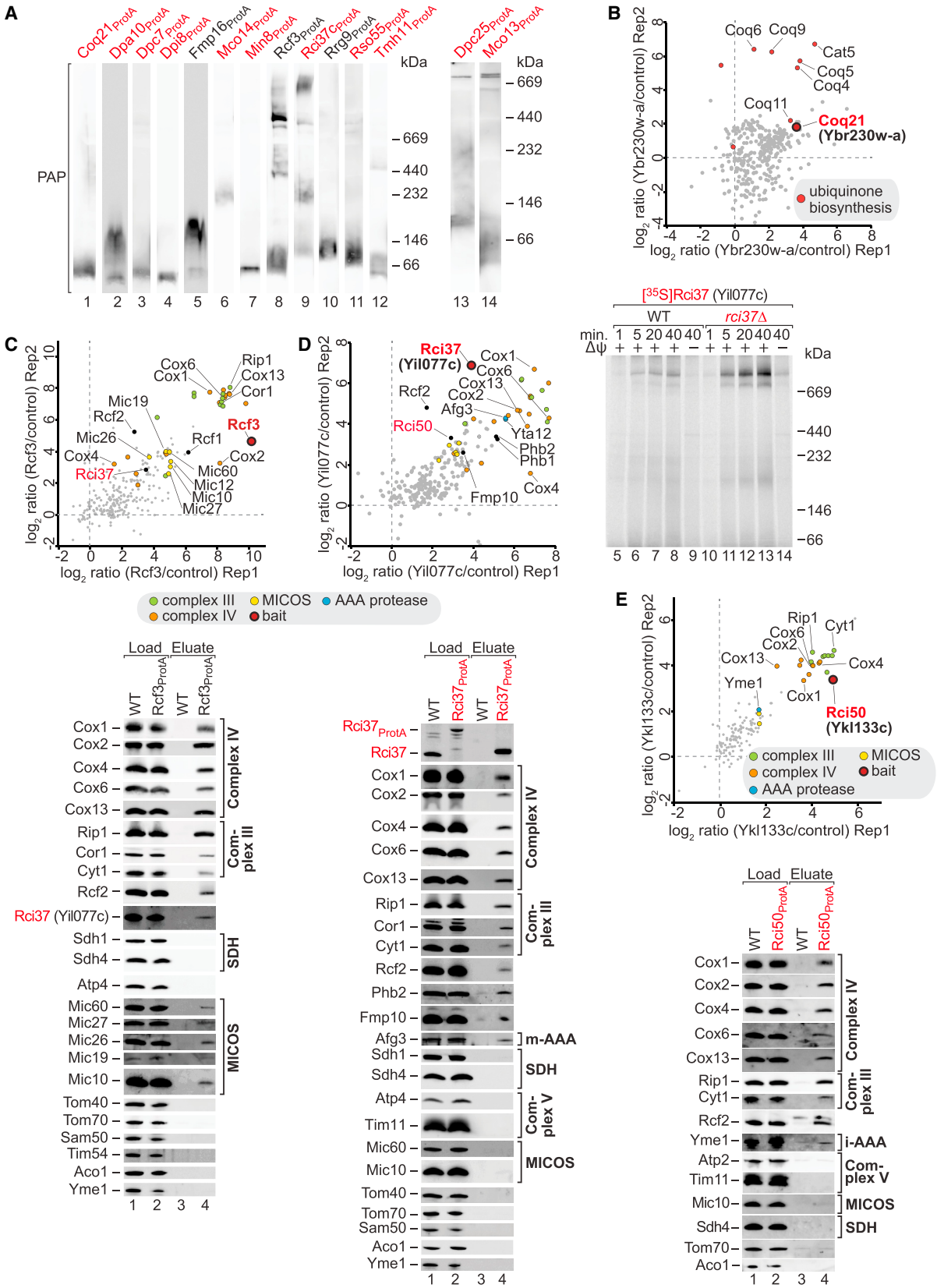

(legend on next page)

proteins with dual subcellular location (Figures 2, 4, 5, 6, S2, and S4–S6; Tables S2, S6, and S7).

Our high-confidence mitochondrial proteome of 901 proteins includes 82 proteins that were not assigned to mitochondria previously and 119 proteins with a previous ambiguous mitochondrial localization, providing a rich source for the identification and characterization of mitochondrial functions (Figure 1E; Tables S1, S3, and S4). As proof-of-principle for the validity of the proteome and its impact for the analysis of mitochondrial functions, we performed single-protein analysis of 58 identified/ambiguous proteins and demonstrated their bona fide mitochondrial localization, including subfractionation, microscopy, and import of precursor proteins into mitochondria (Table S6). Interaction analysis of selected proteins under native conditions revealed the high potential of the proteome for the definition of interactors of mitochondrial machineries (Figures 7 and S7; Table S2J). We identified an inner membrane complex, formed by Aim11-Gep7-Iai11-Mtc3, that provides a link between the F_1F_o-ATP synthase and a subset of cytochrome *c* oxidase (respiratory complex IV) subunits. Tmh11 interacts with oligomerization-promoting subunits of MICOS and the F_1F_o-ATP synthase (Arnold et al., 1998; Barbot et al., 2015; Bohnert et al., 2015; Rabl et al., 2009), pointing to an interaction of Tmh11 with a special pool of the MICOS core component Mic10. We found that Rcf3 associates not only with respiratory chain supercomplexes (Römpler et al., 2016) but also with the entire MICOS complex, indicating a role of Rcf3 in linking respiratory chain and the cristae organizing system. Mco10 was found as partner protein of the F_1F_o-ATP synthase, and Coq21 was identified as component of the coenzyme Q biosynthesis cluster. We demonstrate that Rso55, a homolog of human C12orf65 that has been linked to spastic paraplegia with optic atrophy and neuropathy SPG55 (Perocchi et al., 2006; Shimazaki et al., 2012), is a high-confidence mitochondrial protein. A further striking example of our proteome is the observation that Rci37 and Rci50 provide a connection between respiratory chain supercomplexes and the AAA proteases of the inner membrane (Rugarli and Langer, 2012; Tatsuta and Langer, 2009). Rci37 interacts with III–IV supercomplexes and the m-AAA protease, which degrades matrix-exposed proteins, whereas Rci50 provides a link between III–IV supercomplexes and the i-AAA protease, which degrades intermembrane space-exposed proteins. These findings suggest that Rci37 and Rci50 provide a system to link respiratory chain complexes to the AAA quality control system on both sides of the mitochondrial inner membrane.

Further intriguing examples of this resource are derived from the list of dual-localized proteins, including the metalloprotease Ste23, the mitochondrial aspartyl-tRNA synthetase Msd1, the cysteinyl-tRNA synthetase Ynl247w, the folic acid biosynthesis enzyme Fol1, and the dihydrofolate synthetase Fol3 (Table S7). The presence of the mitochondria-ER-cortex-anchor Mdm36 (Klecker et al., 2014; Lackner et al., 2013) among the dual-localized proteins as well as the striking distribution of ERMES components between class 1 and class 3 of the proteome (Figure 2F) reveal the potential of this resource for the characterization of proteins that are involved in the formation of contact sites between mitochondria and other cellular membranes.

Taken together, our comprehensive analysis of mitochondria and associated fractions provides a high-confidence resource for the definition of mitochondrial functions, interaction networks, and integration of mitochondria into the cellular context.

EXPERIMENTAL PROCEDURES

Further details and an outline of resources used in this work can be found in Supplemental Experimental Procedures.

Yeast Strains

All yeast strains used in this study are derived from *S. cerevisiae* BY4741, BY4742, or YPH499. For further details, see Supplemental Experimental Procedures.

Statistical Methods

Proteins quantified in the crude/pure mitochondrial dataset were classified based on mean $\log_2$ ratios using equivalence and t tests (p value < 0.01). Error bars in figures represent means ± SEM. For further details, see Supplemental Experimental Procedures.

ACCESSION NUMBERS

The accession numbers for the MS raw data and result files reported in this study are ProteomeXchange Consortium: PXD006128 (subcellular profiling), PXD006151 (pure/crude dataset), PXD006146 (absolute protein quantification under different growth conditions), PXD006128 (submitochondrial profiling), and PXD006147 (q-AP-MS data) (Vizcaíno et al., 2016).

SUPPLEMENTAL INFORMATION

Supplemental Information includes Supplemental Experimental Procedures, seven figures, and seven tables and can be found with this article online at http://dx.doi.org/10.1016/j.celrep.2017.06.014.

AUTHOR CONTRIBUTIONS

M.M., S.B.S., P.L., S.D., U.W., P.H., R.F., and C.S. performed the experiments and analyzed the data (together with C.D.P., F.D., M.G., M.B., M.v.d.L., M.S., S.O., N.P., N.W., and B.W.). B.W., N.W., N.P., and S.O. designed and supervised the project. M.M., S.B.S., P.L., C.D.P., S.D., U.W., P.H., R.F., C.S.,

Figure 7. Mitochondrial Protein Interaction Networks

(A) Mitochondria isolated from indicated yeast strains were analyzed by blue native gel electrophoresis using 3%–13% (lanes 1–13) or 6%–16.5% (lanes 14–16) discontinuous polyacrylamide gels.

(B) Coq21 interaction network identified by SILAC q-AP-MS (n = 2).

(C–E) Rcf3, Rci37, and Rci50 interaction networks identified by SILAC q-AP-MS (n = 2 each). In addition, IgG chromatography eluates were analyzed by SDS-PAGE and immunoblotting using the indicated antisera. Load = 5% (C and D) or 0.4% (E); eluate = 100%. (D, lanes 5–14) ^{35}S-labeled Yil077c was imported into mitochondria isolated from wild-type (WT) or *yil077c⊿* strains for the indicated periods at 25°C and subsequently treated with proteinase K. Where indicated ($-\Delta\psi$), the membrane potential was dissipated prior to import reactions. Samples were solubilized with 1% digitonin and analyzed by blue native gel electrophoresis and digital autoradiography.

See also Figure S7 and Tables S2J and S6.

S.O., and N.W. prepared the figures and tables. B.W., N.W., N.P., and S.O. wrote the manuscript (together with M.M., S.B.S., C.D.P., and C.S., and input of the other authors). All authors discussed results from the experiments and commented on the manuscript.

ACKNOWLEDGMENTS

We thank M. Opalińska, Ł. Opaliński, E. Fitzke, L. Martens, and A. Argentini for discussion and experimental advice, and B. Knapp for technical assistance in LC-MS analyses. Work included in this study has also been performed in partial fulfillment of the requirements for the doctoral theses of M.M., P.L., C.D.P., and S.D., the bachelor's thesis of P.H., and the diploma theses of R.F. and C.S. at the University of Freiburg. This work was supported by the European Research Council (ERC) Consolidator Grants 646604 and 648235, the Excellence Initiative of the German federal and state governments (EXC 294, BIOSS; GSC-4, Spemann Graduate School), Deutsche Forschungsgemeinschaft (PF 202/8-1 and WA 1598/5-1), and Sonderforschungsbereiche 746, 1140, and 1190.

Received: April 4, 2017
Revised: May 23, 2017
Accepted: June 1, 2017
Published: June 27, 2017

REFERENCES

Alder, N.N., Jensen, R.E., and Johnson, A.E. (2008). Fluorescence mapping of mitochondrial TIM23 complex reveals a water-facing, substrate-interacting helix surface. Cell *134*, 439–450.

Arnold, I., Pfeiffer, K., Neupert, W., Stuart, R.A., and Schägger, H. (1998). Yeast mitochondrial F1F0-ATP synthase exists as a dimer: identification of three dimer-specific subunits. EMBO J. *17*, 7170–7178.

Barbot, M., Jans, D.C., Schulz, C., Denkert, N., Kroppen, B., Hoppert, M., Jakobs, S., and Meinecke, M. (2015). Mic10 oligomerizes to bend mitochondrial inner membranes at cristae junctions. Cell Metab. *21*, 756–763.

Becker, T., Wenz, L.-S., Krüger, V., Lehmann, W., Müller, J.M., Goroncy, L., Zufall, N., Lithgow, T., Guiard, B., Chacinska, A., et al. (2011). The mitochondrial import protein Mim1 promotes biogenesis of multispanning outer membrane proteins. J. Cell Biol. *194*, 387–395.

Bohnert, M., Zerbes, R.M., Davies, K.M., Mühleip, A.W., Rampelt, H., Horvath, S.E., Boenke, T., Kram, A., Perschil, I., Veenhuis, M., et al. (2015). Central role of Mic10 in the mitochondrial contact site and cristae organizing system. Cell Metab. *21*, 747–755.

Cherry, J.M., Hong, E.L., Amundsen, C., Balakrishnan, R., Binkley, G., Chan, E.T., Christie, K.R., Costanzo, M.C., Dwight, S.S., Engel, S.R., et al. (2012). *Saccharomyces* Genome Database: the genomics resource of budding yeast. Nucleic Acids Res. *40*, D700–D705.

Chong, Y.T., Koh, J.L.Y., Friesen, H., Duffy, S.K., Cox, M.J., Moses, A., Moffat, J., Boone, C., and Andrews, B.J. (2015). Yeast proteome dynamics from single cell imaging and automated analysis. Cell *161*, 1413–1424.

Duncan, J.A., and Gilman, A.G. (2002). Characterization of *Saccharomyces cerevisiae* acyl-protein thioesterase 1, the enzyme responsible for G protein alpha subunit deacylation in vivo. J. Biol. Chem. *277*, 31740–31752.

Dunn, C.D., Tamura, Y., Sesaki, H., and Jensen, R.E. (2008). Mgr3p and Mgr1p are adaptors for the mitochondrial i-AAA protease complex. Mol. Biol. Cell *19*, 5387–5397.

Eisenberg-Bord, M., Shai, N., Schuldiner, M., and Bohnert, M. (2016). A tether is a tether is a tether: tethering at membrane contact sites. Dev. Cell *39*, 395–409.

Ellenrieder, L., Opaliński, Ł., Becker, L., Krüger, V., Mirus, O., Straub, S.P., Ebell, K., Flinner, N., Stiller, S.B., Guiard, B., et al. (2016). Separating mitochondrial protein assembly and endoplasmic reticulum tethering by selective coupling of Mdm10. Nat. Commun. *7*, 13021.

Ghaemmaghami, S., Huh, W.-K., Bower, K., Howson, R.W., Belle, A., Dephoure, N., O'Shea, E.K., and Weissman, J.S. (2003). Global analysis of protein expression in yeast. Nature *425*, 737–741.

Huh, W.-K., Falvo, J.V., Gerke, L.C., Carroll, A.S., Howson, R.W., Weissman, J.S., and O'Shea, E.K. (2003). Global analysis of protein localization in budding yeast. Nature *425*, 686–691.

Hung, V., Zou, P., Rhee, H.W., Udeshi, N.D., Cracan, V., Svinkina, T., Carr, S.A., Mootha, V.K., and Ting, A.Y. (2014). Proteomic mapping of the human mitochondrial intermembrane space in live cells via ratiometric APEX tagging. Mol. Cell *55*, 332–341.

Itzhak, D.N., Tyanova, S., Cox, J., and Borner, G.H. (2016). Global, quantitative and dynamic mapping of protein subcellular localization. eLife *5*, e16950.

Jones, J.M., Nau, K., Geraghty, M.T., Erdmann, R., and Gould, S.J. (1999). Identification of peroxisomal acyl-CoA thioesterases in yeast and humans. J. Biol. Chem. *274*, 9216–9223.

Klecker, T., Böckler, S., and Westermann, B. (2014). Making connections: interorganelle contacts orchestrate mitochondrial behavior. Trends Cell Biol. *24*, 537–545.

Kornmann, B., Currie, E., Collins, S.R., Schuldiner, M., Nunnari, J., Weissman, J.S., and Walter, P. (2009). An ER-mitochondria tethering complex revealed by a synthetic biology screen. Science *325*, 477–481.

Kulak, N.A., Pichler, G., Paron, I., Nagaraj, N., and Mann, M. (2014). Minimal, encapsulated proteomic-sample processing applied to copy-number estimation in eukaryotic cells. Nat. Methods *11*, 319–324.

Kumar, A., Agarwal, S., Heyman, J.A., Matson, S., Heidtman, M., Piccirillo, S., Umansky, L., Drawid, A., Jansen, R., Liu, Y., et al. (2002). Subcellular localization of the yeast proteome. Genes Dev. *16*, 707–719.

Labbé, K., Murley, A., and Nunnari, J. (2014). Determinants and functions of mitochondrial behavior. Annu. Rev. Cell Dev. Biol. *30*, 357–391.

Lackner, L.L., Ping, H., Graef, M., Murley, A., and Nunnari, J. (2013). Endoplasmic reticulum-associated mitochondria-cortex tether functions in the distribution and inheritance of mitochondria. Proc. Natl. Acad. Sci. USA *110*, E458–E467.

Lauffer, S., Mäbert, K., Czupalla, C., Pursche, T., Hoflack, B., Rödel, G., and Krause-Buchholz, U. (2012). *Saccharomyces cerevisiae* porin pore forms complexes with mitochondrial outer membrane proteins Om14p and Om45p. J. Biol. Chem. *287*, 17447–17458.

Li, J.M., and Shore, G.C. (1992). Protein sorting between mitochondrial outer and inner membranes. Insertion of an outer membrane protein into the inner membrane. Biochim. Biophys. Acta *1106*, 233–241.

Lill, R. (2009). Function and biogenesis of iron-sulphur proteins. Nature *460*, 831–838.

Mootha, V.K., Bunkenborg, J., Olsen, J.V., Hjerrild, M., Wiśniewski, J.R., Stahl, E., Bolouri, M.S., Ray, H.N., Sihag, S., Kamal, M., et al. (2003). Integrated analysis of protein composition, tissue diversity, and gene regulation in mouse mitochondria. Cell *115*, 629–640.

Müller, C.S., Bildl, W., Haupt, A., Ellenrieder, L., Becker, T., Hunte, C., Fakler, B., and Schulte, U. (2016). Cryo-slicing blue native-mass spectrometry (csBN-MS), a novel technology for high resolution complexome profiling. Mol. Cell. Proteomics *15*, 669–681.

Murphy, J.P., Stepanova, E., Everley, R.A., Paulo, J.A., and Gygi, S.P. (2015). Comprehensive temporal protein dynamics during the diauxic shift in *Saccharomyces cerevisiae*. Mol. Cell. Proteomics *14*, 2454–2465.

Neupert, W., and Herrmann, J.M. (2007). Translocation of proteins into mitochondria. Annu. Rev. Biochem. *76*, 723–749.

Nötzel, C., Lingner, T., Klingenberg, H., and Thoms, S. (2016). Identification of new fungal peroxisomal matrix proteins and revision of the PTS1 consensus. Traffic *17*, 1110–1124.

Nunnari, J., and Suomalainen, A. (2012). Mitochondria: in sickness and in health. Cell *148*, 1145–1159.

Ohlmeier, S., Kastaniotis, A.J., Hiltunen, J.K., and Bergmann, U. (2004). The yeast mitochondrial proteome, a study of fermentative and respiratory growth. J. Biol. Chem. *279*, 3956–3979.

Pagliarini, D.J., Calvo, S.E., Chang, B., Sheth, S.A., Vafai, S.B., Ong, S.-E., Walford, G.A., Sugiana, C., Boneh, A., Chen, W.K., et al. (2008). A mitochondrial protein compendium elucidates complex I disease biology. Cell *134*, 112–123.

Palmieri, F., Agrimi, G., Blanco, E., Castegna, A., Di Noia, M.A., Iacobazzi, V., Lasorsa, F.M., Marobbio, C.M.T., Palmieri, L., Scarcia, P., et al. (2006). Identification of mitochondrial carriers in *Saccharomyces cerevisiae* by transport assay of reconstituted recombinant proteins. Biochim. Biophys. Acta *1757*, 1249–1262.

Paulo, J.A., O'Connell, J.D., Everley, R.A., O'Brien, J., Gygi, M.A., and Gygi, S.P. (2016). Quantitative mass spectrometry-based multiplexing compares the abundance of 5000 *S. cerevisiae* proteins across 10 carbon sources. J. Proteomics *148*, 85–93.

Perocchi, F., Jensen, L.J., Gagneur, J., Ahting, U., von Mering, C., Bork, P., Prokisch, H., and Steinmetz, L.M. (2006). Assessing systems properties of yeast mitochondria through an interaction map of the organelle. PLoS Genet. *2*, e170.

Pflieger, D., Le Caer, J.-P., Lemaire, C., Bernard, B.A., Dujardin, G., and Rossier, J. (2002). Systematic identification of mitochondrial proteins by LC-MS/MS. Anal. Chem. *74*, 2400–2406.

Prokisch, H., Scharfe, C., Camp, D.G., 2nd, Xiao, W., David, L., Andreoli, C., Monroe, M.E., Moore, R.J., Gritsenko, M.A., Kozany, C., et al. (2004). Integrative analysis of the mitochondrial proteome in yeast. PLoS Biol. *2*, e160.

Rabl, R., Soubannier, V., Scholz, R., Vogel, F., Mendl, N., Vasiljev-Neumeyer, A., Körner, C., Jagasia, R., Keil, T., Baumeister, W., et al. (2009). Formation of cristae and crista junctions in mitochondria depends on antagonism between Fcj1 and Su e/g. J. Cell Biol. *185*, 1047–1063.

Rao, R.S.P., Salvato, F., Thal, B., Eubel, H., Thelen, J.J., and Møller, I.M. (2017). The proteome of higher plant mitochondria. Mitochondrion *33*, 22–37.

Reinders, J., Zahedi, R.P., Pfanner, N., Meisinger, C., and Sickmann, A. (2006). Toward the complete yeast mitochondrial proteome: multidimensional separation techniques for mitochondrial proteomics. J. Proteome Res. *5*, 1543–1554.

Renvoisé, M., Bonhomme, L., Davanture, M., Valot, B., Zivy, M., and Lemaire, C. (2014). Quantitative variations of the mitochondrial proteome and phosphoproteome during fermentative and respiratory growth in *Saccharomyces cerevisiae*. J. Proteomics *106*, 140–150.

Rhee, H.-W., Zou, P., Udeshi, N.D., Martell, J.D., Mootha, V.K., Carr, S.A., and Ting, A.Y. (2013). Proteomic mapping of mitochondria in living cells via spatially restricted enzymatic tagging. Science *339*, 1328–1331.

Römpler, K., Müller, T., Juris, L., Wissel, M., Vukotic, M., Hofmann, K., and Deckers, M. (2016). Overlapping role of respiratory supercomplex factor Rcf2 and its N-terminal homolog Rcf3 in *Saccharomyces cerevisiae*. J. Biol. Chem. *291*, 23769–23778.

Rugarli, E.I., and Langer, T. (2012). Mitochondrial quality control: a matter of life and death for neurons. EMBO J. *31*, 1336–1349.

Shimazaki, H., Takiyama, Y., Ishiura, H., Sakai, C., Matsushima, Y., Hatakeyama, H., Honda, J., Sakoe, K., Naoi, T., Namekawa, M., et al.; Japan Spastic Paraplegia Research Consortium (JASPAC) (2012). A homozygous mutation of C12orf65 causes spastic paraplegia with optic atrophy and neuropathy (SPG55). J. Med. Genet. *49*, 777–784.

Sickmann, A., Reinders, J., Wagner, Y., Joppich, C., Zahedi, R., Meyer, H.E., Schönfisch, B., Perschil, I., Chacinska, A., Guiard, B., et al. (2003). The proteome of *Saccharomyces cerevisiae* mitochondria. Proc. Natl. Acad. Sci. USA *100*, 13207–13212.

Stadler, C., Rexhepaj, E., Singan, V.R., Murphy, R.F., Pepperkok, R., Uhlén, M., Simpson, J.C., and Lundberg, E. (2013). Immunofluorescence and fluorescent-protein tagging show high correlation for protein localization in mammalian cells. Nat. Methods *10*, 315–323.

Stefely, J.A., Kwiecien, N.W., Freiberger, E.C., Richards, A.L., Jochem, A., Rush, M.J.P., Ulbrich, A., Robinson, K.P., Hutchins, P.D., Veling, M.T., et al. (2016). Mitochondrial protein functions elucidated by multi-omic mass spectrometry profiling. Nat. Biotechnol. *34*, 1191–1197.

Tatsuta, T., and Langer, T. (2009). AAA proteases in mitochondria: diverse functions of membrane-bound proteolytic machines. Res. Microbiol. *160*, 711–717.

Taylor, S.W., Fahy, E., Zhang, B., Glenn, G.M., Warnock, D.E., Wiley, S., Murphy, A.N., Gaucher, S.P., Capaldi, R.A., Gibson, B.W., and Ghosh, S.S. (2003). Characterization of the human heart mitochondrial proteome. Nat. Biotechnol. *21*, 281–286.

van der Laan, M., Horvath, S.E., and Pfanner, N. (2016). Mitochondrial contact site and cristae organizing system. Curr. Opin. Cell Biol. *41*, 33–42.

Vizcaíno, J.A., Csordas, A., del-Toro, N., Dianes, J.A., Griss, J., Lavidas, I., Mayer, G., Perez-Riverol, Y., Reisinger, F., Ternent, T., et al. (2016). 2016 update of the PRIDE database and its related tools. Nucleic Acids Res. *44* (*D1*), D447–D456.

Vögtle, F.N., Burkhart, J.M., Rao, S., Gerbeth, C., Hinrichs, J., Martinou, J.-C., Chacinska, A., Sickmann, A., Zahedi, R.P., and Meisinger, C. (2012). Intermembrane space proteome of yeast mitochondria. Mol. Cell. Proteomics *11*, 1840–1852.

Wiedemann, N., and Pfanner, N. (2017). Mitochondrial machineries for protein import and assembly. Annu. Rev. Biochem. Published online March 15, 2017. http://dx.doi.org/10.1146/annurev-biochem-060815-014352.

Wiśniewski, J.R., Hein, M.Y., Cox, J., and Mann, M. (2014). A "proteomic ruler" for protein copy number and concentration estimation without spike-in standards. Mol. Cell. Proteomics *13*, 3497–3506.

Yofe, I., Weill, U., Meurer, M., Chuartzman, S., Zalckvar, E., Goldman, O., Ben-Dor, S., Schütze, C., Wiedemann, N., Knop, M., et al. (2016). One library to make them all: streamlining the creation of yeast libraries via a SWAp-Tag strategy. Nat. Methods *13*, 371–378.

Yogev, O., and Pines, O. (2011). Dual targeting of mitochondrial proteins: mechanism, regulation and function. Biochim. Biophys. Acta *1808*, 1012–1020.

Zahedi, R.P., Sickmann, A., Boehm, A.M., Winkler, C., Zufall, N., Schönfisch, B., Guiard, B., Pfanner, N., and Meisinger, C. (2006). Proteomic analysis of the yeast mitochondrial outer membrane reveals accumulation of a subclass of preproteins. Mol. Biol. Cell *17*, 1436–1450.

Cell Reports, Volume *19*

Supplemental Information

Definition of a High-Confidence

Mitochondrial Proteome at Quantitative Scale

Marcel Morgenstern, Sebastian B. Stiller, Philipp Lübbert, Christian D. Peikert, Stefan Dannenmaier, Friedel Drepper, Uri Weill, Philipp Höß, Reinhild Feuerstein, Michael Gebert, Maria Bohnert, Martin van der Laan, Maya Schuldiner, Conny Schütze, Silke Oeljeklaus, Nikolaus Pfanner, Nils Wiedemann, and Bettina Warscheid

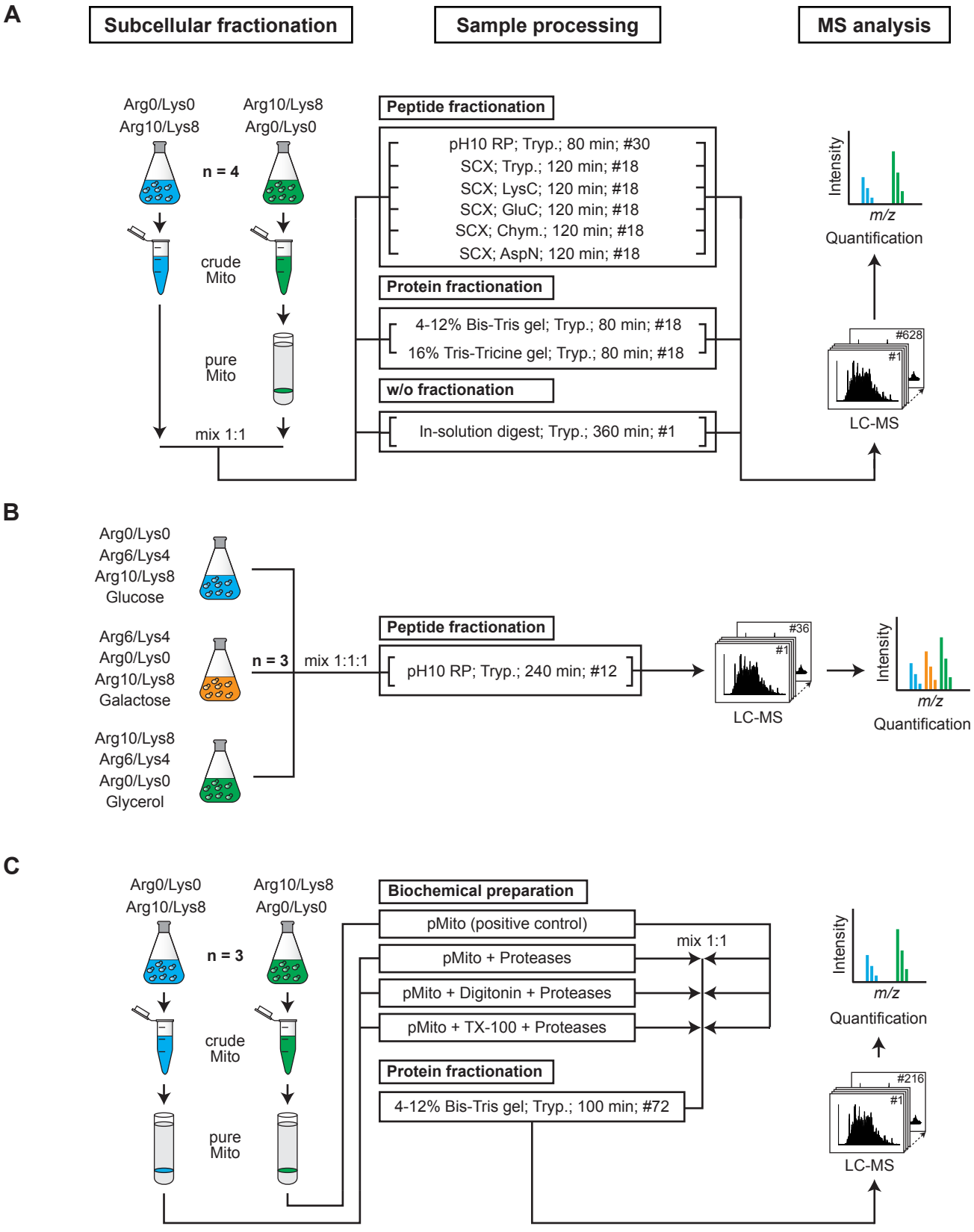
A
Subcellular fractionation
Sample processing
MS analysis
Arg0/Lys0
Arg10/Lys8
Arg10/Lys8
Arg0/Lys0
n = 4
crude Mito
pure Mito
mix 1:1
Peptide fractionation
pH10 RP; Tryp.; 80 min; #30
SCX; Tryp.; 120 min; #18
SCX; LysC; 120 min; #18
SCX; GluC; 120 min; #18
SCX; Chym.; 120 min; #18
SCX; AspN; 120 min; #18
Protein fractionation
4-12% Bis-Tris gel; Tryp.; 80 min; #18
16% Tris-Tricine gel; Tryp.; 80 min; #18
w/o fractionation
In-solution digest; Tryp.; 360 min; #1
Intensity
m/z
Quantification
#628
#1
LC-MS
B
Arg0/Lys0
Arg6/Lys4
Arg10/Lys8
Glucose
Arg6/Lys4
Arg0/Lys0
Arg10/Lys8
Galactose
Arg10/Lys8
Arg6/Lys4
Arg0/Lys0
Glycerol
n = 3
mix 1:1:1
Peptide fractionation
pH10 RP; Tryp.; 240 min; #12
#36
#1
LC-MS
Intensity
m/z
Quantification
C
Arg0/Lys0
Arg10/Lys8
Arg10/Lys8
Arg0/Lys0
n = 3
crude Mito
pure Mito
Biochemical preparation
pMito (positive control)
pMito + Proteases
pMito + Digitonin + Proteases
pMito + TX-100 + Proteases
mix 1:1
Protein fractionation
4-12% Bis-Tris gel; Tryp.; 100 min; #72
Intensity
m/z
Quantification
#216
#1
LC-MS

Figure S1

Figure S1. Illustration of experimental strategies employed for the determination of the mitochondrial proteome and the detailed characterization of individual mitochondrial proteins by quantitative MS

Related to Figure 1

(A) Crude and gradient-purified mitochondrial fractions, prepared from differentially light (Arg0/Lys0) and heavy (Arg10/Lys8) SILAC-labeled yeast cells, were mixed in equal ratio and subsequently analyzed by LC-MS either directly without (w/o) fractionation or following various peptide and protein fractionation techniques such as high pH reversed-phase chromatography (pH 10 RP), strong cation exchange chromatography (SCX), and SDS-PAGE using Bis-Tris gradient and Tricine gels. For enzymatic protein digestion, trypsin (Tryp.), LysC, GluC, chymotrypsin (Chym.), and AspN were used as indicated. The experiment, referred to as 'pure/crude experiment', was performed in four independent biological replicates (including a label-switch). SILAC-based protein quantification and subsequent data analyses facilitated the definition of a mitochondrial core proteome.

(B) For a proteome-wide absolute quantification of yeast proteins grown on different carbon sources, a triple SILAC approach was applied. Cells were cultivated in the presence of glucose, galactose, or glycerol and either labeled with light (Arg0/Lys0), medium-heavy (Arg6/Lys4), or heavy (Arg10/Lys8) amino acids. Whole cell lysates were mixed in equal ratios, proteins were digested with trypsin (Tryp.) and peptides were fractionated by pH 10 RP followed by quantitative LC-MS analysis. The experiment, referred to as 'absolute quantification experiment', was performed in three independent biological replicates including a label-switch. Absolute protein quantification was based on the MS intensities determined by MaxQuant for light, medium-heavy, and heavy SILAC-labeled proteins following the proteomic ruler strategy (Wiśniewski et al., 2014).

(C) To globally profile submitochondrial protein localizations, protease accessibility assays were performed. Gradient-purified mitochondria isolated from differentially SILAC-labeled cells were either treated with proteases (i.e., trypsin and proteinase K) only (S1), digitonin and proteases (S2), or Triton X-100 (TX-100) and proteases (S3). Samples S1 - S3 were mixed with equal amounts of untreated mitochondria (M) serving as reference. Proteins were separated by SDS-PAGE, in-gel digested with trypsin, and analyzed by quantitative MS. The experiment, referred to as 'submitochondrial profiling experiment', was performed in three independent biological replicates including a label-switch.

(A - C) Further information given for each experimental strategy: duration of each LC-MS run and the number (#) of fractions obtained for the indicated sample processing method or LC-MS runs per replicate.

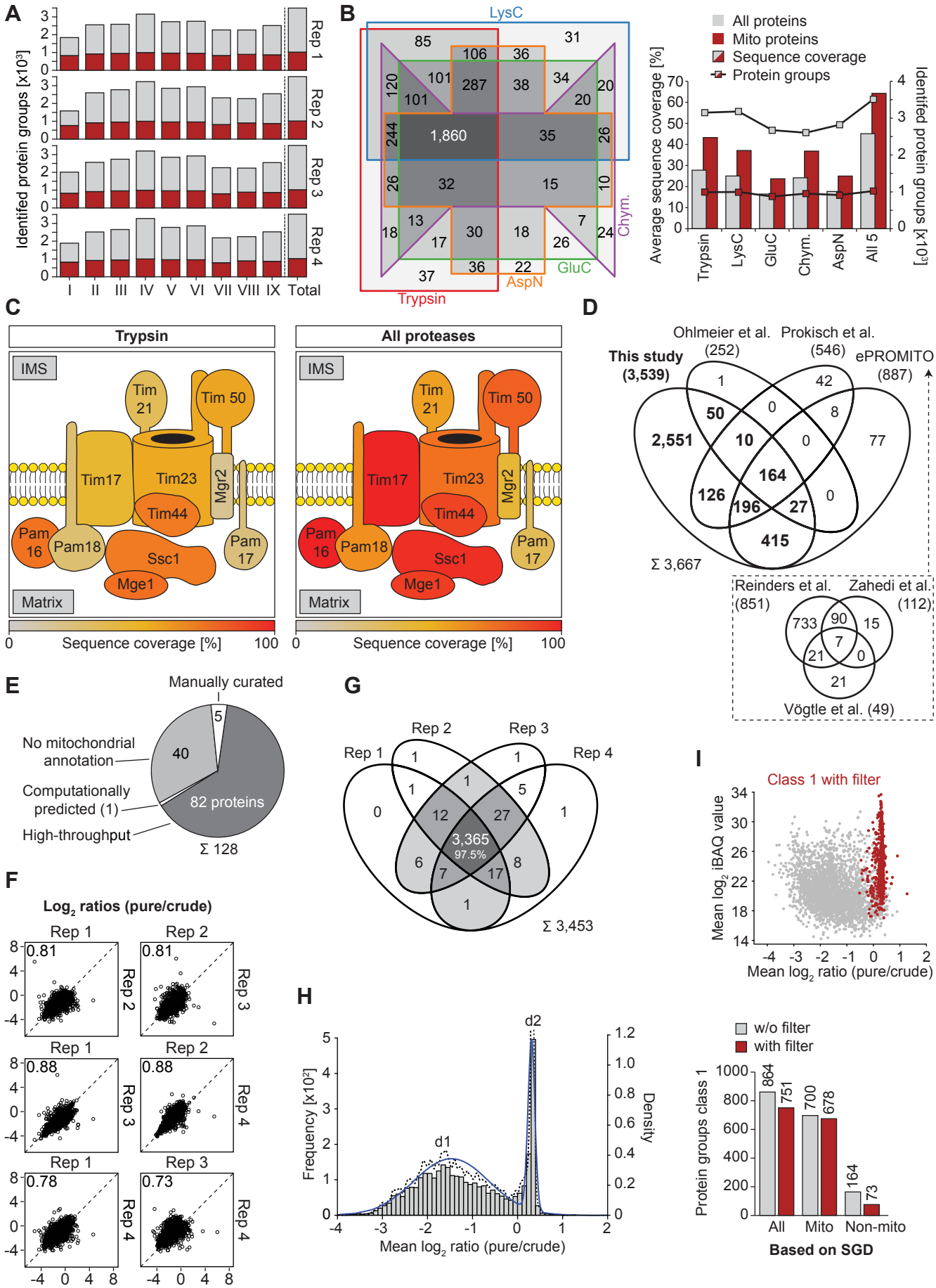
A
Identifed protein groups [x10³]
Rep 1
Rep 2
Rep 3
Rep 4
I II III IV V VI VII VIII IX Total
B
LysC
Trypsin
GluC
AspN
Chym.
85
31
106
36
101
287
38
34
20
120
101
20
244
1,860
35
26
26
32
15
10
13
18
17
30
18
7
26
24
37
36
22
All proteins
Mito proteins
Sequence coverage
Protein groups
Average sequence coverage [%]
Identifed protein groups [x10³]
Trypsin
LysC
GluC
Chym.
AspN
All 5
C
Trypsin
All proteases
IMS
Matrix
Tim 21
Tim 50
Tim17
Tim23
Mgr2
Tim44
Pam 16
Pam18
Pam 17
Ssc1
Mge1
0
Sequence coverage [%]
100
D
This study (3,539)
Ohlmeier et al. (252)
Prokisch et al. (546)
ePROMITO (887)
Reinders et al. (851)
Zahedi et al. (112)
Vögtle et al. (49)
Σ 3,667
E
Manually curated
No mitochondrial annotation
Computationally predicted (1)
High-throughput
40
5
82 proteins
Σ 128
F
Log₂ ratios (pure/crude)
Rep 1
Rep 2
Rep 3
Rep 4
0.81
0.88
0.78
0.73
G
3,365
97.5%
Σ 3,453
H
Frequency [x10²]
Density
d1
d2
Mean log₂ ratio (pure/crude)
I
Class 1 with filter
Mean log₂ iBAQ value
Mean log₂ ratio (pure/crude)
w/o filter
with filter
Protein groups class 1
864
751
700
678
164
73
All
Mito
Non-mito
Based on SGD

Figure S2

Figure S2. Evaluation of the sample processing regime, protein identification and quantification of pure/crude experiments

Related to Figure 2

(A) Number of protein groups identified in individual replicates following different sample fractionation protocols (I - IX; see also Fig. S1A, Tables S2B and S2C) and in total. Proteins were analyzed by LC-MS either without fractionation (I) or following gel electrophoresis using TrisTricine (II) and BisTris (III) gels, high pH reversed-phase chromatography of tryptic peptides (IV), or strong cation exchange chromatography (SCX) of peptides derived from tryptic (V), LysC (VI), GluC (VII), chymotryptic (VIII), and AspN (IX) digests. Red, mitochondrial proteins according to GO cellular component annotations; light grey, other proteins; Rep, replicate.

(B) Overlap of protein groups identified in tryptic, LysC, GluC, chymotryptic, and AspN digests (left) and impact of the protease(s) chosen for proteolytic digestion on sequence coverage and the number of protein groups identified (right). All samples were analyzed by SCX (V - IX in [A]).

(C) Cartoons illustrating the sequence coverage of individual components of the TIM23 complex identified in pure/crude experiments by SCX following proteolytic digestion with trypsin only (V in A; left) or a multi-protease digestion approach using trypsin, LysC, GluC, chymotrypsin, and AspN (V - IX in A; right). IMS, intermembrane space.

(D) Overlap of proteins identified in pure/crude experiments in this study and in previous studies targeting the mitochondrial proteome of *S. cerevisiae*. Numbers in parentheses indicate the number of proteins identified in this study, by (Ohlmeier et al., 2004) and (Prokisch et al., 2004), and the number of proteins present in the ePROMITO list comprising mitochondrial proteins reported by (Reinders et al., 2006) (global mitochondrial proteome), (Zahedi et al., 2006) (mitochondrial outer membrane proteome), and (Vögtle et al., 2012) (mitochondrial intermembrane space proteome). See also Table S2B.

(E) Overview of proteins reported to be mitochondrial in the studies shown in (D) that were not identified in this study in pure/crude experiments. Proteins were classified according to the category of annotation as mitochondrial protein in the SGD, i.e. manually curated, high-throughput (lacking firm evidence for a mitochondrial localization), computational prediction, or none. In case the annotation was based on more than one category, the protein was assigned to the category with the highest reliability (manually curated > high-throughput > computationally predicted).

(F) Multiscatter plot showing the reproducibility of protein quantification between four independent replicates. Protein abundance ratios (pure/crude) calculated for individual replicates were $\log_2$-transformed and plotted against each other. Values in the upper left corner indicate the Pearson correlation coefficient between replicates. Rep, replicate.

(G) Overlap of proteins quantified in four individual replicates.

(H) Histogram and density curve visualizing the distribution of protein abundance changes between pure and crude mitochondria. Shown are the mean of log_2-transformed pure/crude ratios (n = 4) of proteins quantified in all replicates with at least two fractionation methods. The data show a bimodal distribution, as indicated by the density curves (solid blue and black dotted lines), with distribution center d1 at a mean log_2 ratio of -1.47 and d2 at 0.31. For each protein it was tested, to which distribution it belongs using an equivalence test (p value < 0.01). All proteins with inconclusive classification, i.e. proteins that belonged to neither of the distributions according to the equivalence test, were further analyzed employing a two-sample two-sided t test (p value < 0.01). Statistical analysis resulted in the definition of four distinct classes as shown in Fig. 2D. For more details about the statistical analysis, refer to Supplemental Experimental Procedures.

(I) Additional data filter criteria on class 1 proteins. To exclude low abundant non-mitochondrial contaminants that co-migrated with mitochondria in sucrose density gradients from our mitochondrial core proteome, we disregarded all proteins with a standard deviation of > 0.75 of log_2 pure/crude ratios across all replicates and a sequence coverage of ≤ 20%. The ratio-intensity plot (top) shows the distribution of class 1 proteins after filtering (see also Fig. 2D). Information about subcellular localizations were derived from GO cellular component annotations (Table S2B). Non-mito, class 1 proteins without previous association with mitochondria or mitochondrial subcompartments.

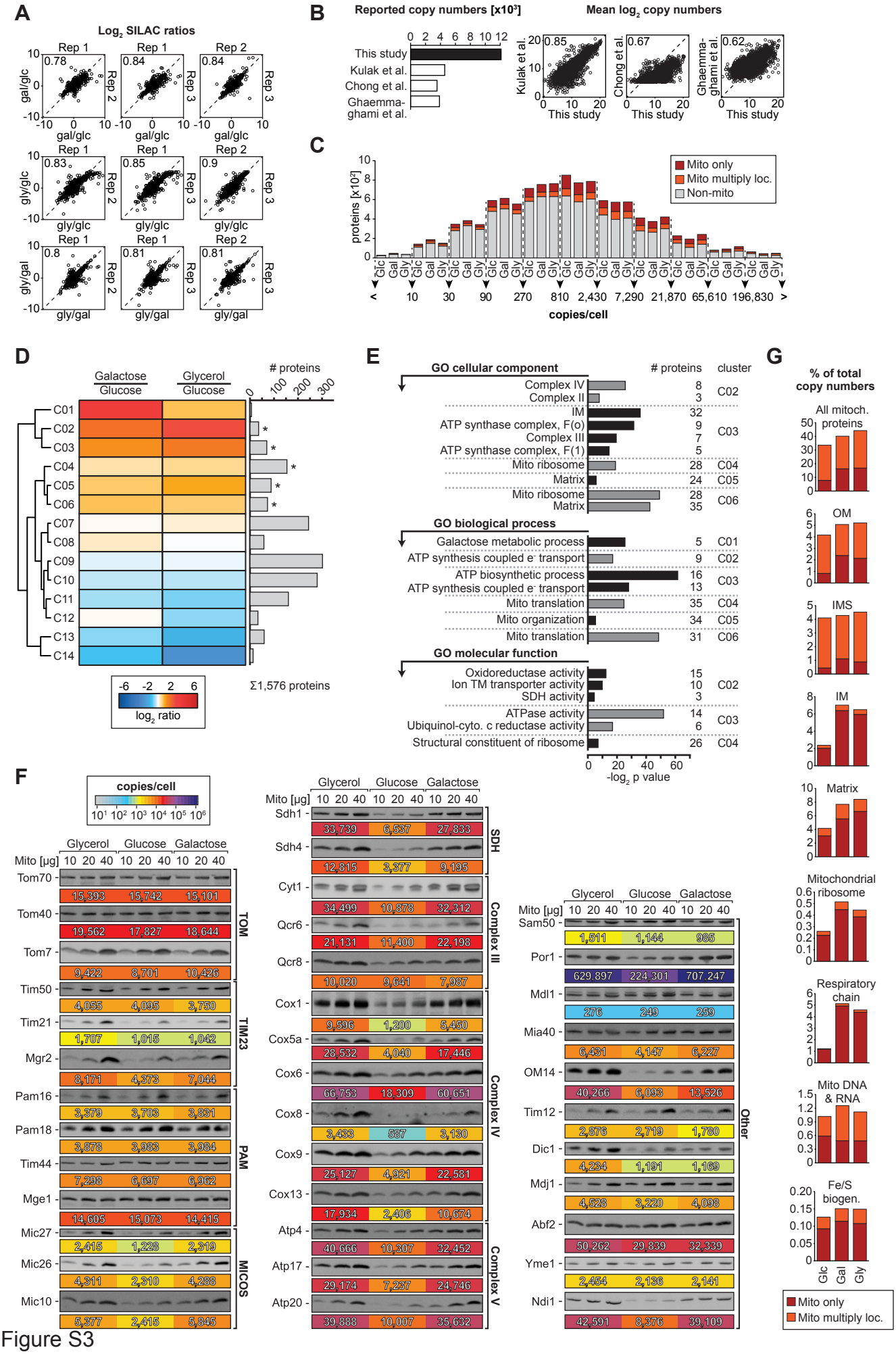
A
Log2 SILAC ratios
Rep 1
Rep 2
Rep 3
gal/glc
gly/glc
gly/gal
0.78
0.84
0.84
0.83
0.85
0.9
0.8
0.81
0.81
B
Reported copy numbers [x10³]
This study
Kulak et al.
Chong et al.
Ghaemma-ghami et al.
Mean log2 copy numbers
0.85
0.67
0.62
C
proteins [x10²]
Mito only
Mito multiply loc.
Non-mito
Glc
Gal
Gly
copies/cell
D
Galactose / Glucose
Glycerol / Glucose
proteins
C01
C02
C03
C04
C05
C06
C07
C08
C09
C10
C11
C12
C13
C14
log2 ratio
Σ1,576 proteins
E
GO cellular component
GO biological process
GO molecular function
proteins
cluster
Complex IV
Complex II
IM
ATP synthase complex, F(o)
Complex III
ATP synthase complex, F(1)
Mito ribosome
Matrix
Galactose metabolic process
ATP synthesis coupled e⁻ transport
ATP biosynthetic process
Mito translation
Mito organization
Oxidoreductase activity
Ion TM transporter activity
SDH activity
ATPase activity
Ubiquinol-cyto. c reductase activity
Structural constituent of ribosome
-log2 p value
F
copies/cell
Glycerol
Glucose
Galactose
Mito [µg]
Tom70
Tom40
Tom7
Tim50
Tim21
Mgr2
Pam16
Pam18
Tim44
Mge1
Mic27
Mic26
Mic10
TOM
TIM23
PAM
MICOS
Sdh1
Sdh4
Cyt1
Qcr6
Qcr8
Cox1
Cox5a
Cox6
Cox8
Cox9
Cox13
Atp4
Atp17
Atp20
SDH
Complex III
Complex IV
Complex V
Sam50
Por1
Mdl1
Mia40
OM14
Tim12
Dic1
Mdj1
Abf2
Yme1
Ndi1
Other
G
% of total copy numbers
All mitoch. proteins
OM
IMS
IM
Matrix
Mitochondrial ribosome
Respiratory chain
Mito DNA & RNA
Fe/S biogen.
Glc
Gal
Gly
Mito only
Mito multiply loc.

Figure S3

Figure S3. Assessment of proteome-wide absolute quantification experiments

Related to Figure 3

(A) Multiscatter plot showing the reproducibility of protein abundance ratios determined in three biological replicates of proteome-wide absolute quantification experiments. Abundance ratios were determined based on triple SILAC experiments (with label-switch) for proteins extracted from cells grown on galactose versus glucose (gal/glc, top row), glycerol versus glucose (gly/glc, middle row), and glycerol versus galactose (gly/gal, bottom row) (see Table S2E). Log_2-transformed ratios of individual replicates were plotted against each other. Values in the upper left corner of each plot indicate the Pearson correlation coefficient between replicates. MS intensities for light, medium-heavy, and heavy labeled proteins of this experiment were used to calculated absolute protein copy numbers for all three carbon sources according to the proteomic ruler strategy (Wiśniewski et al., 2014). Rep, replicate.

(B) Comparison between protein copy numbers determined in this study and copy numbers reported in previous global proteome studies of *S. cerevisiae*. Copy numbers determined in our study for proteins from cells grown on glucose were compared with data previously published by (Ghaemmaghami et al., 2003), (Chong et al., 2015), and (Kulak et al., 2014) (see Table S2D). The calculation of protein copy numbers in these studies was based on Western blot analyses, single cell imaging, and the 'Total Protein Approach' (Wiśniewski et al., 2012), respectively. Values in the upper left corner of the scatter plots indicate the Pearson correlation coefficient between the data of the studies.

(C) Distribution of estimated copy numbers per cell determined for mitochondrial and non-mitochondrial (Non-mito) proteins extracted from yeast grown on glucose (Glu), galactose (Gal) and glycerol (Gly). Classification of proteins as non-mitochondrial, exclusively mitochondrial (Mito only) or mitochondrial and other subcellular localizations (multiply loc.) was based on GO cellular component annotations (see Table S1).

(D) K-means clustering of proteins with altered expression in yeast grown on galactose or glycerol in relation to glucose. Bar chart indicates the number of proteins per cluster. *, clusters in which mainly mitochondria-related terms are enriched as determined in (E).

(E) GO term enrichment analysis. For clusters C07-C14, no GO term was significantly enriched. Cyto., cytochrome; SDH, succinate dehydrogenase; TM, transmembrane.

(F) Biochemical confirmation of carbon source-dependent effects on mitochondrial protein expression levels revealed by MS-based copy number estimation. Mitochondria were isolated from YPH499 Δ*arg4* cells that were grown in the presence of the different carbon sources glycerol, glucose or galactose in SILAC medium. 10, 20, and 40 µg of mitochondria (protein amount) were lysed, subjected to SDS-PAGE and analyzed by immunoblotting. For direct comparison, immunoblot results are shown together with the corresponding copy numbers. Mito, mitochondria.

(G) Percentage of total protein copy numbers per cell determined for all mitochondrial proteins and mitochondrial proteins of distinct submitochondrial categories quantified in cells grown on different carbon sources as indicated.

Mito, mitochondrial; OM/IM, mitochondrial outer/inner membrane; IMS, intermembrane space; Mito DNA and RNA, associated with mitochondrial DNA and RNA biology; Fe/S biog., iron-sulfur cluster biogenesis.

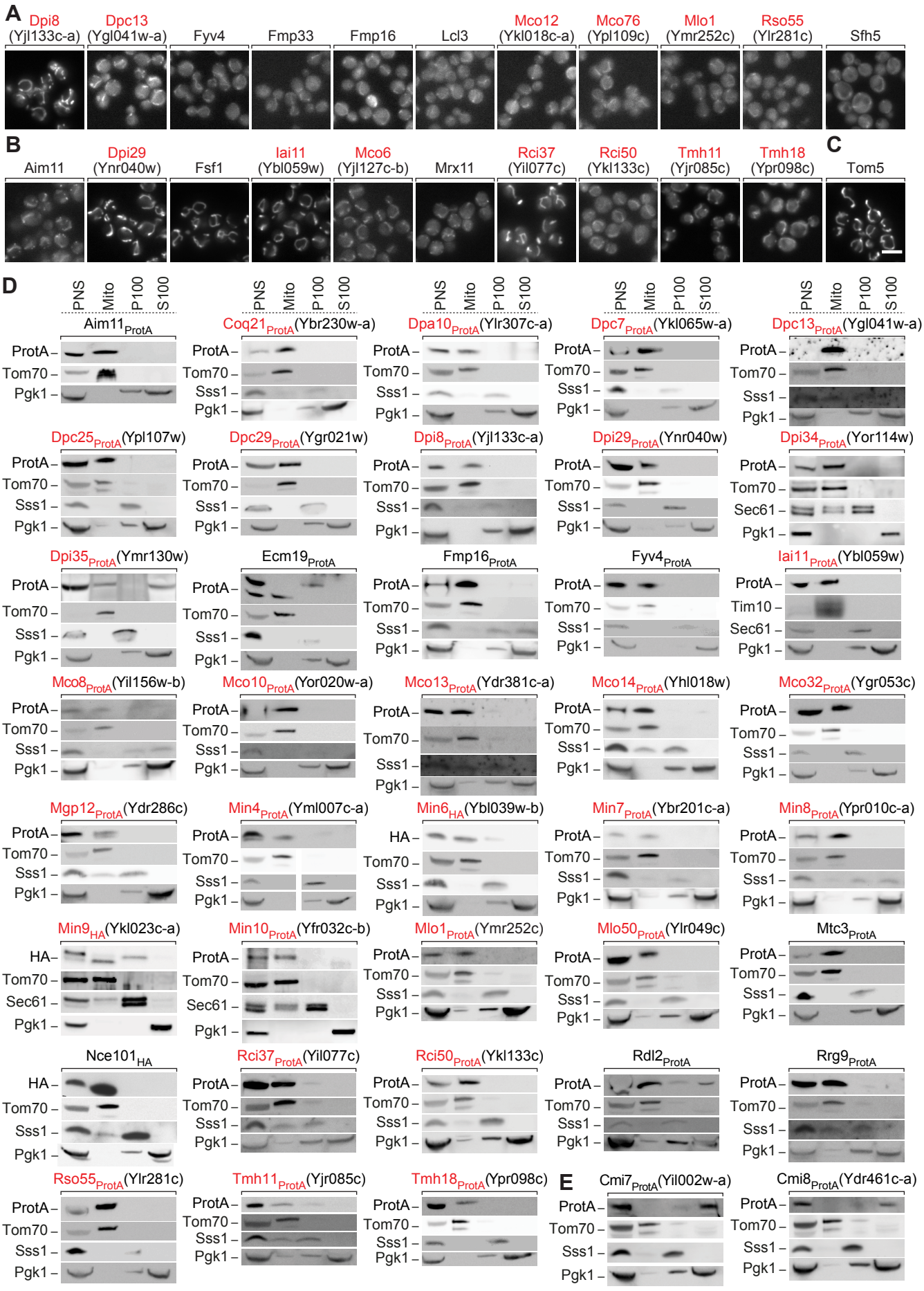
A
Dpi8 (Yjl133c-a)
Dpc13 (Ygl041w-a)
Fyv4
Fmp33
Fmp16
Lcl3
Mco12 (Ykl018c-a)
Mco76 (Ypl109c)
Mlo1 (Ymr252c)
Rso55 (Ylr281c)
Sfh5
B
Aim11
Dpi29 (Ynr040w)
Fsf1
Iai11 (Ybl059w)
Mco6 (Yjl127c-b)
Mrx11
Rci37 (Yil077c)
Rci50 (Ykl133c)
Tmh11 (Yjr085c)
Tmh18 (Ypr098c)
C
Tom5
D
PNS
Mito
P100
S100
Aim11ProtA
Coq21ProtA(Ybr230w-a)
Dpa10ProtA(Ylr307c-a)
Dpc7ProtA(Ykl065w-a)
Dpc13ProtA(Ygl041w-a)
Dpc25ProtA(Ypl107w)
Dpc29ProtA(Ygr021w)
Dpi8ProtA(Yjl133c-a)
Dpi29ProtA(Ynr040w)
Dpi34ProtA(Yor114w)
Dpi35ProtA(Ymr130w)
Ecm19ProtA
Fmp16ProtA
Fyv4ProtA
Iai11ProtA(Ybl059w)
Mco8ProtA(Yil156w-b)
Mco10ProtA(Yor020w-a)
Mco13ProtA(Ydr381c-a)
Mco14ProtA(Yhl018w)
Mco32ProtA(Ygr053c)
Mgp12ProtA(Ydr286c)
Min4ProtA(Yml007c-a)
Min6HA(Ybl039w-b)
Min7ProtA(Ybr201c-a)
Min8ProtA(Ypr010c-a)
Min9HA(Ykl023c-a)
Min10ProtA(Yfr032c-b)
Mlo1ProtA(Ymr252c)
Mlo50ProtA(Ylr049c)
Mtc3ProtA
Nce101HA
Rci37ProtA(Yil077c)
Rci50ProtA(Ykl133c)
Rdl2ProtA
Rrg9ProtA
Rso55ProtA(Ylr281c)
Tmh11ProtA(Yjr085c)
Tmh18ProtA(Ypr098c)
E
Cmi7ProtA(Yil002w-a)
Cmi8ProtA(Ydr461c-a)
ProtA
HA
Tom70
Sss1
Sec61
Tim10
Pgk1

Figure S4

Figure S4. Fluorescence microspopy and biochemical subcellular localization analysis of mitochondrial proteins

Related to Figure 4

(A-C) Fluorescent images of yeast cells expressing N' GFP-tagged proteins. Scale bar, 5 µm.

(D) Subcellular fractionation of yeast cells as described in Figure 4E. This supplementary figure shows the fractionations from Figure 4E with the appropriate controls plus further experiments.

(E) Fractionation of two uncharacterized proteins that do not localize to mitochondria. Cmi7 has a negative mean $\log_2$ ratio (pure/crude) and Cmi8 was not quantified.

PNS, post-nuclear supernatant; Mito, mitochondrial fraction; P100, microsomal fraction; S100, cytosolic fraction; MloX, Mitochondrially localized protein; CmiX, Cytosolic mini protein of ~X kDa.

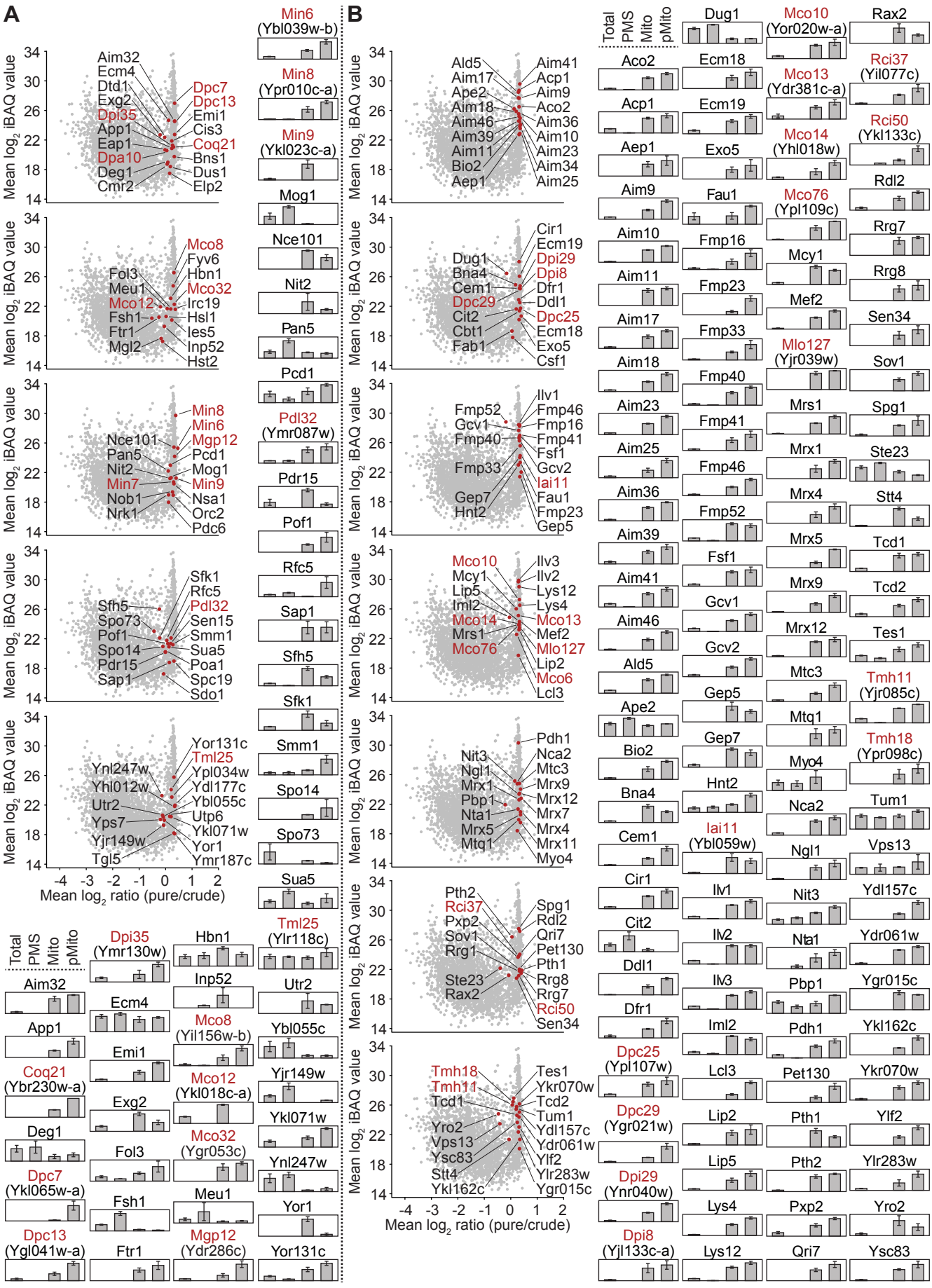
A
B
Mean log2 iBAQ value
Mean log2 ratio (pure/crude)
Total
PMS
Mito
pMito
Aim32
Ecm4
Dtd1
Exg2
Dpi35
App1
Eap1
Dpa10
Deg1
Cmr2
Dpc7
Dpc13
Emi1
Cis3
Coq21
Bns1
Dus1
Elp2
Fol3
Meu1
Mco12
Fsh1
Ftr1
Mgl2
Mco8
Fyv6
Hbn1
Mco32
Irc19
Hsl1
Ies5
Inp52
Hst2
Nce101
Pan5
Nit2
Min7
Nob1
Nrk1
Min8
Min6
Mgp12
Pcd1
Mog1
Min9
Nsa1
Orc2
Pdc6
Sfh5
Spo73
Pof1
Spo14
Pdr15
Sap1
Sfk1
Rfc5
Pdl32
Sen15
Smm1
Sua5
Poa1
Spc19
Sdo1
Ynl247w
Yhl012w
Utr2
Yps7
Yjr149w
Tgl5
Yor131c
Tml25
Ypl034w
Ydl177c
Ybl055c
Utp6
Ykl071w
Yor1
Ymr187c
Ald5
Aim17
Ape2
Aim18
Aim46
Aim39
Aim11
Bio2
Aep1
Aim41
Acp1
Aim9
Aco2
Aim36
Aim10
Aim23
Aim34
Aim25
Dug1
Bna4
Cem1
Dpc29
Cit2
Cbt1
Fab1
Cir1
Ecm19
Dpi29
Dpi8
Dfr1
Ddl1
Dpc25
Ecm18
Exo5
Csf1
Fmp52
Gcv1
Fmp40
Fmp33
Gep7
Hnt2
Ilv1
Fmp46
Fmp16
Fmp41
Fsf1
Gcv2
Iai11
Fau1
Fmp23
Gep5
Mco10
Mcy1
Lip5
Iml2
Mco14
Mrs1
Mco76
Ilv3
Ilv2
Lys12
Lys4
Mco13
Mef2
Mlo127
Lip2
Mco6
Lcl3
Nit3
Ngl1
Mrx1
Pbp1
Nta1
Mrx5
Mtq1
Pdh1
Nca2
Mtc3
Mrx9
Mrx12
Mrx7
Mrx4
Mrx11
Myo4
Pth2
Rci37
Pxp2
Sov1
Rrg1
Ste23
Rax2
Spg1
Rdl2
Qri7
Pet130
Pth1
Rrg8
Rrg7
Rci50
Sen34
Tmh18
Tmh11
Tcd1
Yro2
Vps13
Ysc83
Stt4
Ykl162c
Tes1
Ykr070w
Tcd2
Tum1
Ydl157c
Ydr061w
Ylf2
Ylr283w
Ygr015c
Min6 (Ybl039w-b)
Min8 (Ypr010c-a)
Min9 (Ykl023c-a)
Mog1
Nce101
Nit2
Pan5
Pcd1
Pdl32 (Ymr087w)
Pdr15
Pof1
Rfc5
Sap1
Sfh5
Sfk1
Smm1
Spo14
Spo73
Sua5
Tml25 (Ylr118c)
Utr2
Ybl055c
Yjr149w
Ykl071w
Ynl247w
Yor1
Yor131c
Dpi35 (Ymr130w)
Inp52
Ecm4
Mco8 (Yil156w-b)
Emi1
Mco12 (Ykl018c-a)
Exg2
Mco32 (Ygr053c)
Fol3
Meu1
Fsh1
Mgp12 (Ydr286c)
Ftr1
Aim32
App1
Coq21 (Ybr230w-a)
Deg1
Dpc7 (Ykl065w-a)
Dpc13 (Ygl041w-a)
Dug1
Aco2
Ecm18
Acp1
Ecm19
Aep1
Exo5
Aim9
Fau1
Aim10
Fmp16
Aim11
Fmp23
Aim17
Fmp33
Aim18
Fmp40
Aim23
Fmp41
Aim25
Fmp46
Aim36
Fmp52
Aim39
Fsf1
Aim41
Gcv1
Aim46
Gcv2
Ald5
Gep5
Ape2
Gep7
Bio2
Hnt2
Bna4
Nca2
Cem1
Iai11 (Ybl059w)
Cir1
Ilv1
Cit2
Ilv2
Ddl1
Ilv3
Dfr1
Iml2
Dpc25 (Ypl107w)
Lcl3
Dpc29 (Ygr021w)
Lip2
Lip5
Dpi29 (Ynr040w)
Lys4
Dpi8 (Yjl133c-a)
Lys12
Mco10 (Yor020w-a)
Mco13 (Ydr381c-a)
Mco14 (Yhl018w)
Mco76 (Ypl109c)
Mcy1
Mef2
Mlo127 (Yjr039w)
Mrs1
Mrx1
Mrx4
Mrx5
Mrx9
Mrx12
Mtc3
Mtq1
Myo4
Nca2
Ngl1
Nit3
Nta1
Pbp1
Pdh1
Pet130
Pth1
Pth2
Pxp2
Qri7
Rax2
Rci37 (Yil077c)
Rci50 (Ykl133c)
Rdl2
Rrg7
Rrg8
Sen34
Sov1
Spg1
Ste23
Tcd1
Tcd2
Tes1
Tmh11 (Yjr085c)
Tmh18 (Ypr098c)
Tum1
Vps13
Ydl157c
Ydr061w
Ygr015c
Ykl162c
Ykr070w
Ylf2
Ylr283w
Yro2
Ysc83

Figure S5

Figure S5. MS-based subcellular localization analysis of mitochondrial proteins

Related to Figure 4

(A, B) Ratio-intensity plots as shown in Figures 4A and 4B highlighting individual proteins from Tables S4A and S4B. Bar charts represent from left to right the mean of normalized MS intensities of the indicated proteins for total cell lysate, the post mitochondrial supernatant, the mitochondrial fraction and gradient-purified mitochondria of wild-type yeast analyzed by LC-MS as shown in Figure 4E. Error bars indicate SEM for $n \geq 3$ and the range for $n = 2$ (see Table S2A).

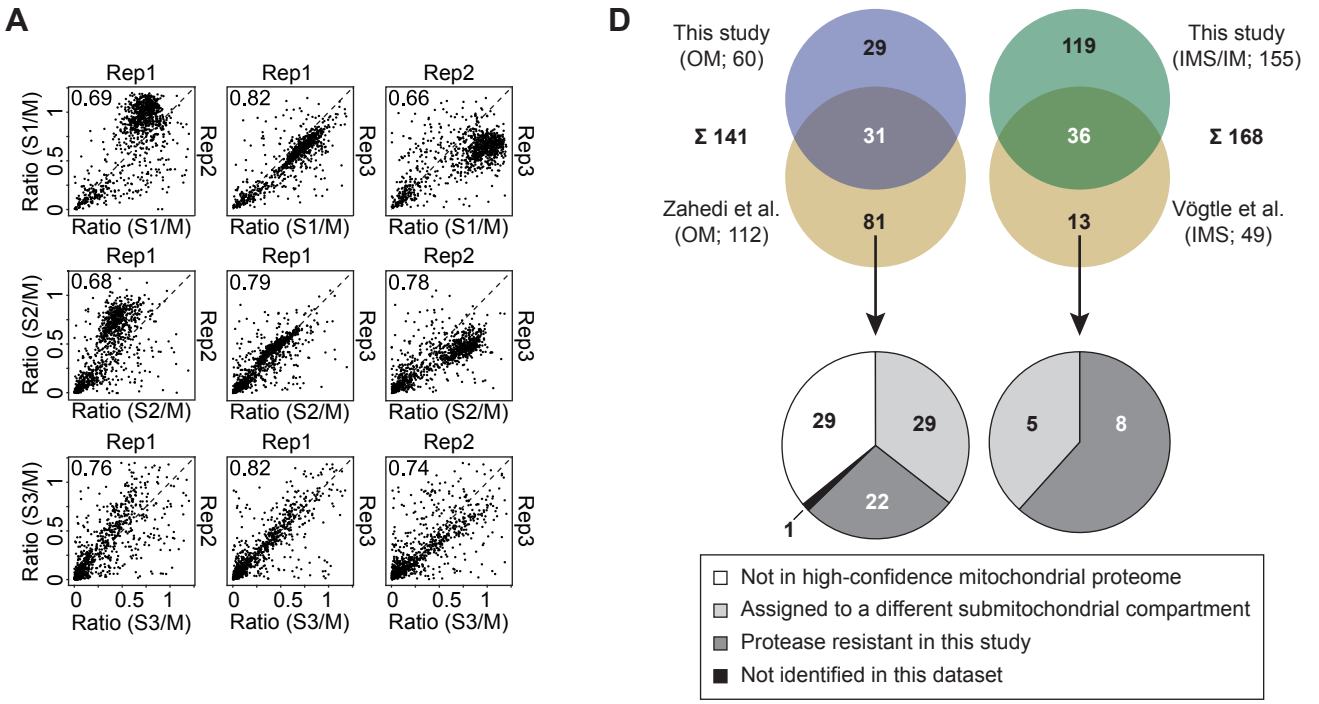
A
Rep1
Rep1
Rep2
0.69
0.82
0.66
Ratio (S1/M)
Rep2
Rep3
Ratio (S1/M)
Ratio (S1/M)
0.68
0.79
0.78
Ratio (S2/M)
Ratio (S2/M)
Ratio (S2/M)
0.76
0.82
0.74
Ratio (S3/M)
Ratio (S3/M)
Ratio (S3/M)
0
0.5
1
D
This study
(OM; 60)
29
119
This study
(IMS/IM; 155)
Σ 141
31
36
Σ 168
Zahedi et al.
(OM; 112)
81
13
Vögtle et al.
(IMS; 49)
29
29
22
1
5
8
Not in high-confidence mitochondrial proteome
Assigned to a different submitochondrial compartment
Protease resistant in this study
Not identified in this dataset

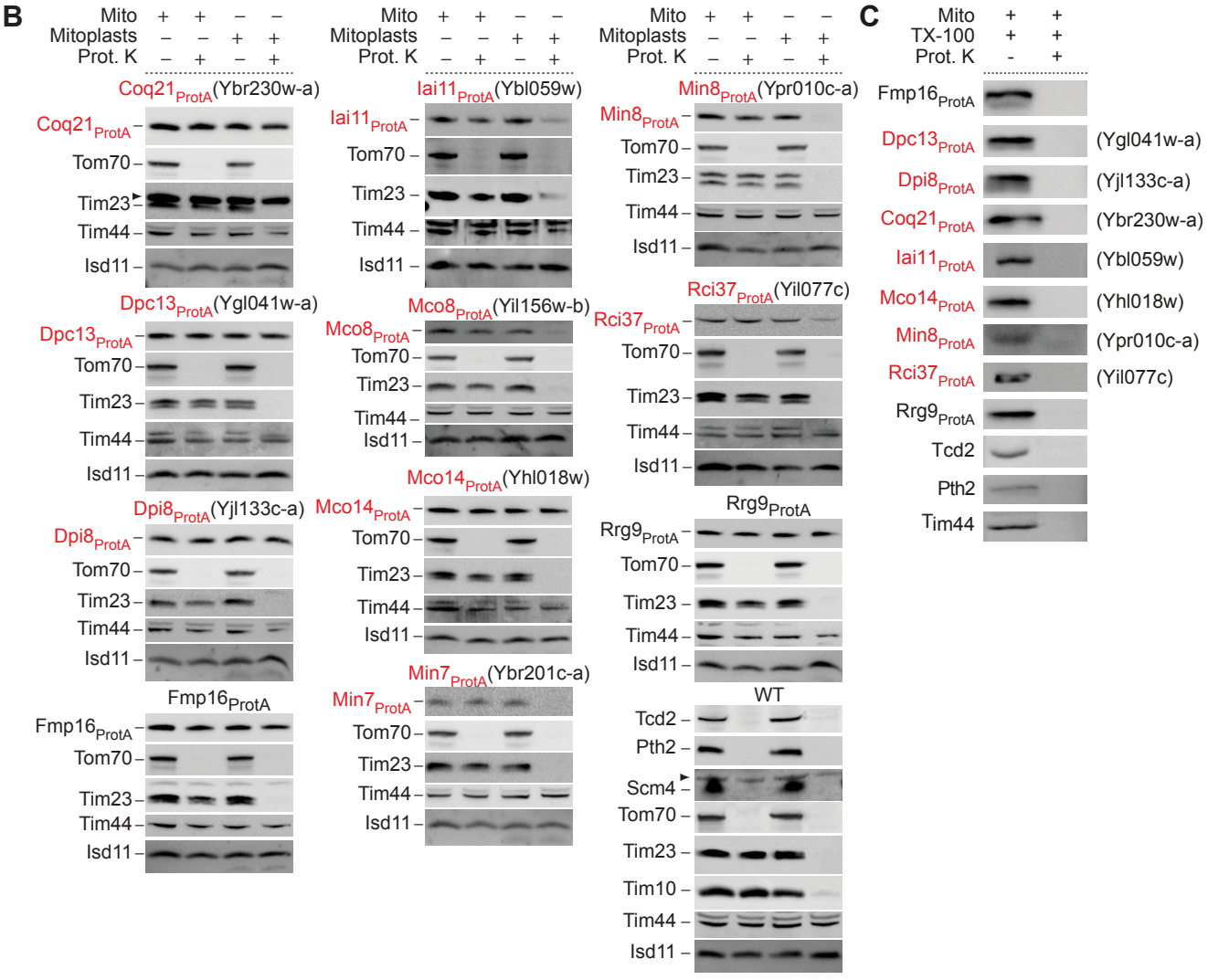
B
Mito
Mitoplasts
Prot. K
Coq21ProtA(Ybr230w-a)
Coq21ProtA
Tom70
Tim23
Tim44
Isd11
Dpc13ProtA(Ygl041w-a)
Dpc13ProtA
Dpi8ProtA(Yjl133c-a)
Dpi8ProtA
Fmp16ProtA
Iai11ProtA(Ybl059w)
Iai11ProtA
Mco8ProtA(Yil156w-b)
Mco8ProtA
Mco14ProtA(Yhl018w)
Mco14ProtA
Min7ProtA(Ybr201c-a)
Min7ProtA
Min8ProtA(Ypr010c-a)
Min8ProtA
Rci37ProtA(Yil077c)
Rci37ProtA
Rrg9ProtA
WT
Tcd2
Pth2
Scm4
Tim10
C
Mito
TX-100
Prot. K
Fmp16ProtA
Dpc13ProtA
(Ygl041w-a)
Dpi8ProtA
(Yjl133c-a)
Coq21ProtA
(Ybr230w-a)
Iai11ProtA
(Ybl059w)
Mco14ProtA
(Yhl018w)
Min8ProtA
(Ypr010c-a)
Rci37ProtA
(Yil077c)
Rrg9ProtA
Tcd2
Pth2
Tim44

Figure S6

Figure S6. Submitochondrial profiling experiments

Related to Figure 5

(A) Multiscatter plots showing the reproducibility of protein abundance ratios across three biological replicates of MS-based global submitochondrial profiling experiments. Gradient-purified mitochondria (M) isolated from light or heavy SILAC-labeled yeast were mixed in equal ratio with mitochondria (S1), mitoplasts (S2) or lysed mitochondria (S3) that had been treated with proteases and were obtained from differentially SILAC-labeled yeast. Samples of three independent replicates were analyzed by SDS-PAGE followed by quantitative MS analysis (see Fig. S1C). For each of 24 gel slices per replicate, protein abundance ratios (S/M) were determined (Table S2H). For each protein quantified, the ratio of the slice with the highest MS intensity for M is plotted (Table S2G). Values in the upper left corner indicate the Pearson correlation coefficient between replicates. Rep, replicate.

(B) Western blots from Figures 5E and 5F together with the respective controls. Tom70, outer membrane protein; Tim10, intermembrane space protein; Tim23, intermembrane space-exposed inner membrane protein; Tim44, matrix protein peripherally attached to the inner membrane; Isd11, soluble matrix protein.

(C) Triton X-100 controls for indicated proteins. WT (for analysis of Tcd2, Pth2, Tim44) or Protein A-tagged strains were treated with 1% Triton X-100 in SEM buffer and incubated for 7 minutes on ice. Where indicated, samples were subjected to proteinase K (Prot. K) treatment at a final concentration of 7 µg/mL for 15 minutes. Samples were subjected to SDS-PAGE and analyzed by immunoblotting. Tim44, matrix protein.

(D) Overlap of proteins identified in this study to be associated with the mitochondrial outer membrane (OM; left) or exposed to the intermembrane space (IMS; right) with previous proteomics studies targeting these submitochondrial proteomes. Numbers in parentheses indicate the number of proteins assigned to OM or IMS in our study or the work published by Zahedi et al. (2006) and Vögtle et al. (2012), respectively. Our study targets OM proteins exposed to the cytosol; Zahedi et al. (2006) detected OM proteins and a number of (precursor) proteins that are destined for internal mitochondrial compartments. Our study of IMS/IM includes soluble IMS proteins and membrane proteins (mostly of the inner membrane, IM) exposed to the IMS, whereas Vögtle et al. (2012) mainly analyzed soluble IMS proteins (and loosely membrane-attached proteins).

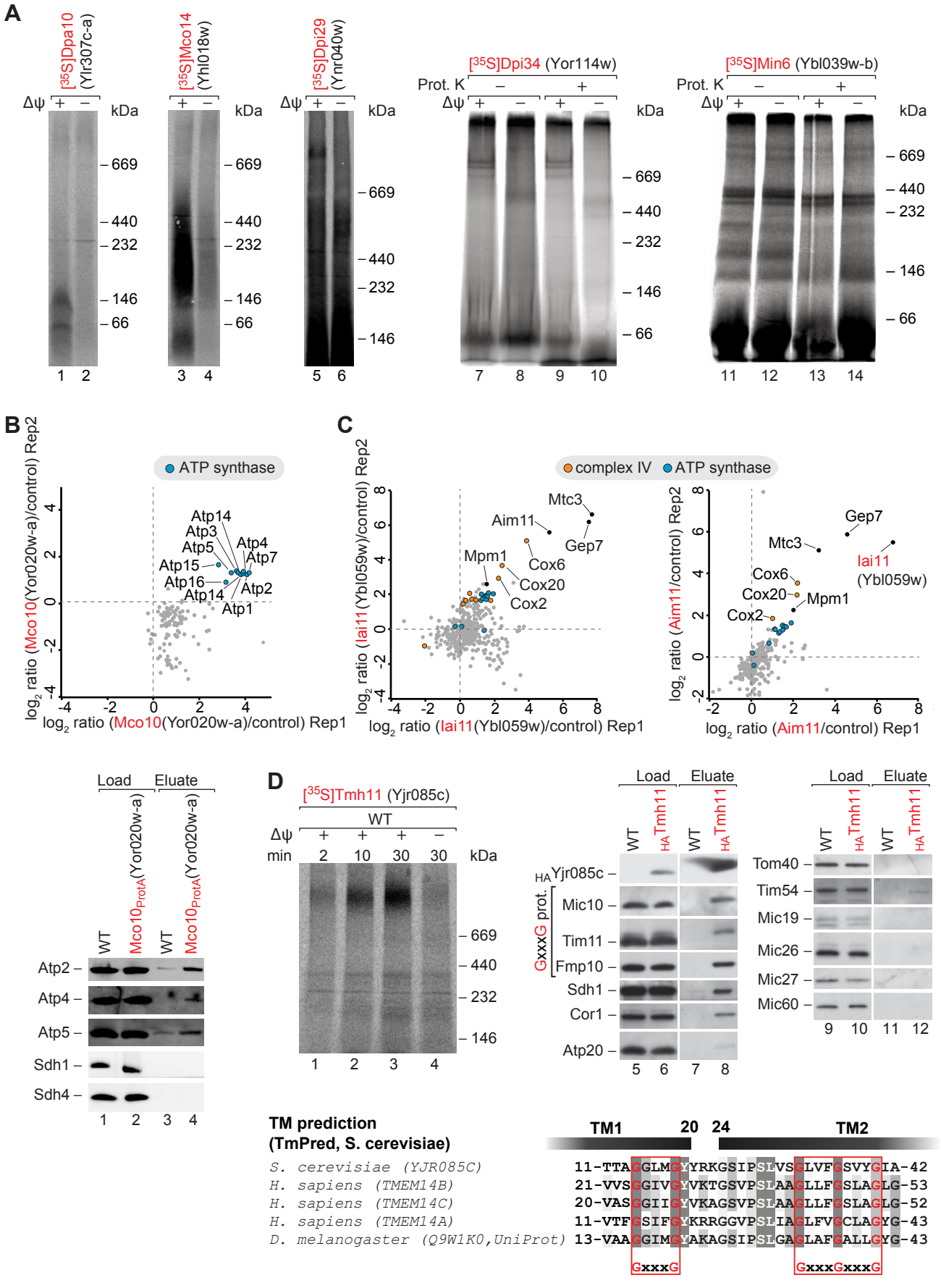
A
[35S]Dpa10 (Yir307c-a)
[35S]Mco14 (Yhl018w)
[35S]Dpi29 (Ynr040w)
[35S]Dpi34 (Yor114w)
[35S]Min6 (Ybl039w-b)
Prot. K
Δψ
kDa
669
440
232
146
66
1 2 3 4 5 6 7 8 9 10 11 12 13 14
B
ATP synthase
Atp14
Atp3
Atp5
Atp4
Atp7
Atp15
Atp16
Atp14
Atp2
Atp1
log2 ratio (Mco10(Yor020w-a)/control) Rep2
log2 ratio (Mco10(Yor020w-a)/control) Rep1
C
complex IV
ATP synthase
Mtc3
Aim11
Gep7
Mpm1
Cox6
Cox20
Cox2
log2 ratio (Iai11(Ybl059w)/control) Rep2
log2 ratio (Iai11(Ybl059w)/control) Rep1
Gep7
Mtc3
Iai11 (Ybl059w)
Cox6
Cox20
Mpm1
Cox2
log2 ratio (Aim11/control) Rep2
log2 ratio (Aim11/control) Rep1
Load
Eluate
WT
Mco10ProtA(Yor020w-a)
Atp2
Atp4
Atp5
Sdh1
Sdh4
1 2 3 4
D
[35S]Tmh11 (Yjr085c)
WT
Δψ
min
2 10 30 30
kDa
669
440
232
146
1 2 3 4
HATmh11
HAYjr085c
GxxxG prot.
Mic10
Tim11
Fmp10
Sdh1
Cor1
Atp20
5 6 7 8
Tom40
Tim54
Mic19
Mic26
Mic27
Mic60
9 10 11 12
TM prediction
(TmPred, S. cerevisiae)
TM1
20
24
TM2
S. cerevisiae (YJR085C) 11-TTAGGLMGYYRKGSIPSLVSGLVFGSVYGIA-42
H. sapiens (TMEM14B) 21-VVSGGIVGYVKTGSVPSLAAGLLFGSLAGLG-53
H. sapiens (TMEM14C) 20-VASGGIIGYVKAGSVPSLAAGLLFGSLAGLG-52
H. sapiens (TMEM14A) 11-VTFGSIFGYKRRGGVPSLIAGLFVGCLAGYG-43
D. melanogaster (Q9W1K0,UniProt) 13-VAAGGIMGYAKAGSIPSLGAGLAFGALLGYG-43
GxxxG
GxxxGxxxG

Figure S7

Figure S7. Mitochondrial protein interaction networks

Related to Figure 7

(A) Assembly of [^{35}S]-labeled mitochondrial proteins into high molecular weight complexes. The radiolabeled precursors were mixed with isolated mitochondria and incubated for 45 min at 30°C in the presence (+Δψ) or absence (-Δψ) of the membrane potential. Where indicated, mitochondria were subjected to proteinase K (Prot. K) treatment after import.

(B) SILAC mitochondria isolated from wild-type (WT) and Yor020w-a$_{ProtA}$ yeast strains were solubilized with 1% digitonin and subjected to IgG affinity chromatography, followed by elution of proteins specifically bound to Yor020w-a$_{ProtA}$ using TEV protease. Top, Ratio-versus-ratio plot visualizing the Mco10 (Yor020w-a) interaction network. Data were obtained in q-AP-MS experiments using Protein A-tagged Mco10 (Yor020w-a) as bait (Table S2J). Bottom, Samples were analyzed by SDS-PAGE and immunoblotting using the indicated antisera. Load, 0.5%; Elution, 100%.

(C) Reciprocal interaction networks of Iai11 (left) and its interaction partner Aim11 (right) obtained in q-AP-MS experiments of Protein A-tagged baits (Table S2J).

(D) Left (lanes 1-4), radiolabeled Tmh11 precursor was imported into isolated wild-type (WT) mitochondria. [^{35}S]Tmh11 was incubated with the reaction buffers for 10 min at 25°C followed by centrifugation for 10 min at 14,000 rpm. Import was started by the addition of 60 µg of mitochondria to pre-incubated samples and import reaction was allowed to proceed for the indicated time points at 25°C. Where indicated (-Δψ), membrane potential was dissipated. Non-imported precursor was digested by the addition of proteinase K. Samples were analyzed by Blue-Native electrophoresis followed by autoradiography. Right (lanes 5-12), mitochondria from wild-type (WT) and $_{HA}$Tmh11 were solubilized with 1% digitonin and incubated with anti-HA affinity matrix. After washing, a denaturing elution was performed and samples were subjected to SDS-PAGE and immunoblotting using antisera directed against the indicated proteins Load, 2%; Elution, 100%. Bottom, Sequence alignment of Tmh11 and the transmembrane protein 14A family members of higher eukaryotes. The conserved GxxxG transmembrane domain interaction motives are highlighted.

Table S4. Mitochondrial proteins identified and validated in this study. Related to Figures 1 and 4. (A) List of identified mitochondrial proteins that were not assigned to mitochondria previously. (B) List of mitochondrial proteins with annotation inferred from high-throughput studies without further verification. Proteins in bold were subjected to additional experimental validation of their mitochondrial localization (outlined in Figures 4, 5, 6, 7, S4, S5, S6, S7 plus Table S7 and summarized in Table S6). Coq21, COQ interacting protein; Dpa10, Delta-Psi dependent mitochondrial assembly, protein of 10 kDa; DpcX, Delta-psi ($\Delta\psi$)-dependent import and cleavage, protein of ~X kDa; DpiX, Delta-psi ($\Delta\psi$)-dependent import, protein of ~X kDa; Iai11, Interactor of Aim11; Mgp12, Mitochondrial glutaredoxin-like protein of 12 kDa; McoX, Mitochondrial class one protein of X kDa; MinX, Mini mitochondrial protein of ~X kDa; MloX, Mitochondrially localized protein, Pdl32, Protein of dual localization, protein of 32 kDa; RciX, Respiratory chain interacting protein of ~X kDa; Rso55, Mitochondrial protein related to spastic paraplegia with optic atrophy and neuropathy SPG55; Tmh11, TMEM14 homolog of 11 kDa; Tmh18, Mitochondrial TMEM205 homolog of 18 kDa; Tml25, Acyl-protein thioesterase with multiple localizations, protein of 25 kDa.

A

Systematic name	Gene name	kDa	Systematic name	Gene name	kDa	Systematic name	Gene name	kDa	Systematic name	Gene name	kDa
YML050W	AIM32	36.0	YER145C	FTR1	45.7	YJR074W	MOG1	24.3	YDR201W	SPC19	18.9
YNL094W	APP1	66.1	YNL133C	FYV6	20.0	**YJL205C**	**NCE101**	**6.3**	YKR031C	SPO14	195.2
YGR230W	BNS1	15.9	**YCL026C-B**	**HBN1**	**21.0**	YJL126W	NIT2	34.7	YER046W	SPO73	16.6
YJL158C	CIS3	23.2	YKL101W	HSL1	169.6	YOR056C	NOB1	51.7	**YGL169W**	**SUA5**	**46.5**
YOR093C	CMR2	186.9	YPL015C	HST2	40.0	YNL129W	NRK1	27.7	YOR081C	TGL5	84.7
YBR230W-A	**COQ21**	**7.6**	YER092W	IES5	14.3	YGL111W	NSA1	51.9	**YLR118C**	**TML25**	**24.7**
YFL001W	**DEG1**	**50.9**	YNL106C	INP52	133.3	YBR060C	ORC2	71.3	YDR449C	UTP6	52.4
YLR307C-A	**DPA10**	**9.6**	YLL033W	IRC19	27.4	YHR063C	PAN5	42.8	YEL040W	UTR2	49.9
YKL065W-A	**DPC7**	**8.5**	**YIL156W-B**	**MCO8**	**8.2**	YLR151C	PCD1	39.8	YGR281W	YOR1	166.7
YGL041W-A	**DPC13**	**18.1**	**YKL018C-A**	**MCO12**	**11.8**	YGR087C	PDC6	61.6	YDR349C	YPS7	64.5
YOR114W	**DPI34**	**35.0**	**YGR053C**	**MCO32**	**32.2**	**YMR087W**	**PDL32**	**32.1**	YBL055C		47.4
YMR130W	**DPI35**	**35.3**	**YLR017W**	**MEU1**	**37.9**	YDR406W	PDR15	172.3	YDL177C		19.1
YDL219W	DTD1	16.7	YMR210W	MGL2	51.4	YBR022W	POA1	19.9	YHL012W		56.0
YML080W	DUS1	48.1	**YDR286C**	**MGP12**	**13.4**	YCL047C	POF1	9.7	YJR149W		45.2
YKL204W	EAP1	69.8	**YMR182W-A**	**MIN3**	**3.1**	YBR087W	RFC5	39.9	YKL071W		28.0
YKR076W	**ECM4**	**43.3**	**YBL039W-B**	**MIN6**	**6.9**	YER047C	SAP1	100.3	YMR187C		50.3
YGR200C	ELP2	89.4	**YBR201C-A**	**MIN7**	**7.7**	YLR022C	SDO1	28.3	YNL247W		87.5
YDR512C	EMI1	21.1	**YPR010C-A**	**MIN8**	**7.9**	YMR059W	SEN15	14.9	YOR131C		24.8
YDR261C	EXG2	63.5	**YKL023C-A**	**MIN9**	**8.5**	**YJL145W**	**SFH5**	**34.4**	YPL034W		18.9
YMR113W	FOL3	47.8	**YFR032C-B**	**MIN10**	**10.0**	YKL051W	SFK1	40.5			
YHR049W	FSH1	27.3	**YLR049C**	**MLO50**	**49.5**	**YNR015W**	**SMM1**	**42.8**			

B

Systematic name	Gene name	kDa	Systematic name	Gene name	kDa	Systematic name	Gene name	kDa	Systematic name	Gene name	kDa
YJL200C	ACO2	86.6	YFR044C	DUG1	52.9	**YOR020W-A**	**MCO10**	**9.6**	YDL104C	QRI7	45.5
YKL192C	ACP1	13.9	YDR125C	ECM18	53.2	**YDR381C-A**	**MCO13**	**12.7**	YLR084C	RAX2	133.9
YMR064W	AEP1	59.8	**YLR390W**	**ECM19**	**12.5**	**YHL018W**	**MCO14**	**14.0**	**YIL077C**	**RCI37**	**37.0**
YER080W	AIM9	72.4	YBR163W	EXO5	67.6	**YPL109C**	**MCO76**	**76.2**	**YKL133C**	**RCI50**	**54.5**
YER087W	AIM10	65.9	YFR019W	FAB1	257.4	YGR012W	MCY1	42.8	**YOR286W**	**RDL2**	**16.7**
YER093C-A	**AIM11**	**15.8**	YER183C	FAU1	24.1	YJL102W	MEF2	91.3	YDR065W	RRG1	42.9
YHL021C	AIM17	53.1	**YDR070C**	**FMP16**	**10.9**	**YML007C-A**	**MIN4**	**4.4**	YOR305W	RRG7	28.0
YHR198C	AIM18	36.5	YBR047W	FMP23	20.5	**YMR252C**	**MLO1**	**15.6**	YPR116W	RRG8	31.1
YJL131C	AIM23	41.5	**YJL161W**	**FMP33**	**20.2**	**YJR039W**	**MLO127**	**127.4**	YAR008W	SEN34	31.3
YJR100C	AIM25	37.5	YPL222W	FMP40	78.3	YIR021W	MRS1	41.3	YMR066W	SOV1	104.8
YMR003W	AIM34	22.8	YNL168C	FMP41	28.8	YER077C	MRX1	79.6	YGR236C	SPG1	10.5
YMR157C	AIM36	29.1	YKR049C	FMP46	15.7	**YPL041C**	**MRX11**	**24.2**	YLR389C	STE23	117.6
YOL053W	AIM39	45.9	YER004W	FMP52	25.1	YJR003C	MRX12	59.8	YLR305C	STT4	214.6
YOR215C	AIM41	21.2	**YOR271C**	**FSF1**	**35.4**	YPL168W	MRX4	48.9	YHR003C	TCD1	48.9
YHR199C	AIM46	34.1	YDR019C	GCV1	44.5	YJL147C	MRX5	44.9	**YKL027W**	**TCD2**	**50.3**
YER073W	ALD5	56.7	YMR189W	GCV2	114.4	YNL211C	MRX7	10.7	**YJR019C**	**TES1**	**40.3**
YKL157W	APE2	107.8	YLR091W	GEP5	33.9	YDL027C	MRX9	48.3	**YJR085C**	**TMH11**	**11.3**
YGR286C	BIO2	41.9	YGL057C	GEP7	33.0	**YGL226W**	**MTC3**	**14.5**	**YPR098C**	**TMH18**	**17.7**
YBL098W	BNA4	52.4	YDR305C	HNT2	24.8	YNL063W	MTQ1	35.9	**YOR251C**	**TUM1**	**34.2**
YKL208W	CBT1	31.2	**YBL059W**	**IAI11**	**22.3**	YAL029C	MYO4	169.3	YLL040C	VPS13	357.8
YER061C	CEM1	47.6	YER086W	ILV1	63.8	YPR155C	NCA2	70.9	YHL014C	YLF2	45.7
YGR207C	CIR1	28.8	YMR108W	ILV2	74.9	YOL042W	NGL1	42.4	YBR054W	YRO2	38.7
YCR005C	CIT2	51.4	YJR016C	ILV3	62.9	YLR351C	NIT3	32.5	YHR017W	YSC83	44.2
YLR087C	CSF1	338.2	YJL082W	IML2	82.5	YJR062C	NTA1	51.9	YDL157C		13.6
YOR022C	DDL1	81.8	**YGL085W**	**LCL3**	**32.1**	YGR178C	PBP1	78.8	YDR061W		61.2
YOR236W	DFR1	24.3	YLR239C	LIP2	37.2	YPR002W	PDH1	57.7	YGR015C		37.9
YPL107W	**DPC25**	**28.6**	YOR196C	LIP5	46.3	YJL023C	PET130	39.8	YKL162C		46.5
YGR021W	**DPC29**	**31.7**	YIL094C	LYS12	40.1	YHR189W	PTH1	21.0	YKR070W		39.4
YJL133C-A	**DPI8**	**7.7**	YDR234W	LYS4	75.2	**YBL057C**	**PTH2**	**22.4**	YLR283W		36.6
YNR040W	**DPI29**	**28.7**	**YJL127C-B**	**MCO6**	**6.0**	**YJR111C**	**PXP2**	**32.2**			

Table S6: Mitochondrial proteins with localization validated in this study. Related to Figures 4-7 and S4-S7.

Systematic name	Gene name	Dual loc.	kDa	Subcell. fractio-nation	Δψ dependent import into mitochondria	Mitochon-drial GFP-signal	Submito. fractionation MS (exp. val. ✔)	Additional experiments performed in this study	Copy# Gly/Glc (−6 log$_2$ ratio 6)	Pred. no. TM helices (TMHMM)	Previous studies	Name description
YER093C-A	AIM11		15.8	✔	import	N-term	IMS/IM	Co-IP (Iai11, Mtc3, Gep7)		2	§	Altered inheritance rate of mitochondria
YBR230W-A	COQ21		7.6	✔	import		matrix/IM ✔	BN, Co-IP (Coqx, Cat5)				COQ interacting protein
YFL001W	DEG1	✔	50.9	✔	import				242/363			Depressed growth rate
YLR307C-A	DPA10		9.6	✔	assembly			BN				Delta-Psi dependent mitochondrial assembly, protein of 10 kDa
YKL065W-A	DPC7		8.5	✔	import & cleavage	C-term	matrix/IM	BN	7824/1704	1		Delta-Psi dependent mitochondrial import and cleavage, protein of 7 kDa
YGL041W-A	DPC13		18.1	✔	import & cleavage	N-term	matrix/IM ✔		689/525			Delta-Psi dependent mitochondrial import and cleavage, protein of ~13 kDa
YPL107W	DPC25		28.6	✔	import & cleavage		matrix/IM	BN	367/168		*	Delta-Psi dependent mitochondrial import and cleavage, protein of ~25 kDa
YGR021W	DPC29		31.7	✔	import & cleavage				595/231		*‡¶	Delta-Psi dependent mitochondrial import and cleavage, protein of ~29 kDa
YJL133C-A	DPI8		7.7	✔	import	N-term	matrix/IM ✔	BN	1139/554		‡¶	Delta-Psi dependent mitochondrial Import, protein of 8 kDa
YNR040W	DPI29		28.7	✔	import & assembly	N-term	matrix/IM		779/594		*β‡¶	Delta-Psi dependent mitochondrial Import, protein of 29 kDa
YOR114W	DPI34		35.0	✔	import & assembly							Delta-Psi dependent mitochondrial Import, protein of ~34 kDa
YMR130W	DPI35		35.2	✔	import		matrix/IM		363/467			Delta-Psi dependent mitochondrial Import, protein of 35 kDa
YKR076W	ECM4	✔	43.3	✔					7027/1368			Extracellular mutant
YLR390W	ECM19		12.5	✔			IMS/IM		844/598	1	‡	Extracellular mutant
YDR070C	FMP16		10.9	✔	import & cleavage	N-term	matrix/IM ✔	BN	66971/3414		*β‡¶	Found in mitochondrial proteome
YJL161W	FMP33		20.2			N-term	IMS/IM		3729/1341		*β‡	Found in mitochondrial proteome
YOR271C	FSF1		35.4			N-term			8923/11250	4	*‡¶§	Fungal sideroflexin 1
YHR059W	FYV4		15.3	✔		N-term	matrix/IM		391/201		*ϕ	Function required for yeast viability
YCL026C-B	HBN1	✔	21.0		import				4571/1469			Homologous to bacterial nitroreductases
YBL059W	IAI11		22.3	✔		N-term	IMS/IM	Co-IP (Aim11, Mtc3, Gep7)	795/296	2	*‡§	Interactor of Aim11
YGL085W	LCL3		32.0			N-term	matrix/IM			1	*	Long chronological lifespan 3
YJL127C-B	MCO6		6.0			N-term	OM				§	Mitochondrial class one protein of 6 kDa
YIL156W-B	MCO8		8.2	✔			IMS/IM ✔		4789/2340			Mitochondrial class one protein of 8 kDa
YOR020W-A	MCO10		9.6	✔			IMS/IM	Co-IP (CV)	2788/853	1	‡¶	Mitochondrial class one protein of 10 kDa
YKL018C-A	MCO12		11.8			N-term	OM		522/165			Mitochondrial class one protein of 12 kDa
YDR381C-A	MCO13		12.7	✔			IMS/IM	BN	2555/1411	1	‡¶°	Mitochondrial class one protein of 13 kDa
YHL018W	MCO14		14.0	✔	import & assembly		matrix/IM ✔	BN	165/117		*	Mitochondrial class one protein of 14 kDa
YGR053C	MCO32		32.2	✔			matrix/IM		10/3			Mitochondrial class one protein of 32 kDa
YPL109C	MCO76		76.1			N-term	IMS/IM		100/35		*β‡	Mitochondrial class one protein of 76 kDa
YLR017W	MEU1	✔	37.9	✔	import		matrix/IM		1852/3152			Multicopy enhancer of UAS2
YDR286C	MGP12		13.4	✔	import & cleavage				989/828			Mitochondrial glutaredoxin-like protein of 12 kDa
YMR182W-A	MIN3		3.1			C-term				1		Mini mitochondrial protein of 3 kDa
YML007C-A	MIN4		4.4	✔							*	Mini mitochondrial protein of 4 kDa
YBL039W-B	MIN6		6.9	✔		C-term	OM	BN		1		Mini mitochondrial protein of ~6 kDa
YBR201C-A	MIN7		7.7	✔			IMS/IM ✔			1		Mini mitochondrial protein of ~7 kDa
YPR010C-A	MIN8		7.9	✔			IMS/IM ✔	BN	13017/2464	1		Mini mitochondrial protein of 8 kDa
YKL023C-A	MIN9		8.5	✔		C-term	matrix/IM			1		Mini mitochondrial protein of 9 kDa
YFR032C-B	MIN10		10.0	✔		C-term				1		Mini mitochondrial protein of 10 kDa
YMR252C	MLO1		15.6	✔		N-term					*	Mitochondrially localized protein
YLR049C	MLO50		49.5	✔								Mitochondrially localized protein of 50 kDa
YJR039W	MLO127		127.4	✔							β‡	Mitochondrially localized protein of 127 kDa
YPL041C	MRX11		24.2			N-term	matrix/IM			2	§	Mitochondrial organization of gene expression (MIOREX)
YGL226W	MTC3		14.5	✔			IMS/IM		1268/452	1	*¶	Maintenance of telomere capping
YJL205C	NCE101		6.3	✔					931/389	1		Nonclassical export
YMR087W	PDL32	✔	32.1	✔			matrix/IM		221/139			Protein of dual localization, protein of 32 kDa
YBL057C	PTH2		22.4				OM ✔		4545/6624	1	β‡¶°	Peptidyl-trna hydrolase
YJR111C	PXP2	✔	32.2	✔					1786/1763		*	Peroxisomal protein
YIL077C	RCI37		37.0	✔	import & assembly	N-term	IMS/IM ✔	BN, Co-IP (CIII, CIV, m-AAA)	540/258	2	*‡	Respiratory chain interacting protein of 37 kDa
YKL133C	RCI50		54.5	✔	import & cleavage	N-term	IMS/IM	Co-IP (CIII, CIV, i-AAA)		1	§	Respiratory chain interacting protein of ~50 kDa
YOR286W	RDL2		16.7	✔	import & cleavage				6638/4974		*β‡¶	Rhodanese-like protein
YNL213C	RRG9		25.3	✔	import & cleavage		matrix/IM ✔	BN			‡Ω	Required for respiratory growth
YLR281C	RSO55		18.2	✔	import & cleavage	N-term		BN			*ϕ	Mitochondrial protein related to spastic paraplegia with optic atrophy and neuropathy SPG55
YJL145W	SFH5		34.4			N-term	OM		2441/2547			Sec fourteen homolog
YNR015W	SMM1	✔	42.8	✔	import		matrix/IM		788/1081			Suppressor of mitochondrial mutation
YGL169W	SUA5	✔	46.5	✔			IMS/IM		784/699			Suppressor of upstream AUG
YKL027W	TCD2		50.3				OM ✔		4295/3584	1	*β‡¶°	tRNA Threonylcarbamoyladenosine dehydratase
YJR019C	TES1	✔	40.3		import		matrix/IM		10404/1398		β‡¶	Thioesterase
YJR085C	TMH11		11.3	✔	import	N-term		BN, Co-IP (GxxxG-cont. prot.)	1752/937	3	β‡	TMEM14 homolog of 11 kDa
YPR098C	TMH18		17.7	✔		N-term	OM		5832/2902	3	*‡°	Mitochondrial TMEM205 homolog of 18 kDa
YLR118C	TML25	✔	24.7	✔	import				2635/2937			Acyl-protein thioesterase with multiple localizations, protein of 25 kDa
YOR251C	TUM1	✔	34.2	✔	import		matrix/IM		7954/6424			Thiouridine modification

* Huh WK, et al. (2003) Global analysis of protein localization in budding yeast. Nature 425(6959):686-91

ϕ Perocchi F, et al. (2006) Assessing Systems Properties of Yeast Mitochondria through an Interaction Map of the Organelle. PLoS Genet 2(10):e170

β Sickmann A, et al. (2003) The proteome of Saccharomyces cerevisiae mitochondria. Proc Natl Acad Sci U S A 100(23):13207-12

‡ Reinders J, et al. (2006) Toward the complete yeast mitochondrial proteome: multidimensional separation techniques for mitochondrial proteomics. J Proteome Res 5(7):1543-54

¶ Renvoise M, et al. (2014) Quantitative variations of the mitochondrial proteome and phosphoproteome during fermentative and respiratory growth in Saccharomyces cerevisiae. J Proteomics 106:140-50

Ω Wysocki R, et al. (1999) Disruption and basic phenotypic analysis of 18 novel genes from the yeast Saccharomyces cerevisiae. Yeast 15(2):165-71

§ Yofe I, et al. (2016) One library to make them all: streamlining the creation of yeast libraries via a SWAp-Tag strategy. Nat Methods 13(4):371-8

° Zahedi RP, et al. (2006) Proteomic analysis of the yeast mitochondrial outer membrane reveals accumulation of a subclass of preproteins. Mol Biol Cell 17(3):1436-50

Table S7. Dual-localized mitochondrial proteins. Related to Figure 6. To identify soluble mitochondrial proteins with dual/multiple cellular localization, filtered high-confidence mitochondrial class 1 proteins were selected from Table S1 when they displayed a significant amount in the post mitochondrial supernatant (PNS/total > 0.5) and in both mitochondrial fractions (pure mito/crude mito > 0). α-helical membrane proteins (transmembrane helix TMHMM prediction) and β-barrel membrane proteins were removed. The list of 57 mitochondrial proteins includes proteins with known (grey) dual/multiple cellular localizations, proteins validated in this study (green) and high-confidence candidates. Upon completion of this study we noticed that Tum1 was previously imported as y-rho into isolated mitochondria (Dubaquié et al., 1998) in full agreement with our study.

Systematic name	PMS/ Total	Gene name	Mitochondrial proteome class 1	Mitochondrial localization (other evidence)	Extra-mito. annotation	Extra-mitochondrial localization	Gene description
YKL157W	1.42	APE2	✔	HT	Manual	Plasmamembrane	Aminopeptidase yscII
YMR098C	0.87	ATP25	✔	Manual			Mito. protein required for Oli1p ring formation and stability of Oli1p (Atp9p) mRNA
YJL060W	0.67	BNA3	✔	Manual	Manual	Cytosol	Kynurenine aminotransferase
YMR038C	1.60	CCS1	✔	Manual	Manual	Cytosol, Nucleus	Copper chaperone for superoxide dismutase Sod1p
YDL164C	0.99	CDC9	✔	Manual	Manual	Nucleus	DNA ligase I found in nucleus and mitochondria
YGR255C	5.90	COQ6	✔	Manual			Flavin-dependent monooxygenase involved in ubiquinone biosynthesis
YFL001W	1.13	**DEG1**	✔	This study	Manual	Cytosol (this study), Nucleus	tRNA:pseudouridine synthase
YHR011W	6.21	DIA4	✔	Manual	Manual	Cytosol	Probable mitochondrial seryl-tRNA synthetase
YFR044C	1.26	DUG1	✔	HT			Cys-Gly metallo-di-peptidase
YKR076W	1.16	**ECM4**	✔	This study	Manual	Cytosol & Microsome (this study)	S-glutathionyl-(chloro)hydroquinone reductase (GS-HQR)
YIL098C	2.45	FMC1	✔	Manual			Mito. matrix protein that is required for assembly or stability at high temperature of the F1 sector of mitochondrial F1F0 ATP synthase
YNL256W	0.67	FOL1	✔	Manual			Multifunctional enzyme of the folic acid biosynthesis pathway
YMR113W	0.53	FOL3	✔				Dihydrofolate synthetase that is involved in folic acid biosynthesis
YHR049W	2.82	FSH1	✔		HT	Cytoplasm, Nucleus	Putative serine hydrolase
YHR100C	0.91	GEP4	✔	Manual			Mitochondrial phosphatidylglycerophosphatase (PGP phosphatase)
YPL091W	1.16	GLR1	✔	Manual	Manual	Cytosol, Nucleus	Cytosolic and mitochondrial glutathione oxidoreductase
YOL059W	1.37	GPD2	✔	Manual	Manual	Cytosol	NAD-dependent glycerol 3-phosphate dehydrogenase
YCL026C-B	1.10	**HBN1**	✔	This study	HT	Cytosol, Nucleus	Protein of unknown function that is similar to bacterial nitroreductases
YMR207C	1.22	HFA1	✔	Manual			Mitochondrial acetyl-coenzyme A carboxylase that catalyzes production of malonyl-CoA in mitochondrial fatty acid biosynthesis
YDR305C	1.20	HNT2	✔	HT	HT	Cytoplasm, Nucleus	Dinucleoside triphosphate hydrolase
YPR033C	1.15	HTS1	✔	Manual	Manual	Cytosol	Cytoplasmic and mitochondrial histidine tRNA synthetase
YPR083W	0.66	MDM36	✔	Manual			Component of the mitochondria-ER-cortex-ancor (MECA)
YLR017W	3.05	**MEU1**	✔	This study	Manual	Cytosol (this study)	Methylthioadenosine phosphorylase (MTAP)
YMR002W	0.88	MIX17	✔	Manual	HT	Cytoplasm, Nucleus	Mitochondrial intermembrane space protein that is required for normal oxygen consumption
YOR274W	0.71	MOD5	✔	Manual	Manual	Cytosol, Nucleus	Delta 2-isopentenyl pyrophosphate:tRNA isopentenyl transferase
YNL306W	1.70	MRPS18	✔	Manual			Mitochondrial ribosomal protein of the small subunit
YBR251W	2.15	MRPS5	✔	Manual			Mitochondrial ribosomal protein of the small subunit
YPL104W	0.62	MSD1	✔	Manual			Mitochondrial aspartyl-tRNA synthetase that is required for acylation of aspartyl-tRNA
YCL033C	1.21	MXR2	✔	Manual			Methionine-R-sulfoxide reductase
YAL029C	0.87	MYO4	✔	HT			Type V myosin motor involved in actin-based transport of cargos
YGL221C	1.19	NIF3	✔	Manual	Manual	Cytosol	Protein of unknown function
YLR351C	1.36	NIT3	✔	HT			Nit protein
YGR178C	0.58	PBP1	✔	HT	Manual	Cytoplasm, Nucleus (HT)	Component of glucose deprivation induced stress granules that is involved in P-body-dependent granule assembly
YMR087W	1.02	**PDL32**	✔	This study		Cytosol (this study)	Putative ADP-ribose-1"-monophosphatase that converts ADP-ribose-1"-monophosphate to ADP-ribose
YCL057W	1.25	PRD1	✔	Manual	Manual	Cytoplasm, Golgi, Vacuole	Zinc metalloendopeptidase
YNL292W	1.25	PUS4	✔	Manual	Manual	Nucleus	Pseudouridine synthase
YJR111C	0.66	**PXP2**	✔	This study	Manual	Cytosol (this study), Peroxisome	Peroxisomal matrix protein with naturally active promoter
YKL113C	1.41	RAD27	✔	Manual	Manual	Cytosol, Nucleus	5' to 3' exonuclease / 5' flap endonuclease
YLR059C	1.37	REX2	✔	Manual			3'-5' RNA exonuclease
YBR087W	1.85	RFC5	✔		Manual	Nucleus	Subunit of heteropentameric Replication factor C (RF-C)
YLR139C	2.31	SLS1	✔	Manual			Mitochondrial membrane protein that coordinates this studyression of mitochondrially-encoded genes
YNR015W	0.97	**SMM1**	✔	This study	HT	Cytosol (this study), Nucleus	Dihydrouridine synthase
YMR066W	8.73	SOV1	✔	HT			Mitochondrial protein of unknown function
YLR389C	1.32	STE23	✔	HT			Metalloprotease that is involved in N-terminal processing of pro-a-factor to mature form
YLR305C	2.13	STT4	✔	HT	Manual	Plasmamembrane	Phosphatidylinositol-4-kinase that functions in the Pkc1p protein kinase pathway
YGL169W	2.41	**SUA5**	✔	This study	HT	Cytosol (this study)	Protein involved in threonylcarbamoyl adenosine biosynthesis
YGR046W	2.90	TAM41	✔	Manual			Mitochondrial phosphatidate cytidylyltransferase (CDP-DAG synthase)
YJR019C	0.58	**TES1**	✔	This study	Manual	Peroxisome	Peroxisomal acyl-CoA thioesterase
YLR118C	0.97	**TML25**	✔	This study	Manual	Cytosol (this study)	Acyl-protein thioesterase responsible for depalmitoylation of Gpa1p
YHR070W	4.83	TRM5	✔	Manual	Manual	Cytoplasm	tRNA(m(1)G37)methyltransferase
YOR251C	0.87	**TUM1**	✔	This study	Manual	Cytosol (this study)	Rhodanese domain sulfur transferase
YGR094W	1.12	VAS1	✔	Manual	Manual	Cytoplasm	Mitochondrial and cytoplasmic valyl-tRNA synthetase
YLL040C	1.02	VPS13	✔	HT	Manual	Golgi, Vacuole	Protein involved in prospore membrane morphogenesis
YBL055C	1.33	YBL055C	✔				3'-->5' exonuclease and endonuclease
YGR234W	0.81	YHB1	✔	Manual	Manual	Cytosol	Nitric oxide oxidoreductase
YJR149W	2.43	YJR149W	✔				Putative protein of unknown function
YNL247W	1.26	YNL247W	✔				Cysteinyl-tRNA synthetase

SUPPLEMENTAL EXPERIMENTAL PROCEDURES

Media, growth conditions and metabolic labeling

Yeast cells were grown at 30°C and 160 rpm in in YPG (1% [w/v] yeast extract, 2% [w/v] peptone, 3% [v/v] glycerol), YPD (1% [w/v] yeast extract, 2% [w/v] peptone, 2% [w/v] glucose), or SC medium (0.17% [w/v] yeast nitrogen base [YNB] without amino acids, 0.5% [w/v] ammonium sulfate, 3% [v/v] glycerol, 20 mg/L of L-histidine, L-tryptophan, L-methionine, adenine and uracil, 23 mg/L of L-arginine and L-lysine, 30 mg/L of L-isoleucine and L-tyrosine, 50 mg/L of L-phenylalanine, 100 mg/L of L-leucine, 150 mg/L of L-valine, and 200 mg/L of L-threonine and proline). To assess differences in protein expression levels in YPH499Δ*arg4* after growth on different carbon sources, cells were grown in SC medium containing 3% (w/v) glycerol, 2% (w/v) galactose or 2% (w/v) glucose. For metabolic labeling of yeast, media were supplemented with stable isotope-coded amino acids (Euriso-Top GmbH), i.e. 'heavy' arginine ($^{13}C_6/^{15}N_4$) and lysine ($^{13}C_6/^{15}N_2$) or 'medium-heavy' arginine ($^{13}C_6/^{14}N_2$) and lysine ($^{4}H_2$) instead of the respective 'light' amino acids. To ensure complete incorporation of isotopically labeled amino acids, cells were grown for at least five cell doublings in precultures and four doublings in main cultures. Cells were generally harvested during exponential growth phase.

For selection of yeast strains on solid media, YPD plates (1% [w/v] yeast extract, 2% [w/v] peptone, 2% [w/v] glucose, 2.5% [w/v] Bacto™ Agar) containing antibiotics or minimal medium plates (0.67% [w/v] YNB without amino acids [Becton, Dickinson and Company Inc.], appropriate amino acid drop-out mix [MP Biomedicals LLC], 2% [w/v] glucose, 2.5% Bacto™ Agar [Becton, Dickinson and Company Inc.]) lacking the amino acid used as selection marker were used.

Generation of yeast strains

All *Saccharomyces cerevisiae* strains used in this study have been derived from the wild type strains BY4741 (*MATa, his3Δ1, leu2Δ0, met15Δ0, ura3Δ0*), BY4742 (*Matα, his3Δ1, leu2Δ0, met15Δ0, ura3Δ0, lys2Δ0)* or YPH499 (*MATa, ura3-52, lys2-801, ade2-101, trp1-Δ63, his3-Δ200, leu2-Δ1*).

C-terminal Protein A-, HA- or EGFP-tagging of chromosomal genes was performed by introducing the genetic information for the respective tag, followed by a selection marker, in front of the stop codon of the respective gene. In this study, the *kanMX4*, *kanMX6*, *HIS3MX6* (Knop et al., 1999), and *hphNT1* cassettes (Janke et al., 2004) served as selection markers. Chromosomal deletions were obtained by substitution of the respective gene by a *kanMX6* cassette (Longtine et al., 1998). For generation of YPH499 Δ*arg4* strain, the *kanMX4* selection marker was

introduced (von der Malsburg et al., 2011). Yeast cells were transformed as previously described (Gietz and Woods, 2002) and transformants were selected on minimal medium -HIS plates. Selections of strains containing an antibiotics resistance cassette were performed on YPD plates supplemented with 200 µM KP_i and 200 mg/L G418 (Enzo Biochem Inc.; ALX-380-013-G005) for selection of strains containing a *kanMX6* cassette or 300 mg/L hygromycin B (Carl Roth GmbH + Co. KG; CP13.3) for selection of strains containing a *hphNT1* cassette. Chromosomal insertion of *hphNT1* and *kanMX6* cassettes at the correct position was confirmed by colony PCR and/or immunoblotting of whole cell yeast extracts using antibodies raised against the Protein A, HA or GFP epitope tag. For colony PCR, a tiny number of cells was transferred with a toothpick to 10 µL of a 1 mg/mL Zymolyase solution (Zymolyase®-20T, Nacalai Tesque Inc.) and incubated for 10 min at 25°C. Afterwards, forward and reverse primers that bind to the 5'-UTR and 3'-UTR of the respective open reading frame were added. For some of the Protein A-tagged strains a reverse primer was employed that binds to the linker region of the Protein A tag. RedMastermix (2X) (Genaxxon Bioscience GmbH; M3029.0500) was used for amplification of DNA fragments. For the generation of N-terminal GFP-tagged proteins, strain BY4741 was genomically transformed to tag proteins at their start codon with GFP under the control of the constitutive NOP1 gene promoter. Using the SWAT approach, excision of the selection cassette and NOP1 promoter resulted in restoration of the gene's endogenous promoter (Yofe et al., 2016). Tagging was verified using a genomic PCR check.

The pRS425-$_{HA}$YJR085C plasmid was generated as follows: the YJR085C open reading frame including 537 nucleotides upstream (containing the endogenous promoter) and 369 nucleotides downstream (comprising the endogenous terminator) was amplified from yeast genomic DNA. At their 5'-ends, the forward (YJR085C_pRS425_FW) and reverse (YJR085C_pRS425_REV) primers were fused to a HindIII or BamHI cleavage site, respectively. The resulting HindIII-$P_{YJR085C}$-YJR085C (*S. cerevisiae*)-$T_{YJR085C}$-BamHI PCR fragment was cloned into pRS425 plasmid using HindIII and BamHI restriction enzymes. Site-directed mutagenesis was employed to introduce the N-terminal HA-tag in front of YJR085C. To this end the forward and reverse primers NHA_YJR085C_FW and NHA_YJR085C_Rev as well as the QuikChange™ Site-Directed Mutagenesis Kit (Agilent Technologies Inc.) were used.

$_{HA}$YJR085C and its corresponding wild-type strain (YPH499 + *pRS425*) were generated by transforming YPH499 cells with the pRS425 plasmid encoding for the $_{HA}$YJR085C protein (under control of its endogenous promoter and terminator) or the empty plasmid followed by several rounds of selection on minimal medium plates depleted from leucine.

To generate the pFA6a-TEV-ProtA-7His-hphNT1 plasmid, the TEV-ProtA-7His module was amplified from pYM10 plasmid (Knop et al., 1999) using TEV-ProtA_fwd and TEV-ProtA_rev primers and cloned into pFA6a-hphNT1 plasmid (Janke et al., 2004) using HindIII and XmaI restriction sites.

To generate the BY4741 Δ*arg4* strain, BY4741 and BY4742 Δ*arg4* (Euroscarf) were crossed and several tetrads were dissected. Correct genotype (*MATa*; *ura3*Δ0, *leu2*Δ0, his3Δ*1, lys2*Δ*0, met15*Δ*0, arg4::kanMX4*) was selected by replica plating. To this end, minimal media devoid of either arginine, methionine or lysine were used. Mating type was determined by colony PCR using the primers MATlocus_fw, Mat(a)_rv and Mat(alpha)_rv (Huxley et al., 1990).

Preparation of cell lysates, subcellular fractionation, and isolation of mitochondria

Subcellular fractionation and isolation of mitochondria for quantitative MS experiments were performed as described before (Meisinger et al., 2000) with slight modifications. Differentially SILAC-labeled cells were harvested by centrifugation for 5 min at 3,000 x g and RT, washed with deionized water, and incubated for 20 min at 160 rpm and 30°C in 2 mL of DTT buffer (100 mM Tris-H_2SO_4 [pH 9.4], 10 mM DTT) per g wet weight (ww). Following centrifugation (5 min, 3,000 x g, RT), cells were washed with 7 mL/g ww zymolyase buffer (1.2 M sorbitol, 20 mM K_3PO_4 [pH 7.4]) and incubated for 45 min at 160 rpm and 30°C in 7 mL/g ww zymolyase buffer containing 3 mg/g ww Zymolyase 20-T (MP Biomedicals Life Sciences) to digest cell walls. Spheroplasts were harvested by centrifugation (5 min, 3,000 x g, 4°C) and homogenized in 7 mL/g ww ice-cold homogenization buffer (0.6 M sorbitol, 10 mM Tris-HCl [pH 7.4], 1 mM PMSF [dissolved in isopropanol]) containing 1 mM EDTA using a glass-Teflon potter (15 strokes). Cell debris and nuclei were removed from the homogenate (referred to as 'cell lysate' in this work) by centrifugation for 5 min at 1,500 x g and 4°C followed by centrifugation of the supernatants for 5 min at 4,000 x g and 4°C. Crude mitochondrial fractions were pelleted from the resulting postnuclear supernatants (PNS) by centrifugation for 15 min at 12,000 x g and 4°C. The post-mitochondrial supernatants (PMS) were taken off and the pellets were resuspended in SEM buffer (250 mM sucrose, 1 mM EDTA, 10 mM MOPS-KOH [pH 7.2]).

To obtain mitochondrial fractions of higher purity, crude mitochondria were loaded onto sucrose density gradients consisting of 2 mL of 60%, 6 mL of 32%, 2 mL of 23%, and 2 mL of 15% (w/v each) sucrose in EM buffer (10 mM MOPS-KOH [pH 7.2], 1 mM EDTA). Following centrifugation for 1 h at 134,000 x g and 2°C, pure mitochondrial fractions were collected from the interface between 60% and 32% sucrose, diluted with the two-fold volume of SEM buffer, pelleted for 10 min at 12,000 x g and 2°C, resuspended in 100 µL/g ww of SEM buffer, shock-frozen in liquid nitrogen, and stored at -80°C until further use.

To reveal differences in protein abundance between crude mitochondrial fractions and gradient-purified mitochondria and, thus, identify putative mitochondrial proteins, crude and pure mitochondria from differentially SILAC-labeled cells were mixed in equal ratios based on protein concentration and analyzed by LC-MS following different protein and peptide fractionation methods. This experiment (referred to as 'pure/crude' experiment in this work) was performed in four biological replicates including label-switch (see Figure S1A). For subcellular profiling experiments, performed to verify the mitochondrial localization of candidate proteins, aliquots of subcellular fractions (i.e., cell lysates, the post-mitochondrial supernatant PMS, crude and gradient-purified mitochondria; n = 4) generated during pure/crude experiments were analyzed separately by LC-MS following tryptic in-solution digestion. To absolutely quantify the yeast proteome and determine protein copy numbers, cell lysates were prepared from light, medium-heavy, and heavy SILAC-labeled, mixed in 1:1:1 ratios, and analyzed by LC-MS in three biological replicates including a label switch (see Figure S1B).

For medium-scale preparations of mitochondria from up to 20 yeast strains in parallel, performed for validation experiments, the protocol was as follows: *S. cerevisiae* strains were grown to mid-logarithmic phase in 360 mL of YPG medium in a 1-L flask. 400 OD_{600} of cells were pelleted by centrifugation (3,000 x g, 5 min, 25°C, SLA-300 rotor [Sorvall™, Thermo Fisher Scientific Inc.]). Yeast pellets were washed with dH_2O in 50 mL concial tubes, suspended in 3.5 mL of DTT buffer and transferred to 5-mL Eppendorf Tubes® (Eppendorf AG). Samples were incubated at 30°C and 900 rpm for 20 min (ThermoMixer® C, Eppendorf AG) and collected by centrifugation at 3,000 x g for 5 min at 25°C (Rotor FA-45-20-17, Centrifuge 5804 R [Eppendorf AG]). Pellets were dissolved in 4.5 mL of zymolyase buffer, 30 mg Zymolyase®-20T (Nacalai Tesque Inc.) were added to each sample and samples were incubated for 45 min at 30°C. Spheroplasts were pelleted by centrifugation (1,500 x g, 5 min, 25°C), washed with 3.5 mL of 1.2 M sorbitol and dissolved in 4.5 mL homogenization buffer containing 0.2% (w/v) bovine serum albumin. Cells were opened on ice using an Omnifix® 10 mL LL syringe (B. Braun Melsungen AG, 4617100V) and a Sterican® 0.90 x 0.40 mm cannula (B. Braun Melsungen AG, 4657519) by 15-20 repetitions of drawing up the dissolved yeast cells through the cannula into the syringe and pushing the cells back to the 5 mL Eppendorf tube. Cell debris was removed by centrifugation (1,500 x g, 5 min, 4°C) and supernatant was transferred to a fresh 5 mL Eppendorf tube and subjected to two consecutive centrifugation steps at 3,000 x g for 5 min at 4°C. Afterwards mitochondria were pelleted by centrifugation at 20,913 x g for 5 min at 4°C. Mitochondrial pellet was suspended in 3.5 mL SEM buffer and subjected to a low-speed centrifugation (3,000 x g for 5 min at 4°C). Supernatant was transferred to a fresh 5 mL Eppendorf cup and mitochondria were collected by centrifugation at 20,913 x g for 5 min

at 4°C. Mitochondria were dissolved in 200 µL of SEM buffer and protein concentration was determined using the Bradford assay. Afterwards, mitochondria were aliquoted, snap frozen in liquid nitrogen and stored at -80°C.

Subcellular fractionation for biochemical validation of subcellular protein localization

70 OD_{600} of cells (corresponds to 70 mL of cultured cells grown to an OD_{600} of 1.0) were harvested by centrifugation at 3,000 x g for 5 min at 25°C. Cells were suspended in 2 mL DTT buffer and incubated for 20 min at 30°C. Afterwards, yeast cells were collected by centrifugation (3,000 x g, 5 min, 25°C) and suspended in 1 mL of zymolyase buffer containing 8 mg/mL Zymolyase®-20T (Nacalai Tesque Inc.). Spheroplasts were pelleted by centrifugation (1,500 x g, 5 min, 25°C) and suspended in 2 mL of homogenization buffer. Cells were opened by 20 strokes with a PTFE pestle (Sartorius, BBI-8542708) in a 5 mL Homogenizer Vessel (Sartorius, BBI-8542309) on ice. Cell debris, nuclei and intact cells were pelleted (1,500 x g, 5 min, 4°C) and supernatant (containing crude mitochondria) was subjected to another 10 strokes. Half of the post-nuclear supernatant (PNS) was precipitated with trichloroacetic acid (TCA) and dissolved in 2x SDS sample (120 mM Tris-HCl [pH 6.8], 4% [w/v] SDS, 20% [v/v] glycerol, 0.02% [w/v] bromphenolblue) supplemented with 10 mM DTT and 2 mM of PMSF.
Mitochondria were isolated from the other half of the PNS by centrifugation at 13,000 x g for 10 min at 4°C. To remove loosely attached proteins of other cellular compartments from the surface of mitochondria, mitochondria were suspended in 200 µL of SEM buffer, loaded onto 500 µL of S_{500}EM (500 mM sucrose, 1 mM EDTA, 10 mM MOPS-KOH [pH 7.2]) and re-isolated by centrifugation (13,000 x g for 10 min at 4°C). The mitochondrial pellet (Mito) was dissolved in 200 µL of 2x SDS sample buffer supplemented with 10 mM DTT and 2 mM of PMSF. For isolation of microsomal fraction, the supernatant was subjected to ultracentrifugation at 100,000 x g for 1 h at 4°C. The microsomal pellet (P100) was suspended in 200 µL of 2x SDS sample buffer supplemented with 10 mM of DTT and 2 mM of PMSF whereas the supernatant (S100) was treated with trichloroacetic acid before addition of SDS sample buffer. 20 µL of PNS, 20 µL of Mito, 23 µL of P100 and 23 µL of S100 fractions were subjected to SDS-PAGE.

Protease accessibility assay

For the global analysis of the suborganellar localization of mitochondrial proteins by quantitative MS, gradient-purified mitochondria (100 µg per replicate, 5 mg/mL) obtained from heavy SILAC-labeled (replicates 1 and 3) or unlabeled cells (replicate 2) were treated with (i) protease only (referred to as S1), (ii) protease following rupture of

the outer membrane (OM) using digitonin (S2), and (iii) protease following lysis of mitochondria using Triton X-100 (S3). Same amounts of mitochondria from differentially SILAC-labeled cells (replicates 1 and 3, unlabeled; replicate 2, heavy labeled) remained untreated and served as control (M). For the perforation of OM, mitochondria were incubated with digitonin (0.1% [w/v] final concentration) for 3 min at 4°C. Membrane perforation was stopped by adding the 14-fold volume of SEM buffer. To lyse mitochondria, Triton X-100 was added to a final concentration of 1% (w/v) and samples were incubated for 10 min at 4°C. Volumes of all samples were adjusted with SEM buffer to the volume of S2. For the digestion of accessible proteins in S1, S2, and S3, trypsin and proteinase K were added (final concentration of 5 µg/mL each) and samples were incubated for 15 min at 4°C. Proteases were inactivated by adding PMSF (1 mM final concentration) and incubation for 15 min at 4°C. Mitochondria (M, S1) and mitoplasts (S2) were collected by centrifugation (10 min, 12,000 x g, 4°C), layered with SEM buffer containing 1 mM PMSF to inactivate residual protease activity, and recollected by centrifugation (10 min, 12,000 x g, 4°C). Pellets were resuspended in 100 µL SDS sample buffer containing 50 mM DTT and 1 mM PMSF and boiled for 20 min at 94°C. Proteins in S3 were precipitated by adding TCA (15% [w/v], final concentration) followed by incubation for 30 min at 4°C and centrifugation (15 min, 14,000 x g, 4°C). The resulting pellets were washed with 80% ice-cold acetone (v/v) and centrifuged again (15 min, 14,000 x g, 4°C). Supernatants were carefully removed and the pellets were resuspended in 100 µL SDS sample buffer containing 50 mM DTT and 1 mM PMSF and boiled for 20 min at 94°C. S1, S2, and S3 were each mixed with equal amounts of M for subsequent quantitative MS analysis (see Figure S1C). This experiment is referred to as 'submitochondrial profiling experiment' in this work.

Swelling assay for determination of submitochondrial protein localization

Crude mitochondria were suspended in SEM buffer and split into samples of equal volume (each sample containing 50-70 µg of mitochondria). Half of the samples were subjected to hypoosmotic swelling by addition of 8 volumes of EM buffer. The other half of the samples were diluted with the same volume of SEM buffer (mitochondria were left intact). Where indicated, samples were treated with proteinase K (final concentration: 7 µg/mL) for 15 min on ice. PMSF was added to all samples to a final concentration of 2.5 mM. Mitochondria were washed with SEM buffer and dissolved in 2x SDS sample buffer supplemented with 2% (v/v) of β-mercaptoethanol and 2 mM of PMSF. Samples were analyzed by SDS-PAGE and immunoblotting. To control for protein aggregates, 70 µg of mitochondria were suspended in 50 µL of 1% Triton X-100 (diluted in SEM buffer) and incubated on ice for 7 minutes. Where indicated, samples were subjected to proteinase K treatment for 15 min at a final concentration of 7 µg/mL. Protease

was inhibited by the addition of PMSF to a final concentration of 2 mM. After addition of SDS sample buffer, samples were separated by SDS-PAGE and analyzed by immuoblotting.

Purification of mitochondrial protein complexes using IgG and HA affinity chromatography

Two milligram of wild-type and Protein A-tagged mitochondria, respectively, were suspended in 2 mL of solubilization buffer (1% [w/v] digitonin, 20 mM Tris-HCl [pH 7.4], 50 mM NaCl, 10% glycerol, 0.1 mM EDTA) supplemented with 1.5 mM PMSF and 1x cOmplete^{TM}, EDTA-free Protease Inhibitor Cocktail (F. Hoffmann-La Roche AG). Mitochondria were incubated end-over-end for 30 min at 4°C. Non-solubilized material was removed by centrifugation. Afterwards, 50 µL of solubilized mitochondria were mixed with 12.5 µL of 4x SDS sample buffer containing 4% (v/v) β-mercaptoethanol and 4 mM PMSF (Load fraction).

For co-immunoprecipitation of Protein A-tagged mitochondrial proteins, 150 µL of 50% slurry human IgG-coupled Sepharose beads were equilibrated with solubilization buffer, mixed with solubilized mitochondria and incubated end-over-end for 2 h at 4°C. After binding of Protein A-tagged proteins to IgG, beads were re-collected by centrifugation (100 x g, 1 min, 4°C) and transferred to Mobicol Mini-Columns. To remove unspecifically-bound proteins beads were washed 12 times with 500 µL of wash buffer (0.1-0.3% [w/v] digitonin, 20 mM Tris-HCl [pH 7.4], 60 mM NaCl, 10% glycerol, 0.5 mM EDTA) supplemented with 1.5 mM PMSF and 1x cOmplete^{TM}, EDTA-free Protease Inhibitor Cocktail (F. Hoffmann-La Roche AG). Specifically bound proteins were eluted by the addition of 10 µL of AcTEV Protease (Thermo Fisher Scientific Inc.) in 150 µL of wash buffer, followed by vigorous shaking at 4°C for 16 h. For removal of His-tagged AcTEV protease from elution mixture, 10 µL of Ni-NTA agarose (Qiagen N.V.) were equilibrated with wash buffer and added to eluate, followed by vigorous shaking for 30 min at 4°C. Eluted mitochondrial proteins were collected by centrifugation (200 x g, 1 min, 4°C). To remove residual proteins, another 50 µL of wash buffer was added to the IgG-coupled Sepharose beads and collected by centrifugation yielding a total of 215 µL of eluate. 115 µL of eluate were mixed with 30 µL of 4x SDS sample buffer. For the analysis of protein complexes by SILAC-based quantitative MS, 100 µL of eluates obtained from differentially labeled wild-type cells and cells expressing the Protein A-tagged bait were mixed and analyzed by LC-MS.

For co-immunoprecipitation from $_{HA}$Tmh11 and corresponding wild-type mitochondria one milligram of mitochondria were used per strain. They were suspended in 1 mL of solubilization buffer (supplemented with 1 mM PMSF) and incubated end-over-end for 30 min at 4°C. After removal of non-solubilized material by centrifugation,

20 µL of supernatant were mixed with 20 µL of 2x SDS sample buffer containing 2% (v/v) β-mercaptoethanol and 2 mM PMSF (Load fraction). HA-tagged proteins were bound to 100 µL of pre-equilibrated anti-HA Affinity Matrix slurry (F. Hoffmann-La Roche AG, 11815016001) by incubation end-over-end for 1 h at 4°C. Samples were washed 10 times with 600 µL of HA wash buffer (0.1% [w/v] digitonin, 20 mM Tris-HCl [pH 7.4], 50 mM NaCl, 10% glycerol, 0.1 mM EDTA, 1 mM PMSF) and proteins were eluted in 200 µL of 1x SDS sample buffer and afterwards supplemented with 1% (v/v) of β-mercaptoethanol.

SDS-PAGE and tryptic in-gel digestion

Mixtures of crude mitochondrial fractions and gradient-purified mitochondria obtained in pure/crude experiments (n = 4) were boiled in SDS sample buffer for 5 min at 94°C. Proteins (25 µg each per gel lane) were separated on 4 - 12% NuPAGE™ Bis-Tris and Novex™ 16% Tricine gels (Thermo Fisher Scientific) according to the manufacturer's protocol. Following visualization of proteins using colloidal Coomassie Brilliant Blue, gel lanes were cut into 18 slices of equal size. Slices were washed and destained by alternatingly incubating them with 10 mM NH_4HCO_3 and 50% (v/v) acetonitrile (ACN)/10 mM NH_4HCO_3 (10 min at RT each). Cysteine residues were reduced (10 mM DTT/10 mM NH_4HCO_3, 30 min at 56°C) and alkylated (50 mM iodoacetamide/10 mM NH_4HCO_3; 30 min at RT in the dark) followed by proteolytic digestion of proteins using trypsin (60 ng per slice; overnight at 37°C). Peptides were eluted with 0.05% (v/v) trifluoroacetic acid (TFA)/50% (v/v) ACN, dried *in vacuo* and resuspended in 15 µL 0.1% TFA prior to LC-MS analysis. Samples obtained in submitochondrial profiling experiments (n = 3; 25 µg of mixed treated and untreated mitochondria per gel lane) were separated using 4 - 12% NuPAGE Bis-Tris gradient gels and processed as described above except that lanes were cut into 24 slices each.

Proteolytic in-solution digestion

Proteins of pure/crude, subcellular profiling, and q-AP-MS experiments were acetone-precipitated and resuspended in 8 M urea/50 mM NH_4HCO_3. Samples of the absolute quantification experiment were adjusted to 8 M urea and 50 mM NH_4HCO_3 by directly adding the required amounts of the chemicals to the samples. Cysteine residues were reduced with 5 mM Tris(2-carboxyethyl)phosphine (30 min, 37°C) and free thiol groups were subsequently alkylated with 50 mM iodoacetamide/50 mM NH_4HCO_3 (30 min at RT in the dark). The alkylation reaction was quenched by adding DTT to a final concentration of 25 mM. For proteolytic digestion, urea concentration was adjusted to 4 M (LysC), 1.6 M (trypsin), or 1 M (AspN, chymotrypsin, GluC) using 50 mM NH_4HCO_3. Proteases were added at a

protease-to-protein ratio of 1:50 for trypsin, 1:100 for chymotrypsin, LysC, and GluC, or 1:150 for AspN. Proteins were digested overnight at 37°C. In case of LysC/trypsin double-digestion, incubation with LysC was performed for 4 h (37°C) followed by incubation with trypsin overnight (37°C). Proteolysis was stopped by acidifying the samples with 100% TFA. For the direct analysis (i.e. without further sample fractionation, referred to as '1-shot' analysis) of peptides from pure/crude and subcellular profiling experiments, 10 µg of protein were digested. Acidified peptides were cleared by centrifugation (5 min, 12,000 x g, RT) and one-fifth of each digest was analyzed by LC-MS. For the analysis of peptide samples that were further fractionated by strong cation exchange chromatography (SCX) or high pH reversed-phase (RP) chromatography, 300 µg of protein were digested and peptides were desalted using C18 cartridges (3M Empore, St. Paul, USA) according to the manufacturer's protocol and dried *in vacuo*.

Strong cation exchange chromatography

Dried peptides of tryptic, chymotryptic, AspN, LysC, and GluC digests of differentially SILAC-labeled, mixed crude and gradient-purified mitochondria from pure/crude experiments (n = 4) were resuspended in 500 µL SCX buffer (10 mM KH_2PO_4 [pH 3.0], 25% [v/v] ACN) and loaded onto cation exchange mini-columns (POROS™ 50 HS strong cation exchange resin; 4 x 15 mm; particle size, 50 µm; AB Sciex) equilibrated with SCX buffer. Peptides were eluted step-wise with 35, 55, 75, 100, 125, 150, 200, 250 and 350 mM KCl in SCX buffer (500 µL each). The resulting nine fractions were lyophylized. Peptides were resuspended in 500 µL 0.5% (v/v) acetic acid, desalted using StageTips, dried in vacuo, and resuspended in 60 µL of 0.1% TFA, of which 15 µL were analyzed by LC-MS.

High pH reversed-phase chromatography

High pH RP chromatography (Delmotte et al., 2007; Lasaosa et al., 2009) was used for the fractionation of peptides derived from pure/crude samples and from samples of the absolute quantification experiment. Tryptic peptides of mitochondrial fractions were resuspended in 99% solvent A (72 mM triethylamine, 52 mM acetic acid, pH 10) and 1% solvent B (72 mM triethylamine and 52 mM acetic acid in ACN) and loaded onto a Gemini-NX column (150 mm x 2 mm inner diameter, particle size 3 µm, pore size 110 Å; Phenomenex, Aschaffenburg, Germany) using an Ultimate 3000 HPLC system (Thermo Fisher Scientific, Dreieich, Germany) at a flow rate of 200 µL/min and a column temperature of 40°C. For peptide separation, a gradient of 1 - 55% solvent B (starting after 5 min) in 55 min followed by 55 - 70% B in 2 min and 2 min at 70% B was used. Fractions were collected in 30 s intervals starting at minute 8.5 and ending at minute 56.5 and pooled into 30 non-contiguously concatenated fractions by combining

every 30st fraction. Peptides of mixed cell lysates, generated by a LysC/trypsin double digestion, were resuspended in 99% solvent A' (10 mM NH_4OH, pH 10) and 1% solvent B' (10 mM NH_4OH in 90% [v/v] ACN) and loaded onto a Gemini-NX column as described above. Peptides were eluted by applying a gradient of 1 - 54% solvent B' (starting after 5 min) in 53 min followed by 54 - 78% B' in 5 min, 5 min at 78% B', and 78 - 1% B' in 7 min. Fractions were collected in 40 s intervals between minute 1 and minute 73 in a non-contiguous, concatenated way resulting in a total of 12 fractions. Peptides of all high pH RP chromatography experiments were lyophylized, washed with 70% (v/v) ACN, dried again *in vacuo*, and resuspended in 60 µL (pure/crude experiments) or 150 µL (absolute quantification experiments) of 0.1% TFA, of which 15 µL were analyzed by LC-MS.

LC-MS analysis

Peptide mixtures were analyzed by nano-HPLC-ESI-MS/MS using an LTQ Orbitrap XL, an Orbitrap Elite, or a Q Exactive instrument (Thermo Fisher Scientific, Bremen, Germany) each directly coupled to an UltiMate 3000 RSLCnano HPLC system (Thermo Fisher Scientific, Dreieich, Germany). Peptides were washed and preconcentrated on PepMap™ C18 precolumns (5 mm x 300 µm inner diameter; Thermo Scientific) and separated using AcclaimPepMap™ RSLC columns (50 cm x 75 µm inner diameter; pore size, 100 Å; particle size, 2 µm) at a flow rate of 250 nl/min and 40 - 43°C. For peptide elution, binary solvent systems were used consisting of (i) 0.1% (v/v) formic acid (FA)/4% (v/v) DMSO (solvent A) and 0.1% (v/v) FA/4% (v/v) DMSO/48% (v/v) methanol/30% (v/v) ACN (solvent B) for LC-MS analyses using the LTQ Orbitrap XL and Orbitrap Elite or (ii) 0.1% (v/v) FA (solvent A') and 0.1% (v/v) FA/86% (v/v) ACN (solvent B') for measurements using the Q Exactive. Length and slope of the gradients were adjusted according to the complexity of individual samples. Peptide mixtures of pure/crude experiments, obtained following various protein and peptide fractionation methods, were analyzed at the Orbitrap Elite using the LC gradients detailed in the following. Tryptic peptides, analyzed without fractionation, were eluted with a gradient of 5 - 25% solvent B in 115 min followed by 25 - 45% in 110 min, 45 - 60% in 50 min, 60 - 80% in 20 min, 80 - 99% in 10 min, and 5 min at 99%. Peptides derived from tryptic in-gel digests were separated with 1 - 65% solvent B in 50 min, 65 - 95% in 5 min and 5 min at 95%. For the separation of peptides collected by high pH RP chromatography, a gradient ranging from 1 - 67.5% solvent B in 50 min, 67.5 - 95% in 5 min, and 5 min at 95% was applied, and peptides of SCX samples were eluted with 1 - 40% solvent B in 55 min followed by 40 - 70% in 30 min, 70 - 99% in 10 min, and 5 min at 99%. Separation of tryptic peptides of absolute quantification experiments, analyzed at the Q Exactive, was performed using a gradient of 4 - 39% solvent B' in 195 min, 39 - 54% in 15 min, 54

- 95% in 5 min, and 5 min at 95%'. Tryptic peptides of subcellular profiling experiments, analyzed without fractionation at the Orbitrap Elite, were separated by applying a gradient ranging from 1 - 25% solvent B in 115 min, 25 - 45% in 110 min, 45 - 60% in 50 min, 60 - 80% in 20 min, 80 - 99% in 10 min, and 5 min at 99%. Tryptic peptides derived from submitochondrial profiling experiments were eluted with a gradient ranging from 1 - 65% solvent B in 70 min, 65 - 95% in 5 min, and 5 min 95% followed by MS analysis at the Orbitrap Elite (replicates 1 and 2) or with 4 - 40% solvent B' in 50 min, 40 - 95% in 5 min and 5 min at 95% when analyzed at the Q Exactive (replicate 3). For the separation of peptides from q-AP-MS experiments, a gradient of 1 - 30% solvent B in 65 min, 30 - 45% in 30 min, 45 - 70% in 25 min, 70 - 99% in 15 min, and 5 min at 99% was applied followed by MS analysis at the Orbitrap Elite (Aim11, Coq21, Iai11, Rci37 and Rcf3 complexes) or the LTQ Orbitrap XL (Mco10 and Rci50 complexes). Replicate 1 of Coq21, Rci37, and Rcf3 complexes were analyzed in two technical replicates.

Mass spectrometers were equipped with a Nanospray Flex ion source with DirectJunction (Thermo Scientific; Q Exactive and Orbitrap Elite) or a Finnigan Nanospray ion source with dynamic NSI probe (Thermo Scientific; LTQ-Orbitrap XL) and stainless steel (Thermo Scientific) or fused silica emitters (New Objective, Woburn, USA). MS instruments were externally calibrated using standard compounds. The Orbitrap Elite was operated with the following mass spectrometric parameters: MS survey scans ranging from *m/z* 370 - 1,700 were acquired in the orbitrap at a resolution (R) of 120,000 (at *m/z* 400). Automatic gain control (AGC) was set to 1×10^6 ions and the maximum injection time (IT) to 200 ms. A TOP15 (samples of pure/crude experiments fractionated by SDS-PAGE), TOP20 (pure/crude samples fractionated by high pH RP and samples of submitochondrial profiling experiments), or TOP25 method (all other samples) was used for low energy collision-induced dissociation (CID) of multiply charged precursor peptides in the linear ion trap applying a normalized collision energy (NCE) of 35%, an activation q of 0.25, an activation time of 10 ms, an AGC of 5×10^3, and a max. IT of 150 ms. Singly charged precursor peptides were generally rejected from fragmentation, except for the analysis of samples derived from SCX experiments, which were additionally analyzed allowing fragmentation of singly charged precursor peptides to increase the likelihood to identify small mitochondrial proteins. The dynamic exclusion time (DE) for previously fragmented precursors was set to 45 s. For analyses at the Q Exactive, the following parameters were applied: MS scans, *m/z* 375 - 1,700; R, 70,000 (at *m/z* 200); AGC, 3×10^6 ions; max. IT, 60 ms; TOP12 (samples of submitochondrial profiling experiments) or TOP15 method (samples of absolute quantification experiments) for higher energy collisional dissociation (HCD) of precursor peptides ($z \geq 2$) in the orbitrap; NCE, 28%; AGC, 1×10^5 ions, max. IT, 120 ms; DE, 45 s. LTQ Orbitrap XL parameters were as follows: MS scans, *m/z* 370 - 1,700; R, 60,000 (at *m/z* 400); AGC, 5

x 10^5 ions; max. IT, 500 ms; TOP5 CID method for fragmentation of precursor peptides ($z \geq 2$); NCE, 35%; activation q, 0.25; activation time, 30 ms; AGC, 1 x 10^4 ions, max. IT, 100 ms; DE, 45 s.

MS data analysis

For peptide and protein identification and quantification, mass spectrometric raw data were processed using the MaxQuant software package (version 1.5.3.12) with its integrated search engine Andromeda (Cox and Mann, 2008; Cox et al., 2011). MS/MS data of different experiments (i.e., pure/crude, absolute quantification, subcellular and submitochondrial profiling, and q-AP-MS experiments) were searched separately against a custom-made protein database containing all entries of the *Saccharomyces* Genome Database (SGD; http://www.yeastgenome.org/, downloaded 02/04/2016; 6,726 entries including protein sequences of verified, uncharacterized, and dubious open reading frames [ORFs]) and 47 entries for putative small ORFs reported by Smith et al. (2014). Data were also correlated with a list of common contaminants provided by MaxQuant. Database searches were performed with mass tolerances of 4.5 ppm for precursor and 0.5 Da (CID data) or 20 ppm (HCD data) for fragment ions and the appropriate enzymatic specificity allowing two (AspN), three (trypsin/P, LysC), or four missed cleavages (chymotrypsin, GluC). The cleavage sites for chymotrypsin were defined as C-terminal to tyrosine, phenylalanine, tryptophan, leucine, and methionine. Acetylation of protein N-termini and oxidation of methionine were considered as variable and carbamidomethylation of cysteine residues as fixed modification. Arg10 and Lys8 were set as heavy labels and Arg6/Lys4 as medium-heavy labels. The options 'requantify', 'match between runs' (match from and to), and 'iBAQ' were generally enabled except for the analysis of data from subcellular profiling experiments ('requantify' disabled) and submitochondrial profiling experiments ('match between runs' and 'iBAQ' disabled). For the analysis of data from submitochondrial profiling experiments, which were analyzed following a gel-based approach, each gel slice (n = 24 per replicate; 3 replicates) was defined as individual 'experiment' in the experimental design template. Proteins were identified based on at least one unique peptide with a length of six amino acids and a maximum mass of 4,600 Da or 6,000 Da (for data from pure/crude experiments only). Lists of peptides and proteins identified by MaxQuant were filtered applying a false discovery rate of 0.01. Proteins identified by the same set of peptides were combined to a single protein group by MaxQuant. For SILAC-based protein quantification, at least one unique peptide and a minimum ratio count of one were required. Lists of all proteins identified and quantified in individual experiments are provided in Table S2A (subcellular profiling), S2B and S2C (pure/crude data), S2D and S2E

(absolute proteome quantification under fermentable and non-fermentable growth conditions), S2F - S2H (submitochondrial profiling), and S2I (q-AP-MS data).

Mean protein abundance ratios for pure/crude experiments (n = 4) were calculated based on normalized peptide SILAC ratios determined by MaxQuant. For each replicate, the logarithmic pure/crude ratio (normalized) for a protein was computed as the median of log2 peptide ratios across values obtained for all different fractionation techniques. Ratios for two of the four replicates were inverted to account for the label switch. MaxQuant additionally reports non-normalized peptide ratios. In cases when the major population of proteins remains unchanged in abundance, the normalization may compensate for slight differences in the mixing of differentially SILAC-labeled samples by shifting the values to a median logarithmic ratio of zero per experiment. In the pure/crude experiment, however, the distribution of logarithmic ratios is not unimodal and includes a major population reflecting proteins of higher abundance in crude mitochondrial fractions compared to gradient-purified mitochondria with log pure/crude ratios < 0 (see *'Classification of proteins of the pure/crude dataset*' in 'Bioinformatics and statistics'). To take into account the bimodal distribution of the values, log pure/crude protein ratios based on normalized peptide ratios were subsequently shifted back by calculating the mean difference between normalized and non-normalized protein ratios for each replicate and subtracting the mean of that differences determined across all replicates.

For visualization of pure/crude data, mean $\log_2$ ratios (pure/crude) were plotted against mean $\log_2$ iBAQ values. Only proteins that were quantified in all four biological replicates with at least two fractionation techniques were considered for subsequent statistical and bioinformatics data analyses.

Protein copy numbers for cells grown on galactose, glycerin, or glucose were determined based on the MS intensities for light, medium-heavy, and heavy SILAC-labeled proteins according to the 'Proteomic Ruler' strategy (Wiśniewski et al., 2014) using Perseus (Tyanova et al., 2016) with the 'protemic ruler' plugin.

The analysis of data obtained in subcellular profiling experiments was based on MS intensities determined for proteins identified in cell lysates, the non-mitochondrial fraction PMS, crude and gradient-purified mitochondria. MS intensities of proteins in distinct subcellular fractions were normalized to the total intensity per fraction. For each protein and fraction, the mean of the normalized intensities across all replicates (n = 2 - 4) was determined. For visualization, the value of the subcellular fraction with the highest mean normalized intensity was set to one (see Figures 1B, 4E, and S5).

The setup of the MaxQuant analysis of data derived from submitochondrial profiling experiments enabled the quantification of each protein in each of the 24 gel slices per replicate. For each protein, the slice with the highest intensity for M (i.e., untreated gradient-purified mitochondria, serving as control) was determined and the SILAC

ratio for this slice was used for further data processing. In case a protein was missing from treated mitochondria in S1, S2, and S3 due to digestion by the proteases added to the sample and, thus, an S/M protein ratio could not be calculated for a slice, the ratio for this protein was set to 0.01. Mean SILAC ratios across all replicates (n = 2 - 3) were determined. For this, only ratios from adjacent gel slices were taken into account. For further bioinformatics analyses, proteins were required to exhibit ratios for all three experimental conditions in at least two replicates. Data used to analyze the topology of membrane proteins were derived from the MaxQuant peptides.txt results file. Putative membrane proteins were determined based on TMHMM predictions (information was retrieved from the SGD). For each peptide of these proteins, the intensities for each S1, S2, S3, and M across all gel slices were summed up and mean S/M intensity ratios per replicate were determined. In case a peptide intensity was given for M but missing for S, the S/M ratio was set to 0.01. For peptides quantified in at least two replicates, mean S/M intensity ratios across replicates were calculated. In peptide plots, the highest value was set to 1.3 (see Figures 5E and 5F).

Bioinformatics and statistics

Gene Ontology annotations. GO annotations for the domains 'biological process' (BP), 'cellular component' (CC) and 'molecular function' (MF) including child terms were downloaded from the SGD (date of download: 12/08/2016). To compile a list of proteins annotated as mitochondrial in the SGD, all entries of the database were searched for the GOCC term 'mitochondrion' (GO:0005739) including its child terms. The resulting list contained 1,178 proteins. To obtain information about mitochondrial subproteomes, we retrieved proteins annotated as OM (GO:0005741; 107 proteins), intermembrane space (IMS; GO:0005758; 61), inner membrane (IM; GO:0005743; 253), and matrix proteins (GO:0005759; 226). To compare the protein composition of crude mitochondrial fractions (Mito) and gradient-purified mitochondria (pMito), proteins identified in pure/crude experiments were assigned to a distinct subcellular localization based on GOCC terms (see Fig. 2B, Table S2B). Intensity-based absolute quantification (iBAQ) values, calculated by MaxQuant, were used as a measure for the abundance of proteins in crude and pure mitochondria. For each protein and replicate (n = 4), iBAQ values determined for different fractionation strategies were averaged and the mean across the replicates was calculated for pure and crude mitochondria. Mean iBAQ values of all proteins assigned to a distinct subcellular localization were summed up and the percentage of the overall iBAQ value in crude or pure mitochondria was determined.

Classification of proteins of the pure/crude dataset. Proteins quantified with at least two different fractionation techniques in all four replicates of pure/crude experiments (i.e., 3,365 proteins) were classified based on their

pure/crude SILAC ratios (log_2 values). To test for multimodal distribution of the pure/crude data, the 'Hartigan's dip test' was performed (using the 'bimodalitytest' package for R) and revealed two distributions with centers at mean log_2 (pure/crude) of -1.47 for distribution 1 (d1) and 0.31 for d2 (see Fig. S2H). The standard deviation was 0.83 for d1 and 0.08 for d2. For each distribution, 1,000,000 theoretical values were generated taking into account the respective standard deviations. We next determined for each protein present in the dataset to which of the two distributions it belongs using a two-sample two-sided equivalence test (R package 'equivalence') with a significance threshold (p value) of < 0.01. As a result, 544 proteins were assigned to d1 and 812 proteins to d2 (see Table S2B). The remaining proteins were classified based on a two-sample two-sided t test (p value < 0.01; R package 'stats'). 34 of these proteins were determined to be outliers of d1 only and, thus, assigned to d2. *Vice versa*, 1,515 proteins were outliers of d2 only and assigned to d1. 460 proteins were outliers of both d1 and d2. These proteins were distributed at ratios < d1 (referred to as OL1), between d1 and d2 (OL2), and at ratios > d2 (OL3). Based on this classification, four distinct classes were defined for the pure/crude dataset: proteins of d2 and OL3 were combined to class 1 and proteins of OL2, d1, and OL1 are defined as class 2, class 3, and class 4, respectively. Proteins of class 1 were further filtered based on sequence coverage and standard deviation calculated for mean log_2 (pure/crude) abundance ratios across all replicates, i.e. proteins with a sequence coverage of < 20% and a standard deviation of > 0.75 were removed (i.e., 113 proteins).

Clustering analysis. Data obtained in absolute quantification and submitochondrial profiling experiments (see Figs. 3 and 5) were subjected to *k*-means clustering to group proteins showing similar characteristics and low variance in the respective experiment. For absolute quantification experiments, clustering was based on absolute protein copy numbers determined for yeast grown on galactose (Gal), glycerin (Gly), or glucose (Glc). Only proteins for which copy numbers were determined for all carbon sources in all replicates (n = 3) were considered. For each protein, ratios of mean log_2 copy numbers Gal/Glc and Gly/Glc were calculated. To reveal proteins with significant carbon source-dependent changes in copy numbers, an analysis of variance (ANOVA) test was performed between the Gal/Glc and Gly/Glc data (R package 'stats'). 1,576 proteins showed significant differences (p value $\geq$ 0.05) in protein copy numbers and were used for the *k*-means clustering analysis ('stats' package). The Davies-Bouldin index was used to determine the optimal number of clusters for this dataset (i.e., k = 14). Information about the proteins present in the clusters are provided in Table S2D. The clustering analysis of data from submitochondrial profiling experiments was based on SILAC ratios determined in protease accessibility assays for proteins of gradient-purified mitochondria treated with proteases (S1), digitonin and proteases (S2), or Triton X-100 and proteases (S3) versus

untreated mitochondria (M). For clustering, only proteins of class 1 as determined in pure/crude experiments that had S/M ratios for all three experimental conditions (i.e., S1 - S3) in at least two replicates (n = 3) were considered. Furthermore, proteins were required to (i) exhibit mean S/M ratios ≤ 1.1 (since due to the experimental design S/M ratios should not exceed a value of 1) and (ii) be decreased in abundance with increasing protease-accessibility of proteins (S3 > S2 > S1) with a tolerance of ± 0.2. A total of 624 proteins met all criteria and were subjected to *k*-means clustering into 5 clusters, which was determined to be the optimal cluster number for this dataset. Information about the proteins present in the clusters are provided in Table S2F. Clusters defined for both absolute quantification and submitochondrial profiling experiments were further clustered by hierarchical clustering using the mean ratio of each cluster to reveal (dis)similarities between individual clusters ('stats' package).

Gene Ontology overrepresentation analysis. GO term overrepresentation analyses were based on GO terms retrieved from the SGD and were performed with an in-house developed script using all proteins quantified in the respective dataset as background. The two-sided Fisher's exact test was used to calculate mid p values. Raw mid p values were corrected for multiple testing by Benjamini-Hochberg adjustment and GO terms with a corrected mid p value of < 0.05 were considered enriched.

Principal component analysis. Proteins present in the OM, IMS/IM, and matrix/IMS clusters of the submitochondrial profiling experiment (see Fig. 5C) and further proteins meeting the criteria for signature plots (i.e. S1/M < 0.25 for OM proteins; S1/M > 0.25 and S2/M < 0.25 IMS/IM proteins; S1/M and S2/M > 0.25, S3/M < 0.25 for matrix/IM proteins) were subjected to principal component analysis. To this end, S1/M, S2/M, and S3/M protein ratios were $\log_2$-transformed, analyzed using the R package 'stats' with the parameters 'center' and 'scale.' set to 'true', and visualized in two-dimensional scores plots depicting the two principal components providing the best visual separation of protein clusters on the x- and y-axes.

Further bioinformatics tools. An in-house developed software based on R was used to process MaxQuant result files, visualize data, and subsequently analyze the data using statistical and bioinformatics means as described. The following R packages were used: base, bimodalitytest, Biobase, clusterSim, clustpro, convert, curl, data.table, datasets, Deducer, devtools, diptest, dplyr, equivalence, flux, gage, GGally, ggbiplot, ggplot2, gplots, graphics, grDevices, grid, gtools, Hmisc, lattice, methods, outliers, pastecs, plotrix, reshape, reshape2, ROCR, scales, silvermantest, stats, stringr, utils, VennDiagram, Vennerable and xtable. Prediction of N-terminal mitochondrial targeting sequences was performed using MitoFates (Fukasawa et al., 2015). For sequence homology searches the HMMER web server was employed (Fin et al., 2015).

Subcellular in vivo localization of uncharacterized GFP-tagged proteins

C-terminally GFP-tagged yeast strains were grown over night in 50 mL YPD medium at 30°C to an OD_{600} of 1.0. Subsequently, 2 OD_{600} of yeast cells were harvested, washed with dH_2O and suspended in 500 µL dH_2O. 3 µL of yeast cell solution was dispersed on a microscope slide (Diagonal), covered with a microscope cover glass (Diagonal) and samples were analyzed immediately. Fluorescence microscopy was performed using the Olympus BX61 microscope (Olympus K.K.) equipped with the immersion oil objective UPLFLN 100x/1.3 (Olympus K.K.). Visualization of GFP was carried out using the 470/40 nm bandpass excitation filter, a 495 nm dichromatic mirror and a 525/50 nm bandpass emission filter. All digital recordings of cells were taken with the F-view CCD camera (Olympus Soft-Imaging Solutions GmbH) controlled by the Cell-P software (Olympus K.K.).

Strains expressing N-terminally GFP-tagged mitochondrial proteins under the control of their native or the *sp*NOP1 promoter were grown in synthetic defined (SD) complete or SD -URA medium. Imaging of the strains was performed using a wide-field epi-fluorescent Olympus microscope with a 60X air objective (excitation, 490/20 nm; emission, 535/50 nm).

***In vitro* import of radiolabeled precursor proteins into mitochondria**

[^{35}S]-labeled precursor proteins were synthesized using the TnT® Quick Coupled Transcription/Translation System (Promega GmbH) or the Flexi® Rabbit Reticulocyte Lysate System (Promega GmbH). To this end, a PCR template encoding the respective ORF under the SP6 promoter was generated from yeast chromosomal DNA using forward primers containing the SP6 promoter followed by a sequence that corresponds to the 5'-UTR of the respective ORF and reverse primers that bind to the 3'-end of the ORF. The *TMH11* ORF was amplified from yeast chromosomal DNA and cloned into pGEM-4Z plasmid (Promega) using EcoRI and HindIII restriction enzymes. Transcription of respective ORFs from PCR templates was performed using the mMESSAGE mMACHINE® SP6 Transcription Kit (Thermo Fisher Scientific Inc.) and RNA was purified using the MEGAclear™ Transcription Clean-Up Kit (Thermo Fisher Scientific Inc.). The RNA served as template for *in vitro* translation reactions. For generation of [^{35}S]Ybl039w-b, [^{35}S]Ykl023c-a, [^{35}S]Ykl065w-a, [^{35}S]Yor114w and [^{35}S]Yjr085c the PCR templates or the pGEM-4Z-Yjr085c plasmid were directly added to the TnT® Quick Coupled Transcription/Translation System.

For import of radiolabeled precursor proteins, mitochondria were suspended in import buffer (3% [w/v] bovine serum albumin, 250 mM sucrose, 80 mM KCl, 5 mM $MgCl_2$, 5 mM methionine, 2 mM KP_i, 10 mM MOPS-KOH

[pH 7.2]) supplemented with 4 mM ATP, 4 mM NADH and an ATP regenerating system (200 µg/mL creatine kinase, 10 mM creatine phosphate). Where indicated, membrane potential across the inner mitochondrial membrane was dissipated prior to import (–Δψ). To this end, import buffer was instead supplemented with 4 mM ATP, 1 µM valinomycin, 8 µM antimycin A, and 20 µM oligomycin (final concentrations). Import reaction was started by the addition of 5-10% [v/v] of *in vitro* translation/lysate system. If not stated otherwise, import in the presence of membrane potential (+Δψ) was stopped after 30 min by the addition of 1 µM valinomycin, 8 µM antimycin A, and 20 µM oligomycin (final concentrations). Mitochondria were pelleted by centrifugation, washed with SEM buffer and suspended in 48 µL of SEM buffer. Where indicated, mitochondria were subjected to hypoosmotic swelling and/or protease treatment (7 µg/mL in SEM or EM buffer, see above). After inhibition of proteinase K activity by 2 mM PMSF, mitochondria were re-isolated and analyzed by SDS-PAGE or blue native gel electrophoresis and digital autoradiography.

Analysis of protein complexes by Blue Native gel electrophoresis

Mitochondria were solubilized in 1% digitonin buffer (20 mM Tris-HCl [pH 7.4], 0.1 mM EDTA, 50 mM NaCl, 10% [v/v] glycerol, 1% [w/v] digitonin, 1 mM PMSF) and incubated for 15 min on ice. Non-solubilized material was removed by centrifugation, blue native loading dye was added (final concentration: 100 mM Bis-Tris-HCl [pH 7.0], 50 mM ε-amino n-caproic acid, 0.5% [w/v] Coomassie G-250) and samples were subjected to 6–16.5 or 3–13% discontinuous polyacrylamide gels.

Generation of whole yeast cell extracts of *S. cerevisiae*

S. cerevisiae cells were grown overnight in 5-7 mL of YPG or YPD medium in 13 mL cell culture tubes (Sarstedt AG & Co. KG, 62.515.006). 2.5 OD_{600} of cells were pelleted (4,000 x g for 2 min at 25°C) and suspended in 200 µL of 100 mM NaOH, followed by 5 min incubation at 25°C (Kushnirov, 2000). Cells were collected by centrifugation (4,000 x g for 2 min at 25°C), suspended in 75-150 µL of 2x SDS sample buffer supplemented with 2% (v/v) β-mercaptoethanol and incubated at 95°C for 3 min. Samples were centrifuged at 13,000 x g for 5 min at 25°C and a fraction of the supernatant was subjected to SDS-PAGE.

Miscellaneous

Radiolabeled proteins that had been separated by blue native gel electrophoresis or SDS-PAGE were visualized by autoradiography using the FLA-9000 (Fujifilm Holdings K.K.) and Typhoon FLA 7000 (GE Healthcare AG) image scanners as well as the Multi Gauge (Fujifilm) or ImageJ 1.49v software.

PCR primers used in this study

Name	Sequence (5'→ 3')	Description
S3-Aim11_fw	TAAGCAATTGCAAGACCTCCTGT CGAGCGAAAACAACAAGCGTAC GCTGCAGGTCGAC	Amplification of *TEV-ProtA-7HIS-kanMX6* fragment from pYM9 plasmid with N-terminal overhang for 3'-end of *AIM11* ORF and C-terminal overhang for *AIM11* terminator
S2-Aim11_rv	CATTATTTACAGTTTAAAGAGAT TAAGCCAATGCGTAGTGATCGAT GAATTCGAGCTCG	
S3-DEG1_fw	ATGGAACCTGTCGAAGTTGTTAA TGCTAAATACTCCAAGAAAAAGA ACAACAAAAATAAGCGTACGCTG CAGGTCGAC	Amplification of *TEV-ProtA-7HIS-hphNT1* fragment from pFA6a-TEV-ProtA-7His-hphNT1 plasmid with N-terminal overhang for 3'-end of *DEG1* ORF and C-terminal overhang for *DEG1* terminator
S2-DEG1_rv	AGCACGTGATGAAAAGAAATATA GTCTTCAAGGTTATATTATACAG GTTTATATATTATTATCGATGAAT TCGAGCTCG	
S3-ECM4_fw	ACAAGGATCAACCCCTTGGGAAT TACGCCCCTGGGACCCAAGCCAG ATATTCGTCCTTTACGTACGCTGC AGGTCGAC	Amplification of *TEV-ProtA-7HIS-hphNT1* fragment from pFA6a-TEV-ProtA-7His-hphNT1 plasmid with N-terminal overhang for 3'-end of *ECM4* ORF and C-terminal overhang for *ECM4* terminator
S2-ECM4_rv	GTATAGAAAAAGAGGCAACTCA GGGAGATTATAGACATTTGATTA TTTAATTACAGCTTGATCGATGA ATTCGAGCTCG	
S3-ECM19_fwd	TTATCATCCACACCAGCTGCACC ACCTACACCACCTACACCTCCTA CTCCACCACAACAGCGTACGCTG CAGGTCGAC	Amplification of *TEV-ProtA-7HIS-hphNT1* fragment from pFA6a-TEV-ProtA-7His-hphNT1 plasmid with N-terminal overhang for 3'-end of *ECM19* ORF and C-terminal overhang for *ECM19* terminator
S2-ECM19_rev	TTTACTATTGATGCTATATACAGG AAAAGAAAGTATAGAGGTATTTT CTAGTACGCTTCCATCGATGAAT TCGAGCTCG	
S3-FMP16_fw	TTGAAAAAAAAGGGAGATGACG CTAGAATCGAACAAAACAGGCCA GATGACGGTGTTTATCGTACGCT GCAGGTCGAC	Amplification of *TEV-ProtA-7HIS-kanMX6* fragment from pYM9 plasmid with N-terminal overhang for 3'-end of *FMP16* ORF and C-terminal overhang for *FMP16* terminator
S2-FMP16_rv	GAATATAGATATGTGTATGACAG AAACTACATGCATATACGAGTTT GTACCAAGTGCTTCATCGATGAA TTCGAGCTCG	
S3-FYV4_fwd	TTTGGTGGTGAGAGGAAGAGAAA GGCATTTACTGCTAAATGGAAAG CTGAAAACAAGCAACGTACGCTG CAGGTCGAC	Amplification of *TEV-ProtA-7HIS-hphNT1* fragment from pFA6a-TEV-ProtA-7His-hphNT1 plasmid with N-terminal overhang for 3'-end of *FYV4* ORF and C-terminal overhang for *FYV4* terminator
S2-FYV4_rev	TATGGAGTATAATGTGAACATAT ACGTATACATGTATATATTGAGA TCTTGCGAAAGCGTATCGATGAA TTCGAGCTCG	
S3-MEU1_fw	CCAGAGGCTATGTCCAAGGAAAC CTTAGAAAGACTAAGATACTTAT TTCCAAACTATTGGCGTACGCTG CAGGTCGAC	Amplification of *TEV-ProtA-7HIS-hphNT1* fragment from pFA6a-TEV-ProtA-7His-hphNT1 plasmid with N-terminal overhang for 3'-end of *MEU1* ORF and C-terminal overhang for *MEU1* terminator
S2-MEU1_rv	TTCCATAGCTATATATGTTTTCTC TCCTATTTATATTTTACATATGAT	

	TAGCGGCAACCAATCGATGAATT CGAGCTCG	
S3-MLO1_fwd	AATATGAAATCGGGTAGTAGGTT CAGTCACCCCAGCTTTAAACAAT TGTTAATACAGAAGCGTACGCTG CAGGTCGAC	Amplification of *TEV-ProtA-7HIS-hphNT1* fragment from pFA6a-TEV-ProtA-7His-hphNT1 plasmid with N-terminal overhang for 3'-end of *MLO1* ORF and C-terminal overhang for *MLO1* terminator
S2-MLO1_rev	ATGATCGGAAGAAACGGTGTGCG CGGCGGAGGGAAGCGAAAAATT GGGAAACGGAAGCAAATCGATG AATTCGAGCTCG	
S3-MTC3_fwd	ACTGCATTTTATAATTGGAAACA AGATAAAAAGCTAGAGGAACAA TTAAGGGATCTTGTACGTACGCT GCAGGTCGAC	Amplification of *TEV-ProtA-7HIS-hphNT1* fragment from pFA6a-TEV-ProtA-7His-hphNT1 plasmid with N-terminal overhang for 3'-end of *MTC3* ORF and C-terminal overhang for *MTC3* terminator
S2-MTC3_rev	AAATGAATAGAACGTACTCTGCG CAAGCGCATATATATATATACTA TTGTTGCTTCCAATATCGATGAAT TCGAGCTCG	
S3-NCE101_fw	TTTACACGAGCTCATAAAGAAGC GATGGGACGATCGCAAACGTACG CTGCAGGTCGAC	Amplification of *3HA-kanMX6* fragment from pYM1 plasmid with N-terminal overhang for 3'-end of *FMP16* ORF and C-terminal overhang for *FMP16* terminator
S2-NCE101_rv	ATCGCCAGAAACTTATATATACT CCCCTCACGCCGGATTAATCGAT GAATTCGAGCTCG	
S3-PXP2_fw	TTGGCTATACTAATATCTCAGTG GTGTGGTGTTAGTTGGAAATCTG GTGTTGTAAAATTGCGTACGCTG CAGGTCGAC	Amplification of *TEV-ProtA-7HIS-hphNT1* fragment from pFA6a-TEV-ProtA-7His-hphNT1 plasmid with N-terminal overhang for 3'-end of *PXP2* ORF and C-terminal overhang for *PXP2* terminator
S2-PXP2_rv	TTTTAATGAATAAGGGTACATAT ATTATGAGCATAACGAGTGGCCG ATCGGCAAAGGGGCATCGATGAA TTCGAGCTCG	
S3-RDL2_fwd	TATCCTGGTTCTATTACTGAGTGG TTAGCTAAAGGTGGTGCTGACGT TAAGCCCAAAAAACGTACGCTGC AGGTCGAC	Amplification of *TEV-ProtA-7HIS-kanMX6* fragment from pYM9 plasmid with N-terminal overhang for 3'-end of *RDL2* ORF and C-terminal overhang for *RDL2* terminator
S2-RDL2_rev	GAAATACACAAAAGGTTGTCTAT ATACAGGATATATCGATTATACT TGTTTCTTTTTGGCATCGATGAAT TCGAGCTCG	
S3-Rrg9_fwd	CAACAAACTATACATTTTGAAGC ATTTGGGCTCGAAACAACGTACG CTGCAGGTCGAC	Amplification of *TEV-ProtA-7HIS-kanMX6* fragment from pYM9 plasmid with N-terminal overhang for 3'-end of *RRG9* ORF and C-terminal overhang for *RRG9* terminator
S2-Rrg9_rev	ACAAGAAGTTTCGTAATAATATA TAAATCCCTCAAAAGTGATCGAT GAATTCGAGCTCG	
S3-SMM1_fw	ACCGATCACATAGGCAGTGACAC TAAAAAGCAAAAGGTTGTACCCC TTCCCACAGATATACGTACGCTG CAGGTCGAC	Amplification of *TEV-ProtA-7HIS-hphNT1* fragment from pFA6a-TEV-ProtA-7His-hphNT1 plasmid with N-terminal overhang for 3'-end of *SMM1* ORF and C-terminal overhang for *SMM1* terminator
S2-SMM1_rv	CATACATATATATATTATGCGCG TTTTCTTTCATAATCCGTTCTTTTT ACTTAGAATATAATCGATGAATT CGAGCTCG	
S3-SUA5_fw	GAAGGATTAGCTGTTATGAACAG ATTGCGAAAGGCGGCTGCAAATA	Amplification of *TEV-ProtA-7HIS-hphNT1* fragment from pFA6a-TEV-

	ATTGTATACAGTTTCGTACGCTGCAGGTCGAC	ProtA-7His-hphNT1 plasmid with N-terminal overhang for 3'-end of *SUA5* ORF and C-terminal overhang for *SUA5* terminator
S2-SUA5_rv	CTAGATATAAAATCTCCGTAATCAGTGGTTATGATTTTCAAAAGTTAATCACAGTTTTATATCGATGAATTCGAGCTCG	
S3-TUM1_fw	GGATCCTGGACCGAGTGGGTCTTGAAATCCGGGCCCGAGTGGATTGCTGAAAACAGAGATCGTACGCTGCAGGTCGAC	Amplification of *TEV-ProtA-7HIS-hphNT1* fragment from pFA6a-TEV-ProtA-7His-hphNT1 plasmid with N-terminal overhang for 3'-end of *TUM1* ORF and C-terminal overhang for *TUM1* terminator
S2-TUM1_rv	AGATAGATAATTAATATATGTAGCTAAATAAATCGACTTGTCAAGAATATATTTCTCTTAATCGATGAATTCGAGCTCG	
S3-YBL039W-B_f	AATCGACTTCAACTCGAAGAGTAAGAAAAAAAATGATAAACGTACGCTGCAGGTCGAC	Amplification of *3HA-kanMX6* fragment from pYM1 plasmid with N-terminal overhang for 3'-end of *YBL039W-B* ORF and C-terminal overhang for *YBL039W-B* terminator
S2-YBL039W-B_r	TTTCCATGGCGTGCTTTTACCAAAGTACTGAACAGGGAGAATCGATGAATTCGAGCTCG	
S3-YBL059W_f	AAAAGAAGCCAGCAAGTAGTGGACAGCTTAGTTAAGACACACAATTCATCTCTTTGTAAACGTACGCTGCAGGTCGAC	Amplification of *TEV-ProtA-7HIS-hphNT1* fragment from pFA6a-TEV-ProtA-7His-hphNT1 plasmid with N-terminal overhang for 3'-end of *YBL059W* ORF and C-terminal overhang for *YBL059W* terminator
S2-YBL059W_r	ATGCGGGTAACACATATAAGTAGTGGAATATATTATTGAAACTACTACTATGGTATAACAATCGATGAATTCGAGCTCG	
S3-YBR201C-A_f	TACTACAAGGACGAATTTTGTTCTCAACGATCATACACCAGGTTTCGTACGCTGCAGGTCGAC	Amplification of *TEV-ProtA-7HIS-kanMX6* fragment from pYM9 plasmid with N-terminal overhang for 3'-end of *YBR201C-A* ORF and C-terminal overhang for *YBR201C-A* terminator
S2-YBR201C-A_r	CTCGGTAATTTTCTCCCTAATGATAACCCATATTTTCGAAAGACTATCGATGAATTCGAGCTCG	
S3-YBR230W-A_fw	GGCCCTATCACAACGGGTCAAGAAAGAGTATGCCGCCAATCGTACGCTGCAGGTCGAC	Amplification of *TEV-ProtA-7HIS-kanMX6* fragment from pYM9 plasmid with N-terminal overhang for 3'-end of *YBR230W-A* ORF and C-terminal overhang for *YBR230W-A* terminator
S2-YBR230W-A_rv	CCAAATATGTAAGTATATAAAATATATGTATGTGTGTGCAATCGATGAATTCGAGCTCG	
S3-YDR286C_f	GAAGAAGACGATATCAGTGATAAAATAAGGAGAATGCAATCTAGACGTACGCTGCAGGTCGAC	Amplification of *TEV-ProtA-7HIS-kanMX6* fragment from pYM9 plasmid with N-terminal overhang for 3'-end of *YDR286C* ORF and C-terminal overhang for *YDR286C* terminator
S2-YDR286C_r	TTATAAATATTTACAGTGTTGTAACTCTAGTAAAAACAAAAGAGGATCGATGAATTCGAGCTCG	
S3-YDR381C-A_f	AGTGCTGTAACAAGAAAAAGAGGTGACAAATTAGGTTTTTTAGATAGGAGGAGAAACGAGCGTACGCTGCAGGTCGAC	Amplification of *TEV-ProtA-7HIS-kanMX6* fragment from pYM9 plasmid with N-terminal overhang for 3'-end of *YDR381C-A* ORF and C-terminal overhang for *YDR381C-A* terminator
S2-YDR381C-A_r	GATGAATATATATATACATAATACTGCATTGAAAAAATGGATAGGTTGATTAAACGTGTGATCGATGAATTCGAGCTCG	
S3-YDR461C-A_fw	CCGCATCCAAGATCCCACAAGGGATATCCGGGTGCGAAGACCCTTA	Amplification of *TEV-ProtA-7HIS-hphNT1* fragment from pFA6a-TEV-

	CATATACTTCACGGCGTACGCTG CAGGTCGAC	ProtA-7His-hphNT1 plasmid with N-terminal overhang for 3'-end of *YDR461C-A* ORF and C-terminal overhang for *YDR461C-A* terminator
S2-YDR461C-A_rv	ACACGCTCATATATATATATATA TATATATATATGTATATGTACATA TACCGCTTACCACATCGATGAAT TCGAGCTCG	
S3-YGL041W-A_f	CAGTTAGGACCTGAACAACTGGC CCCGCTAATGACCGTTTTAGGCC TTGAGAAGAAAAAACGTACGCTG CAGGTCGAC	Amplification of *TEV-ProtA-7HIS-kanMX6* fragment from pYM9 plasmid with N-terminal overhang for 3'-end of *YGL041W-A* ORF and C-terminal overhang for *YGL041W-A* terminator
S2-YGL041W-A_r	ATATTTATACACGGAAGGCGCTA GTAAGACAGATAGGTAATGTTTT TTTACTTTCACCTCATCGATGAAT TCGAGCTCG	
S3-YGR021W_f	ACCACAGCGCTCGAGGACATCGA CGAAGTGACGTCGTTGTACACTA ACGCTAGCAACGCTCGTACGCTG CAGGTCGAC	Amplification of *TEV-ProtA-7HIS-hphNT1* fragment from pFA6a-TEV-ProtA-7His-hphNT1 plasmid with N-terminal overhang for 3'-end of *YGR021W* ORF and C-terminal overhang for *YGR021W* terminator
S2-YGR021W_r	TGTTTGTTTAGTATATACAGGTAT TTGTGGTATTGATTATTTATTTAC GGTTTGGTTGGAATCGATGAATT CGAGCTCG	
S3-YGR053C_f	GAAGATGTTGAACTGATCCATTA CGAGAAGAAAATTGCCACTCGCG GTGCATTTGCATGTCGTACGCTG CAGGTCGAC	Amplification of *TEV-ProtA-7HIS-hphNT1* fragment from pFA6a-TEV-ProtA-7His-hphNT1 plasmid with N-terminal overhang for 3'-end of *YGR053C* ORF and C-terminal overhang for *YGR053C* terminator
S2-YGR053C_r	TTTATGATGGTGTGTTTATTATTT ACAAATAAAGATGCTATCTAATT CTTGTATATCGTAATCGATGAATT CGAGCTCG	
S3-YHL018W_f	AGCGATATAGACGTCCGGATGGC CAAGAGAATAGATTCCTACATCG ATGAGATGACAACTCGTACGCTG CAGGTCGAC	Amplification of *TEV-ProtA-7HIS-kanMX6* fragment from pYM9 plasmid with N-terminal overhang for 3'-end of *YHL018W* ORF and C-terminal overhang for *YHL018W* terminator
S2-YHL018W_r	AAAATCGATAGGAAAAAAAAAA TGGAAAGAGCAATAGCCTTTTAG ACCTGCCCTGCCTTAATCGATGA ATTCGAGCTCG	
S3-YIL002W-A_fw	GTTCAGTTAGAAGATCTACACAG GGACAACAATGATTTGGCAAAAA GTTCCAGCCAAAAACGTACGCTG CAGGTCGAC	Amplification of *TEV-ProtA-7HIS-hphNT1* fragment from pFA6a-TEV-ProtA-7His-hphNT1 plasmid with N-terminal overhang for 3'-end of *YIL002W-A* ORF and C-terminal overhang for *YIL002W-A* terminator
S2-YIL002W-A_rv	AGATTATATATAAATATATTTATT TAGCGTTCCTTCCCTATGCGGCTG TGAGCGTACTCTATCGATGAATT CGAGCTCG	
S3-YIL077C_fw	TCTTCTGATGACAAATATCAGCG TTTACTGCAGAGCGGGAGATATG GTGGGAACCGCTCCCGTACGCTG CAGGTCGAC	Amplification of *TEV-ProtA-7HIS-kanMX6* fragment from pYM9 plasmid with N-terminal overhang for 3'-end of *YIL077C* ORF and C-terminal overhang for *YIL077C* terminator
S2-YIL077C_rv	TTGGCCCAAACATATACCTATAT ACAAATTAGTGACCATACGCTAT TATTACTCCGTCGTATCGATGAAT TCGAGCTCG	
S3-YIL156W-B_fw	TGTTGCCACTTGTGGCTCCTCGAC GTATTTCGCTAGGAAACGTACGC	Amplification of *TEV-ProtA-7HIS-kanMX6* fragment from pYM9 plasmid

	TGCAGGTCGAC	with N-terminal overhang for 3'-end of *YIL156W-B* ORF and C-terminal overhang for *YIL156W-B* terminator
S2-YIL156W-B_rv	TATACAAAATATTATCAACATAT ATAGAATATAAACGTACATCGAT GAATTCGAGCTCG	
S3-YJL133C_f	TATGGTCCCTTGAGTGCCTCACTA GCTACCAGAAGACACTTGGCTCA CGCGCCAAAGTTGCGTACGCTGC AGGTCGAC	Amplification of *TEV-ProtA-7HIS-kanMX6* fragment from pYM9 plasmid with N-terminal overhang for 3'-end of *YJL133C* ORF and C-terminal overhang for *YJL133C* terminator
S2-YJL133C_r	ATAGGTTAAAGTCATCATCATTA ATAAACCAGGAAAGAAAAGAGC ATAATTAAGATACGCATCGATGA ATTCGAGCTCG	
S3-YJR085C_f	ACAGCTTTGGGTGGGCTCGGCAG TTACTACTATTATAACAAATACA AGGAATTTTACCCTCGTACGCTG CAGGTCGAC	Amplification of *TEV-ProtA-7HIS-kanMX6* fragment from pYM9 plasmid with N-terminal overhang for 3'-end of *YJR085C* ORF and C-terminal overhang for *YJR085C* terminator
S2-YJR085C_r	AGAATATCATATTATATATATAT ATAGGGTCGTATATATATCGTGC GTCTTCTTCCTTCTATCGATGAAT TCGAGCTCG	
S3l-YKL065W-A_f	TTTATAAGAACGATAGCAAACAT AGTGAAATTAAAAAGATATACCA AAATGAGAAAAAAATTCGTACGC TGCAGGTCGAC	Amplification of *TEV-ProtA-7HIS-hphNT1* fragment from pFA6a-TEV-ProtA-7His-hphNT1 plasmid with N-terminal overhang for 3'-end of *YKL065W-A* ORF and C-terminal overhang for *YKL065W-A* terminator
S2l-YKL065W-A_r	GAGCTTCGTGACTCGGTTTACCA TTCTGTGTTATATACGAAAACCCT TATATAACAACTTTATCGATGAA TTCGAGCTCG	
S3-YKL133C_f	TTTAATGAACTCATTGAGGAAGC TCAACGTGAACTTAAAAAGGTTG ATGGTACGCCTATACGTACGCTG CAGGTCGAC	Amplification of *TEV-ProtA-7HIS-hphNT1* fragment from pFA6a-TEV-ProtA-7His-hphNT1 plasmid with N-terminal overhang for 3'-end of *YKL133C* ORF and C-terminal overhang for *YKL133C* terminator
S2-YKL133C_r	TCTTTCGGCATTTCAACATATTGA TGAAAATTTAGAAGAATATATAT ACAAATGTAAGATATCGATGAAT TCGAGCTCG	
S3-YLR049C_f	AAAATCGATTGTGACTTAGTCAT TCTGCTAGAAGATTTAAGGTCAC GGATTGATTTAGATCGTACGCTG CAGGTCGAC	Amplification of *TEV-ProtA-7HIS-hphNT1* fragment from pFA6a-TEV-ProtA-7His-hphNT1 plasmid with N-terminal overhang for 3'-end of *YLR049C* ORF and C-terminal overhang for *YLR049C* terminator
S2-YLR049C_r	ACATATATATATATATATATTCTT CCAGGAGAAATACCTGCCTTCTC TCTTACCCCTTGCATCGATGAATT CGAGCTCG	
S3-YLR118C_fw	TCTACAGTTCCAGATGAATTAGA AGACTTGGCTTCATTTATCAAGA AGAGCTTATCATCACGTACGCTG CAGGTCGAC	Amplification of *TEV-ProtA-7HIS-hphNT1* fragment from pFA6a-TEV-ProtA-7His-hphNT1 plasmid with N-terminal overhang for 3'-end of *YLR118C* ORF and C-terminal overhang for *YLR118C* terminator
S2-YLR118C_rv	ATAAATTATTTAACCAAGTATAA TAGCGGTTAAATTGAACTCGCAA TATTAGGAAAAGAGATCGATGAA TTCGAGCTCG	
S3-YLR281C_f	GTCGAAAAAGAGGAACGCGAGG CCCGAGACAGAGAAATGGTGCGC GAGTTATTCCGCCGGCGTACGCT GCAGGTCGAC	Amplification of *TEV-ProtA-7HIS-hphNT1* fragment from pFA6a-TEV-ProtA-7His-hphNT1 plasmid with N-terminal overhang for 3'-end of

S2-YLR281C_r	AGTTACACTTTTTTTTTCATTTTTTTTTTTCTTTTCTCCTCCATCTAATTTCACCTGCGGATCGATGAATTCGAGCTCG	*YLR281C* ORF and C-terminal overhang for *YLR281C* terminator
S3-YLR307C-A_f	CCAATTGTTATTTGCACTGACAACGAAGAGGTAGAGACTGTATCGGAGCACGTAAAAGTACGTACGCTGCAGGTCGAC	Amplification of *TEV-ProtA-7HIS-hphNT1* fragment from pFA6a-TEV-ProtA-7His-hphNT1 plasmid with N-terminal overhang for 3'-end of *YLR307C-A* ORF and C-terminal overhang for *YLR307C-A* terminator
S2-YLR307C-A_r	CTTTTAGCGTCAAAACGTTACACGTACATTTGAACAGTGTTAAGAGTAGATTAATTCAAAATCGATGAATTCGAGCTCG	
S3-YML007C-A_f	AGATTGGTGAGAAACCTCCAATACTTGCTGTTGCCGATAACTTCTTCATTGCTTTTTATACGTACGCTGCAGGTCGAC	Amplification of *TEV-ProtA-7HIS-hphNT1* fragment from pFA6a-TEV-ProtA-7His-hphNT1 plasmid with N-terminal overhang for 3'-end of *YML007C-A* ORF and C-terminal overhang for *YML007C-A* terminator
S2-YML007C-A_r	AATTACAAAGACGAATGGAAAGAAAAAGAGAGCAGCAGAGGATAGGAGAAAACACCCGAAATCGATGAATTCGAGCTCG	
S3-YMR087W_fw	AATGTAGAAAAAGATGCAATAGAATTGCTCATTCCTAGAAGGATTTTGACCTTGGATTTACGTACGCTGCAGGTCGAC	Amplification of *TEV-ProtA-7HIS-hphNT1* fragment from pFA6a-TEV-ProtA-7His-hphNT1 plasmid with N-terminal overhang for 3'-end of *YMR087W* ORF and C-terminal overhang for *YMR087W* terminator
S2-YMR087W_rv	TACTTACAAACGTAGTTCAAGTTCTTGAAAAATTGAAAATAGACTTTATATTATATACCTATCGATGAATTCGAGCTCG	
S3-YMR130W_f	CAGTTGAGTGAAAGAAAGTACGTTGTTTCGAATCTTGAGGTTTTAGAGGAACTCTTTCCCCGTACGCTGCAGGTCGAC	Amplification of *TEV-ProtA-7HIS-hphNT1* fragment from pFA6a-TEV-ProtA-7His-hphNT1 plasmid with N-terminal overhang for 3'-end of *YMR130W* ORF and C-terminal overhang for *YMR130W* terminator
S2-YMR130W_r	TATTACTGGCGGATATGAATAATATCTATCATACATATTTGTTACTGTAACGTTAGGCGCATCGATGAATTCGAGCTCG	
S3-YMR182W-A_f	GCATGTAACATAATATTTCTTCCCCTCGTTAAGTGTGCATCAGCAACCATAATGCTGAATCGTACGCTGCAGGTCGAC	Amplification of *γEGFP-kanMX4* fragment from pYM12 plasmid with N-terminal overhang for 3'-end of *YMR182W-A* ORF and C-terminal overhang for *YMR182W-A* terminator
S2-YMR182W-A_r	ATGCAGGAGAAAGGGCGAGTTTTGTTTATATGCGATCCTTTATGGTAACCTTTGCGGTTAATCGATGAATTCGAGCTCG	
S3-YNR040W_f	AAGACCCTATTTCACTCGGGGAATTCTAGATCATCCATCAAGAATATCGTGAAGCCCAAACGTACGCTGCAGGTCGAC	Amplification of *TEV-ProtA-7HIS-hphNT1* fragment from pFA6a-TEV-ProtA-7His-hphNT1 plasmid with N-terminal overhang for 3'-end of *YNR040W* ORF and C-terminal overhang for *YNR040W* terminator
S2-YNR040W_r	TGTTTAATTGTTCTTTTATTCGATTATTATTTACATGCATTCTTACGTAGATGTCCGTACATCGATGAATTCGAGCTCG	
S3-YOR020W-A_f	AGTATTGAAGGATTTTTAAATGATTTAGAGAAAGATACGAGGCAGGATACGAAAGCCAACCGTACGCTGCAGGTCGAC	Amplification of *TEV-ProtA-7HIS-kanMX6* fragment from pYM9 plasmid with N-terminal overhang for 3'-end of *YOR020W-A* ORF and C-terminal

S2-YOR020W-A_r	CAGTGCATCCCTTCACTGAACGATGAAGAACACCACCATTTCAGAAATTTTTATACATAAATCGATGAATTCGAGCTCG	overhang for *YOR020W-A* terminator
S3-YPL107W_f	AAGAAAAGATTACAAAAAATTCGCCGACAGGAAGAAATAAAAAAGAGGACAGCTTTGGTTCGTACGCTGCAGGTCGAC	Amplification of *TEV-ProtA-7HIS-hphNT1* fragment from pFA6a-TEV-ProtA-7His-hphNT1 plasmid with N-terminal overhang for 3'-end of *YPL107W* ORF and C-terminal overhang for *YPL107W* terminator
S2-YPL107W_r	ACCAAGATCAAAGAAGACCGCAAATATTGTACATAGGCTTTTCAATAATATATATTTGCTATCGATGAATTCGAGCTCG	
S3-YPR010C-A_fw	ATTATCTAGTTTAGATGAAGTCCTTGCCAAAGATAAGGATCGTACGCTGCAGGTCGAC	Amplification of *TEV-ProtA-7HIS-kanMX6* fragment from pYM9 plasmid with N-terminal overhang for 3'-end of *YPR010C-A* ORF and C-terminal overhang for *YPR010C-A* terminator
S2-YPR010C-A_rv	TAAGTGTAGATATTAATATAACAAATCATCAACATGGTTTATCGATGAATTCGAGCTCG	
S3-YPR098C_f	TGCGGGATGCTTGCGTACGGTGTTTGTTTGTCAGGTGGTTTGTTAAGAAAAATTCCAAAACGTACGCTGCAGGTCGAC	Amplification of *TEV-ProtA-7HIS-hphNT1* fragment from pFA6a-TEV-ProtA-7His-hphNT1 plasmid with N-terminal overhang for 3'-end of *YPR098C* ORF and C-terminal overhang for *YPR098C* terminator
S2-YPR098C_r	ACCTTGGCAAAGGAATGACGAAAAAATGATCTTGCATATATATATTTACTTGTAAAATAAATCGATGAATTCGAGCTCG	
Meo1_S3_fw	GACCCAGAACAAAAAGAGCAAATCAAGCGTCTCCACCAGTTGGACGGCATTCCTCACGCTCGTACGCTGCAGGTCGAC	Amplification of *γEGFP-kanMX4* fragment from pYM12 plasmid with N-terminal overhang for 3'-end of *MEO1* ORF and C-terminal overhang for *MEO1* terminator
Meo1_S2_rv	ATCCGTAATTGAAAAAAAAAAAAGAAAAAGATCAAGGAACACATCACCCTGGGCACATCAATCGATGAATTCGAGCTCG	
YBL039W-B_S3_fw	ATGTTCATGTCATCACCTACAATCGACTTCAACTCGAAGAGTAAGAAAAAAAATGATAAACGTACGCTGCAGGTCGAC	Amplification of *γEGFP-kanMX4* fragment from pYM12 plasmid with N-terminal overhang for 3'-end of *YBL039W-B* ORF and C-terminal overhang for *YBL039W-B* terminator
YBL039W-B_S2_rv	AGGAAGTTCTAAATAATTTTCCATGGCGTGCTTTTACCAAAGTACTGAACAGGGAGATTAATCGATGAATTCGAGCTCG	
YFR032C-B_S3_fw	ATTTTCCCTTCTCTCTTTTTTTCTTTATATCCTCCACTATATGCCACTCAGCGCACCTCAATCGATGAATTCGAGCTCG	Amplification of *TEV-ProtA-7HIS-kanMX6* fragment from pYM9 plasmid and *γEGFP-kanMX4* fragment from pYM12 plasmid with N-terminal overhang for 3'-end of *YFR032C-B* ORF and C-terminal overhang for *YFR032C-B* terminator
YFR032C-B_S2_rv	AGTACGTTATATTATCATGAAGTCCCCATTTCGCCCATTGGAAATGCAGGTAGCCAAATCCGTACGCTGCAGGTCGAC	
YGL204C_S3_fw	GAAATGTGGAAATATGCCTTTGCTGTTTCGCTACTTCTTAATAGTTTGGCACTATTTTTTCGTACGCTGCAGGTCGAC	Amplification of *γEGFP-kanMX4* fragment from pYM12 plasmid with N-terminal overhang for 3'-end of *YGL204C* ORF and C-terminal overhang for *YGL204C* terminator
YGL204C_S2_rv	TATAAGGGAGGAGAAATGATGGT	

	GATATTAATATGCAGAAATATCG ATTCCATTTTTTCAATCGATGAAT TCGAGCTCG	
YKL023C-A_S3_forward	ATTTCGGTAAACTATCAAAAGAA CGAACCAGTTGAATTTCTTGAAC GTACGCTGCAGGTCGAC	Amplification of *3HA-kanMX6* fragment from pYM1 plasmid and *γEGFP-kanMX4* fragment from pYM12 plasmid with N-terminal overhang for 3'-end of *YKL023C-A* ORF and C-terminal overhang for *YKL023C-A* terminator
YKL023C-A_S2_reverse	GCGAGAAAGCTGGCTGTGATGTA GTGGCAGCTGTCATTTGTCTTAAT CGATGAATTCGAGCTCG	
YKL065w-a_fw	TATAAGAACGATAGCAAACATAG TGAAATTAAAAAGATATACCAAA ATGAGAAAAAAATTCGTACGCTG CAGGTCGAC	Amplification of *3HA-kanMX6* fragment from pYM1 plasmid and *γEGFP-kanMX4* fragment from pYM12 plasmid with N-terminal overhang for 3'-end of *YKL065W-A* ORF and C-terminal overhang for *YKL065W-A* terminator
YKL065w-a_rv	TTCGTGACTCGGTTTACCATTCTG TGTTATATACGAAAACCCTTATA TAACAACTTTTTAATCGATGAATT CGAGCTCG	
YOR114W_S3_fw	CACGATACAAATACACAACCAAA TAATATTCTTCCCATGACGTACCT ACTAAAAAAGAAACGTACGCTGC AGGTCGAC	Amplification of *TEV-ProtA-7HIS-kanMX6* fragment from pYM9 plasmid with N-terminal overhang for 3'-end of *YOR114W* ORF and C-terminal overhang for *YOR114W* terminator
YOR114W_S2_fv	TCTTTATGATAGTGAAGTGCTTTC GTGGACTCTTCTTAAAGCCCTAA AAGTCTATTGTCAATCGATGAAT TCGAGCTCG	
AIM11_seq_fwd	GGATGGGGAACTTGATTC	Analysis of genomic integration of ProtA tag behind *AIM11* ORF
AIM11_seq_rev	CGGCTCGTAGTTATACC	
DEG1_SP6_f	TCGATTTAGGTGACACTATAGAA TACGCCGCCGCCCACATGCAATC TTTACTGC	Analysis of genomic integration of ProtA tag behind *DEG1* ORF (together with reverse primer: ProtA_seq_rev)
ECM4_SP6_f	TCGATTTAGGTGACACTATAGAA TACGCCGCCGCCCTTACCATCAC TACAGTG	Analysis of genomic integration of ProtA tag behind *ECM4* ORF (together with reverse primer: ProtA_seq_rev)
ECM19_seq_fwd	CTTCTTCTATCTTTTCCGC	Analysis of genomic integration of ProtA tag behind *ECM19* ORF (together with reverse primer: ProtA_seq_rev)
FMP16_seq_fwd	CTTGTTCCTACAATACTCC	Analysis of genomic integration of ProtA tag behind *FMP16* ORF
FMP16_seq_rev	GACTAAATACGATAGGACC	
FYV4_seq_fwd	CCATCTTCAAACAAGAGC	Analysis of genomic integration of ProtA tag behind *FYV4* ORF (together with reverse primer: ProtA_seq_rev)
MATlocus_fw	AGTCACATCAAGATCGTTTATGG	Discrimination between mating types MATa and MATα Huxley et al., 1990
Mat(a)_rv	ACTCCACTTCAAGTAAGAGTTTG	
Mat(alpha)_rv	GCACGGAATATGGGACTACTTCG	
MEU1_SP6_f	TCGATTTAGGTGACACTATAGAA TACGCCGCCGCCCTTTATTGTCAA TTATGTGAAAAG	Analysis of genomic integration of ProtA tag behind *MEU1* ORF (together with reverse primer: ProtA_seq_rev)
MLO1_seq_fwd	CCATATAAGCAGCAAAACG	Analysis of genomic integration of ProtA tag behind *MLO1* ORF (together with reverse primer: ProtA_seq_rev)
MTC3_seq_fwd	GTACTTGCATCCTTCTTCG	Analysis of genomic integration of ProtA tag behind *MTC3* ORF (together

		with reverse primer: ProtA_seq_rev)
NCE101_seq_fwd	GCATACAAATGTTCACTCC	Analysis of genomic integration of ProtA tag behind *NCE101* ORF
NCE101_seq_rev	GTATAAAGGTAGATCCTAGG	
ProtA_seq_rev	TGGTGGGAATTCGCGTCTAC	Reverse primer for the analysis of genomic integration of ProtA tag behind *DEG1*, *ECM4*, ECM19, *FYV4*, *MEU1*, *MLO1*, *MTC3*, *PXP2*, *SMM1*, *SUA5*, *TUM1*, *YBL059W*, *YDR461C-A*, *YGR021W*, *YGR053C*, *YHL018W-A*, *YIL002W-A*, *YKL133C*, *YLR049C*, *YLR118C*, *YLR281C*, *YML007C-A*, *YMR087W*, *YMR130W*, *YNR040W*, *YPL107W* and *YPR098C* ORFs (together with respective forward primers)
PXP2_SP6_f	TCGATTTAGGTGACACTATAGAA TACGCCGCCGCCCATATATACAA GTGCCACAC	Analysis of genomic integration of ProtA tag behind *PXP2* ORF (together with reverse primer: ProtA_seq_rev)
RDL2_seq_fwd	CTCTCAACAAATGGAAGCG	Analysis of genomic integration of ProtA tag behind *RDL2* ORF
RDL2_seq_rev	GAATGAATCGGAGAGGTG	
RRG9_seq_fwd	GACTTCCTTCTGAATCATTTG	Analysis of genomic integration of ProtA tag behind *RRG9* ORF
RRG9_seq_rev	GTTCCACTAACGATATTACTG	
SMM1_seq_f	CTATTTCATCCATCCAAGC	Analysis of genomic integration of ProtA tag behind *SMM1* ORF (together with reverse primer: ProtA_seq_rev)
SUA5_SP6_f	TCGATTTAGGTGACACTATAGAA TACGCCGCCGCCGTTAACTTACC ACTAAACCTG	Analysis of genomic integration of ProtA tag behind *SUA5* ORF (together with reverse primer: ProtA_seq_rev)
TUM1_SP6_f	TCGATTTAGGTGACACTATAGAA TACGCCGCCGCCCATAAAGTTGT GAAGAAAATTGC	Analysis of genomic integration of ProtA tag behind *TUM1* ORF (together with reverse primer: ProtA_seq_rev)
YBL059W_seq_f	GTTCAGCTTCTAACTGTG	Analysis of genomic integration of ProtA tag behind *YBL059W* ORF (together with reverse primer: ProtA_seq_rev)
YBR201C-A_seq_f	CTGTGACAAGGCGAAAAC	Analysis of genomic integration of ProtA tag behind *YBR201C-A* ORF
YBR201C-A_seq_r	CCTGTCTCAAATGTATAAATG	
YBR230W-A_seq_f	AGGCAAGAACAGAGGAG	Analysis of genomic integration of ProtA tag behind *YBR230W-A* ORF
YBR230W-A_seq_r	GGAGAGATTCTATATACCAC	
YDR286C_seq_f	GTAGAGAGTTCGGAGTTG	Analysis of genomic integration of ProtA tag behind *YDR286C* ORF
YDR286C_seq_r	CCTGCGTAAGAAGTATGC	
YDR381C-A_seq_f	CAATCTTCCTCCTTACAAAC	Analysis of genomic integration of ProtA tag behind *YDR381C-A* ORF
YDR381C-A_seq_r	GGATAGGTTGATTAAACGTG	
YDR461C-A_seq_f	GTGTTGAGTATTCAAAGCAC	Analysis of genomic integration of ProtA tag behind *YDR461C-A* ORF (together with reverse primer: ProtA_seq_rev)
YGL041W-A_seq_f	GATGTAACAAAACCGACG	Analysis of genomic integration of ProtA tag behind *YGL041W-A* ORF
YGL041W-A_seq_r	GCTAGTAAGACAGATAGG	
YGR021W_seq_f	GTACGCACGTACGCAAG	Analysis of genomic integration of

		ProtA tag behind *YGR021W* ORF (together with reverse primer: ProtA_seq_rev)
YGR053C_seq_f	GGATGACAGGTATGAGC	Analysis of genomic integration of ProtA tag behind *YGR053C* ORF (together with reverse primer: ProtA_seq_rev)
YHL018W_SP6_f	TCGATTTAGGTGACACTATAGAA TACGCCGCCGCCATGCACAACAA GATTGTTAGAAT	Analysis of genomic integration of ProtA tag behind *YHL018W* ORF (together with reverse primer: ProtA_seq_rev)
YIL002W-A_seq_f	CAATTACTCTAGAGAAATCG	Analysis of genomic integration of ProtA tag behind *YIL002W-A* ORF (together with reverse primer: ProtA_seq_rev)
YIL077C_seq_f	GCAGCCTAATTTCAAGCG	Analysis of genomic integration of ProtA tag behind *YIL077C* ORF
YIL077C_seq_r	CAAATTAGTGACCATACGC	
YIL156W-B_seq_f	CGGAGAGAAAGATCGAAC	Analysis of genomic integration of ProtA tag behind *YIL156W-B* ORF
YIL156W-B_seq_r	CTGGGTGCCGTTATACA	
YJL133C-A_seq_f	GTAGGGAGATGTTTAATGTG	Analysis of genomic integration of ProtA tag behind *YJL133C-A* ORF
YJL133C-A_seq_r	CAGGACCCCAAAAGAAG	
YJR085C_seq_f	GGAGACAAGACAGAAACG	Analysis of genomic integration of ProtA tag behind *YJR085C* ORF
YJR085_seq_r	CGTATATATATCGTGCGTC	
YKL065W-A_seq_f	GGACTTTGGACCTAACTC	Analysis of genomic integration of ProtA tag behind *YKL065W-A* ORF
YKL065W-A_seq_r	CCACAGAACCGACCATTA	
YKL133C_seq_f	GGCACAAAGTGAGAACG	Analysis of genomic integration of ProtA tag behind *YKL133C* ORF (together with reverse primer: ProtA_seq_rev)
YLR049C_seq_f	CGTTAGCCAAATTCTTTGG	Analysis of genomic integration of ProtA tag behind *YLR049C* ORF (together with reverse primer: ProtA_seq_rev)
YLR118C_SP6_f	TCGATTTAGGTGACACTATAGAA TACGCCGCCGCCGAACACATACA CTATATTTGC	Analysis of genomic integration of ProtA tag behind *YLR118C* ORF (together with reverse primer: ProtA_seq_rev)
YLR281C_seq_f	CCAACCTACAAGCTATGC	Analysis of genomic integration of ProtA tag behind *YLR281C* ORF (together with reverse primer: ProtA_seq_rev)
YLR307C-A_seq_f	GACAGCCAAGTATACTTG	Analysis of genomic integration of ProtA tag behind *YLR307C-A* ORF
YLR307C-A_seq_r	CGTTACACGTACATTTGAAC	
YML007C-A_seq_f	GTAAACTGCTCCACTTCG	Analysis of genomic integration of ProtA tag behind *YML007C-A* ORF (together with reverse primer: ProtA_seq_rev)
YMR087W_SP6_f	TCGATTTAGGTGACACTATAGAA TACGCCGCCGCCCATCTTCGTAA TTTTGAACTG	Analysis of genomic integration of ProtA tag behind *YMR087W* ORF (together with reverse primer: ProtA_seq_rev)

YMR130W_seq_f	CATCCACAGAAATTGGCTC	Analysis of genomic integration of ProtA tag behind *YMR130W* ORF (together with reverse primer: ProtA_seq_rev)
YNR040W_seq_f	GTTATCTTATGTGGACTAGG	Analysis of genomic integration of ProtA tag behind *YNR040W* ORF (together with reverse primer: ProtA_seq_rev)
YOR020W-A_seq_f	GTAAGAAAGGTCGCTACTG	Analysis of genomic integration of ProtA tag behind *YOR020W-A* ORF
YOR020W-A_seq_r	GAAGAACACCACCATTTCA	
YPL107W_SP6_f	TCGATTTAGGTGACACTATAGAATACGCCGCCGCCCAGTCAGAGGGTGCATG	Analysis of genomic integration of ProtA tag behind *YPL107W* ORF (together with reverse primer: ProtA_seq_rev)
YPR010C-A_seq_f	GGTAGTTTCCTGAACGAC	Analysis of genomic integration of ProtA tag behind *YPR010C-A* ORF
YPR010C-A_seq_r	CGATTTGTTCCCGACAATT	
YPR098C_seq_f	GGAGTTGTTTGATGATATAGG	Analysis of genomic integration of ProtA tag behind *YPR098C* ORF (together with reverse primer: ProtA_seq_rev)
AIM11_SP6_fwd	TCGATTTAGGTGACACTATAGAATACGCCGCCGCCATGATCGAAGAGAAGAAGG	Synthesis of SP6-AIM11 PCR product as template for subsequent RNA generation
AIM11_SP6_rev	CTACTTGTTGTTTTCGCTC	
DEG1_SP6_f	TCGATTTAGGTGACACTATAGAATACGCCGCCGCCCACATGCAATCTTTACTGC	Synthesis of SP6-DEG1 PCR product as template for subsequent RNA generation
DEG1_rev	TTACTTATTTTTGTTGTTCTTTTTCTTG	
FMP16_SP6_fwd	TCGATTTAGGTGACACTATAGAATACGCCGCCGCCATGTTGAGAACCACTTTTTTG	Synthesis of SP6-FMP16 PCR product as template for subsequent RNA generation
FMP16_SP6_rev	CCAGATGACGGTGTTTATTAA	
HBN1_SP6_f	TCGATTTAGGTGACACTATAGAATACGCCGCCGCCGTAGACTGAAGTATCCTATATC	Synthesis of SP6-HBN1 PCR product as template for subsequent RNA generation
HBN1_rev	TTAATTGAAGATTTCAACATCGTT	
MEU1_SP6_f	TCGATTTAGGTGACACTATAGAATACGCCGCCGCCCTTTATTGTCAATTATGTGAAAAG	Synthesis of SP6-MEU1 PCR product as template for subsequent RNA generation
MEU1_rev	TTACCAATAGTTTGGAAATAAGTA	
RDL2_SP6_f	TCGATTTAGGTGACACTATAGAATACGCCGCCGCCATGTTCAAGCATAGTACAGG	Synthesis of SP6-RDL2 PCR product as template for subsequent RNA generation
RDL2_SP6_r	TTACATTTTTTTGGGCTTAACGTCAG	
RRG9_SP6_fwd	TCGATTTAGGTGACACTATAGAATACGCCGCCGCCATGAACATTCTGCGAATAGC	Synthesis of SP6-RRG9 PCR product as template for subsequent RNA generation
RRG9_SP6_rev	TTATTGTTTCGAGCCCAAATG	
SMM1_SP6_f	TCGATTTAGGTGACACTATAGAA	Synthesis of SP6-SMM1 PCR product

	TACGCCGCCGCCCTATTTCATCCATCCAAGC	as template for subsequent RNA generation
SMM1_rev	TTATATATCTGTGGGAAGGG	
TES1_SP6_f	TCGATTTAGGTGACACTATAGAATACGCCGCCGCCCCTACAATGAAAAACCACG	Synthesis of SP6-TES1 PCR product as template for subsequent RNA generation
TES1_rev	TCAGAACTTGGCTCGAATG	
TUM1_SP6_f	TCGATTTAGGTGACACTATAGAATACGCCGCCGCCCATAAAGTTGTGAAGAAAATTGC	Synthesis of SP6-TUM1 PCR product as template for subsequent RNA generation
TUM1_rev	TTAATCTCTGTTTTCAGCAATC	
YBL039W-B_Sp6_fw	GATCGATTTAGGTGACACTATAGAAGCGGCCACCATGGGCTTTTTTAACAATAATCCGGTAATT	Synthesis of SP6-YBL039W-B PCR product as template for generation of [^{35}S]Ybl039w-b using the TnT® Quick Coupled Transcription/Translation System
YBL039W-B_Sp6_rv	GATCTTATTTATCATTTTTTTTCTTACTCTTCGA	
YBR230W-A_SP6_f	TCGATTTAGGTGACACTATAGAATACGCCGCCGCCATGAGAAACGAATTATACCAGT	Synthesis of SP6-YBR230W-A PCR product as template for subsequent RNA generation
YBR230W-A_SP6_r	CTACATATTGGCGGCATACTCTTT	
YDR286C_SP6_f	TCGATTTAGGTGACACTATAGAATACGCCGCCGCCATGTTGAGAGCGTTCCG	Synthesis of SP6-YDR286C PCR product as template for subsequent RNA generation
YDR286C_SP6_r	TCACATTCTAGATTGCATTCTCCTTATT	
YGL041W-A_SP6_f	TCGATTTAGGTGACACTATAGAATACGCCGCCGCCATGCTAAGAGTTATATGGAAG	Synthesis of SP6-YGL041W-A PCR product as template for subsequent RNA generation
YGL041W-A_SP6_r	TCATTTTTTCTTCTCAAGGCC	
YGR021W_SP6_f	TCGATTTAGGTGACACTATAGAATACGCCGCCGCCCAGCAAACTTGGTATGAAC	Synthesis of SP6-YGR021W PCR product as template for subsequent RNA generation
YGR021W_rev	TTAAGCGTTGCTAGCGTTAG	
YHL018W_SP6_f	TCGATTTAGGTGACACTATAGAATACGCCGCCGCCATGCACAACAAGATTGTTAGAAT	Synthesis of SP6-YHL018W PCR product as template for subsequent RNA generation
YHL018W_SP6_r	TCAAGTTGTCATCTCATCGA	
YIL077C_SP6_f	TCGATTTAGGTGACACTATAGAATACGCCGCCGCCATGTTGGGAAAAGAAGAAGAA	Synthesis of SP6-YIL077C PCR product as template for subsequent RNA generation (eventually used for generation of radiolabeled Yil077c precursor used for assessment of import and assembly under native conditions; Fig. 6C, lanes 9-18)
YIL077C_SP6_r	CTAGGAGCGGTTCCC	
YIL077C SP6 fw	GATCGATTTAGGTGACACTATAGAAGCGGCCACCATGTTGGGAAAAGAAGAAGAACAGC	Synthesis of SP6-YIL077C PCR product as template for subsequent RNA generation (eventually used for generation of radiolabeled Yil077c precursor used for assessment of import under denaturing conditions; Fig. S5, lanes 1-6)
YIL077C SP6 rv	CTAGGAGCGGTTCCCACC	
YJL133C-A_SP6_f	TCGATTTAGGTGACACTATAGAATACGCCGCCGCCATGATCGCCCAAAGTACC	Synthesis of SP6-YJL133C-A PCR product as template for subsequent RNA generation

YJL133C-A_SP6_r	CTACATCAACTTTGGCGCGTGA	
YKL023C-A_Sp6_fw	GATCGATTTAGGTGACACTATAG AAGCGGCCACCATGAATCCACGC TACAGGTTTATA	Synthesis of SP6-YKL023C-A PCR product as template for generation of [^{35}S]Ykl023c-a using the TnT® Quick Coupled Transcription/Translation System
YKL023C-A_Sp6_rv	GATCTTACATCATTTCAAGAAAT TCAACTGGTTC	
YKL065W-A_Sp6_fw	GATCGATTTAGGTGACACTATAG AAGCGGCCACCATGAGATCTAAT ATTTTGAAATTA	Synthesis of SP6-YKL065W-A PCR product as template for generation of [^{35}S]Ykl065w-a using the TnT® Quick Coupled Transcription/Translation System
YKL065W-A_Sp6_rv	GATCTTAAATTTTTTTCTCATTTT GGTA	
YKL133C_SP6_f	TCGATTTAGGTGACACTATAGAA TACGCCGCCGCCGTAATGAAGAA ATTTATGCTCATTTAG	Synthesis of SP6-YKL133C PCR product as template for subsequent RNA generation
YKL133C_rev	TTATATAGGCGTACCATCAAC	
YLR118C_SP6_f	TCGATTTAGGTGACACTATAGAA TACGCCGCCGCCGAACACATACA CTATATTTGC	Synthesis of SP6-YLR118C PCR product as template for subsequent RNA generation
YLR118C_rev	CTATGATGATAAGCTCTTCTT	
YLR281C_SP6_f	TCGATTTAGGTGACACTATAGAA TACGCCGCCGCCGCTATACGTTC CTAGAAC	Synthesis of SP6-YLR281C PCR product as template for subsequent RNA generation
YLR281C_rev	TTACCGGCGGAATAACTC	
YMR130W_SP6_f	TCGATTTAGGTGACACTATAGAA TACGCCGCCGCCCAGACTTTTGA ACATCCAC	Synthesis of SP6-YMR130W PCR product as template for subsequent RNA generation
YMR130W_rev	TCAGGGAAAGAGTTCCTC	
YNR040W_SP6_f	TCGATTTAGGTGACACTATAGAA TACGCCGCCGCCCATAAGAAGGT GCATTTAGTTATC	Synthesis of SP6-YNR040W PCR product as template for subsequent RNA generation
YNR040W_rev	CTATTTGGGCTTCACGATATTC	
YOR114W_Sp6_fw	GATCGATTTAGGTGACACTATAG AAGCGGCCACCATGAAGGCTACT TTACTGTTGAAGGCCCAG	Synthesis of SP6-YOR114W PCR product as template for generation of [^{35}S]Yor114w using the TnT® Quick Coupled Transcription/Translation System
YOR114W_Sp6_rv	GATCTCATTTCTTTTTTAGTAGGT ACGTCATGGG	
YPL107W_SP6_f	TCGATTTAGGTGACACTATAGAA TACGCCGCCGCCCAGTCAGAGGG TGCATG	Synthesis of SP6-YPL107W PCR product as template for subsequent RNA generation
YPL107W_rev	TCAAACCAAAGCTGTCCTC	
TEV-ProtA_fwd	CCCAAGCTTGGGCGTACGCTGCA GGTCGAC	Generation of HindIII-TEV-ProtA-7HIS-XmaI PCR product for cloning into pFA6a-hphNT1plasmid
TEV-ProtA_rev	TCCCCCCGGGGGGACTAGGAATT CGCGTCTAC	
YJR085C_pGEM-4Z_FW	GGAATTCAGATCACACTATGGAA CATCCA	Generation of EcoRI-YJR085C (*S. cerevisiae*)-HindIII PCR product for cloning into pGEM-4Z plasmid
YJR085C_pGEM-4Z_REV	CCCAAGCTTTCTTCTTCCTTCTCT CTAAGGGTAA	
YJR085C_pRS425_FW	CCCAAGCTTATCAAACATTTAGA GCCTGAAACAA	Generation of HindIII-$P_{YJR085C}$-YJR085C (*S. cerevisiae*)-$T_{YJR085C}$-BamHI PCR product for cloning into pRS425 plasmid
YJR085C_pRS425_REV	CGCGGATCCAGGTGGTCTTCACT CGGTT	

NHA_YJR085C_FW	CATCAGATCACACTATGTACCCA TACGATGTTCCAGATTACGCTGA ACATCCAGCATATAC	Insertion of a single N-terminal HA-tag behind the start codon of *YJR085C* in pRS425-YJR085C resulting in pRS425-$_{HA}$YJR085C plasmid
NHA_YJR085C_Rev	GTATATGCTGGATGTTCAGCGTA ATCTGGAACATCGTATGGGTACA TAGTGTGATCTGATG	
AIM11 N' tag CHK R	TACAAACTCTCTTGCCGTTG	Primer for checking N' tagging of the gene. AIM11
AIM11 N' tag pYM F	TTAGTACGACTATCCTACTTCATC AAGAAACGAAACTATGcgtacgctgca ggtcgac	Primer for N' tagging of gene using pYM plasmids. AIM11
AIM11 N' tag pYM R	GAAGAACCCTGCGTTTCTTAAGT TCCTTCTTCTCTTCGATcatcgatgaatt ctctgtcg	Primer for N' tagging of gene using pYM plasmids. AIM11
FMP16 N' tag CHK R	TTAATAAACACCGTCATCTGG	Primer for checking N' tagging of the gene. FMP16
FMP16 N' tag pYM F	AGTATCACATATATAATACACAG GAATATATTTGATAATGcgtacgctgc aggtcgac	Primer for N' tagging of gene using pYM plasmids. FMP16
FMP16 N' tag pYM R	GCATCAATTGTCTTGGAGTGCGC AAAAAAGTGGTTCTCAAcatcgatgaa ttctctgtcg	Primer for N' tagging of gene using pYM plasmids. FMP16
FMP33 N' tag CHK R	CCAAACAATCGAAAATTGAG	Primer for checking N' tagging of the gene. FMP33
FMP33 N' tag pYM F	AAATAAATCAAGTATATCATAGA GTTCTTTCATTCATATGcgtacgctgca ggtcgac	Primer for N' tagging of gene using pYM plasmids. FMP33
FMP33 N' tag pYM R	TGGTGAATTGTGAGTTGTGACGT AACAACCTTGTGTATAGcatcgatgaat tctctgtcg	Primer for N' tagging of gene using pYM plasmids. FMP33
FSF1 N' tag CHK R	TTTAGACCTAACGCAACACC	Primer for checking N' tagging of the gene. FSF1
FSF1 N' tag pYM F	CAGCATCGAAAGAAAAAAATAA ACAAGGCAGAGAAATATGcgtacgct gcaggtcgac	Primer for N' tagging of gene using pYM plasmids. FSF1
FSF1 N' tag pYM R	GGGATTCGGGCAAATCGATGGGC CCTGGGACTGATGATGCcatcgatgaa ttctctgtcg	Primer for N' tagging of gene using pYM plasmids. FSF1
FYV4 N' tag CHK R	AATGCCTTTCTCTTCCTCTC	Primer for checking N' tagging of the gene. FYV4
FYV4 N' tag pYM F	AAACAATAACAAACCTTCATTCA ACACACGTTTTACTATGcgtacgctgc aggtcgac	Primer for N' tagging of gene using pYM plasmids. FYV4
FYV4 N' tag pYM R	TTAAGAATAGAGGAAATTTGTGG CTAATCCGGGAAGGTATcatcgatgaa ttctctgtcg	Primer for N' tagging of gene using pYM plasmids. FYV4
LCL3 N' tag CHK R	TTCAAGAACTGGCTTTTAGC	Primer for checking N' tagging of the gene. LCL3
LCL3 N' tag pYM F	TTTTTCATAGCTATTAAGGGGGC ATAAATGCACTTATATGcgtacgctgc aggtcgac	Primer for N' tagging of gene using pYM plasmids. LCL3
LCL3 N' tag pYM R	CAACATCCGCAGATTTTTTTGAAT TAGAATCACCTTCCCTcatcgatgaattc tctgtcg	Primer for N' tagging of gene using pYM plasmids. LCL3

MNE1 N' tag CHK R	AGTGCAATTTTGTCATTTGC	Primer for checking N' tagging of the gene. MNE1
MNE1 N' tag pYM F	CGGCGAGAAAAAATGATAGTAGTGTGCCAAGAAGAATATGcgtacgctgcaggtcgac	Primer for N' tagging of gene using pYM plasmids. MNE1
MNE1 N' tag pYM R	TACCAATATGACTAGACGAATATCTTTTAAAAAGTAACTTcatcgatgaattctctgtcg	Primer for N' tagging of gene using pYM plasmids. MNE1
MSS116 N' tag CHK R	AACATCATGGTCTTCACTGG	Primer for checking N' tagging of the gene. MSS116
MSS116 N' tag pYM F	GGCAAGAAAATACCAGAGTTGCACGTTAGGCTGATAAATGcgtacgctgcaggtcgac	Primer for N' tagging of gene using pYM plasmids. MSS116
MSS116 N' tag pYM R	CAAGAACAGGTGTGCGACCTTTTATCAATATAGAGGTCAAcatcgatgaattctctgtcg	Primer for N' tagging of gene using pYM plasmids. MSS116
SFH5 N' tag CHK R	GTGACAGCCTTTTTATTTGC	Primer for checking N' tagging of the gene. SFH5
SFH5 N' tag pYM F	CCAATCGTAATTAATTCACTAAATTAACATCCTTAAAATGcgtacgctgcaggtcgac	Primer for N' tagging of gene using pYM plasmids. SFH5
SFH5 N' tag pYM R	GCTTATCGAAAACCTGCTTCTCACTGTCATTGTCGAATTTcatcgatgaattctctgtcg	Primer for N' tagging of gene using pYM plasmids. SFH5
TOM5 N' tag CHK R	ATTTCCATTGCTTTTTCACC	Primer for checking N' tagging of the gene. TOM5
TOM5 N' tag pYM F	AGGCGTCCATTGGCATCAAATAACTAGATAGTATAAAATGcgtacgctgcaggtcgac	Primer for N' tagging of gene using pYM plasmids. TOM5
TOM5 N' tag pYM R	TTTTCTCCTCTTCGGAGACTTCCTGTTGAGGTAGACCAAAcatcgatgaattctctgtcg	Primer for N' tagging of gene using pYM plasmids. TOM5
YBL059W N' tag CHK R	ACCTGCAAGACTCTTTTGTG	Primer for checking N' tagging of the gene. YBL059W
YBL059W N' tag pYM F	ATCTTGCTTTTGTTCAACTGCACTTGTAAATCAGTGAATGcgtacgctgcaggtcgac	Primer for N' tagging of gene using pYM plasmids. YBL059W
YBL059W N' tag pYM R	TAGAGAAAGACCTATTAAAAAATCGCTGCGCGTCCAATAAcatcgatgaattctctgtcg	Primer for N' tagging of gene using pYM plasmids. YBL059W
YGL041W-A N' tag CHK R	CGTGTCTCAGATCTCTGTCC	Primer for checking N' tagging of the gene. YGL041W-A
YGL041W-A N' tag pYM F	CACAAGAAGCAGAAAGTAGATACTACAGCCACACATAATGcgtacgctgcaggtcgac	Primer for N' tagging of gene using pYM plasmids. YGL041W-A
YGL041W-A N' tag pYM R	AACGAGTGACTCTGGAACTATGCTTCCATATAACTCTTAGcatcgatgaattctctgtcg	Primer for N' tagging of gene using pYM plasmids. YGL041W-A
YIL077C N' tag CHK R	GTACTGCCTTTGATTTCTCG	Primer for checking N' tagging of the gene. YIL077C
YIL077C N' tag pYM F	TTAAGGAGCAGCCTAATTTCAAGCGTAGAACAAGGTGATGcgtacgctgcaggtcgac	Primer for N' tagging of gene using pYM plasmids. YIL077C
YIL077C N' tag pYM R	TACCATTCTGGCCATATTGCTGTT	Primer for N' tagging of gene using

	CTTCTTCTTTTCCCAAcatcgatgaattct ctgtcg	pYM plasmids. YIL077C
YJL127C-B N' tag CHK R	TACTGCACGTATTTCGATTG	Primer for checking N' tagging of the gene. YJL127C-B
YJL127C-B N' tag pYM F	TGCAGCAGTGTACAGTTTACGCG ACAATAAAGAAAGCATGcgtacgctg caggtcgac	Primer for N' tagging of gene using pYM plasmids. YJL127C-B
YJL127C-B N' tag pYM R	AAGCTGTAAATATTGAACGGATC TGGTTGAAAAAGAAAATcatcgatgaa ttctctgtcg	Primer for N' tagging of gene using pYM plasmids. YJL127C-B
YJL133C-A N' tag CHK R	CCATATGTCTTGGCATTTTC	Primer for checking N' tagging of the gene. YJL133C-A
YJL133C-A N' tag pYM F	AATATTACATTCATAAGACAGTA AATAAACGTATTAAATGcgtacgctgc aggtcgac	Primer for N' tagging of gene using pYM plasmids. YJL133C-A
YJL133C-A N' tag pYM R	AAGAAGAGACGGCGGCGGCTAA TCTGGTACTTTGGGCGATcatcgatga attctctgtcg	Primer for N' tagging of gene using pYM plasmids. YJL133C-A
YJR085C N' tag CHK R	AGGGTAAAATTCCTTGTATTTG	Primer for checking N' tagging of the gene. YJR085C
YJR085C N' tag pYM F	AAACGAAGTTTGAGAGAAAGGA ACATCAGATCACACTATGcgtacgct gcaggtcgac	Primer for N' tagging of gene using pYM plasmids. YJR085C
YJR085C N' tag pYM R	CGGCTGTAGTCAAAAGACTCAAT GTATATGCTGGATGTTCcatcgatgaat tctctgtcg	Primer for N' tagging of gene using pYM plasmids. YJR085C
YKL018C-A N' tag CHK R	AGATTGATCTCTTCCCCTTC	Primer for checking N' tagging of the gene. YKL018C-A
YKL018C-A N' tag pYM F	AAAAGAGAGTGAAGATCAGATC GTAACATATTGCAAGATGcgtacgct gcaggtcgac	Primer for N' tagging of gene using pYM plasmids. YKL018C-A
YKL018C-A N' tag pYM R	CTACCAACGTCCCCTCTACTACCC ACCTTATCATTCCCAAcatcgatgaattc tctgtcg	Primer for N' tagging of gene using pYM plasmids. YKL018C-A
YKL044W N' tag CHK R	TATAGGCTGGGAACTGAGG	Primer for checking N' tagging of the gene. YKL044W
YKL044W N' tag pYM F	CTGTGGCCCAGGTAGCGTAGGCA AAATCAAGCTCAGAATGcgtacgctgc aggtcgac	Primer for N' tagging of gene using pYM plasmids. YKL044W
YKL044W N' tag pYM R	CTGACATCCTCGCACTCGAAAAC GTCATAATTACGTAACCcatcgatgaat tctctgtcg	Primer for N' tagging of gene using pYM plasmids. YKL044W
YKL133C N' tag CHK R	AAAGTAGATCCACGTTTTCG	Primer for checking N' tagging of the gene. YKL133C
YKL133C N' tag pYM F	AAAGATATTGTAATGAAGAAATT TATGCTCATTTAGTATGcgtacgctgca ggtcgac	Primer for N' tagging of gene using pYM plasmids. YKL133C
YKL133C N' tag pYM R	CGGTCCCTTCATTTTTGACTGATC TATGAAGGTATTTCCAcatcgatgaattc tctgtcg	Primer for N' tagging of gene using pYM plasmids. YKL133C
YLR281C N' tag CHK R	CGTTCCTCTTTTTCGACTC	Primer for checking N' tagging of the gene. YLR281C
YLR281C N' tag pYM F	CTGGAAAAAGCGCAGAAGAATC CGAGACTAGTAAACTATGcgtacgct	Primer for N' tagging of gene using pYM plasmids. YLR281C

	gcaggtcgac	
YLR281C N' tag pYM R	CTGCGGCACTGCTGATTGACCTC TTACTCGCTCCCCTCATcatcgatgaatt ctctgtcg	Primer for N' tagging of gene using pYM plasmids. YLR281C
YMR252C N' tag CHK R	CTGGGGTGACTGAACCTAC	Primer for checking N' tagging of the gene. YMR252C
YMR252C N' tag pYM F	AAGCAGCAAAACGAAGAAGATC GAGTGTGAAGTGTTAATGcgtacgct gcaggtcgac	Primer for N' tagging of gene using pYM plasmids. YMR252C
YMR252C N' tag pYM R	CAATTCTTGTTCTGATGTAGCTTA CGAAAACTTTACCAAAcatcgatgaatt ctctgtcg	Primer for N' tagging of gene using pYM plasmids. YMR252C
YNR040W N' tag CHK R	CTCCCTCGTGATAGAAACTG	Primer for checking N' tagging of the gene. YNR040W
YNR040W N' tag pYM F	AAGAAGGTGCATTTAGTTATCTT ATGTGGACTAGGGTATGcgtacgctgc aggtcgac	Primer for N' tagging of gene using pYM plasmids. YNR040W
YNR040W N' tag pYM R	AGCTGCTTCCTTTGAACTGATTCT TGGCAGCCATGTTTGTcatcgatgaattc tctgtcg	Primer for N' tagging of gene using pYM plasmids. YNR040W
YPL041C N' tag CHK R	CCAACAAATTTCTCCATAGC	Primer for checking N' tagging of the gene. YPL041C
YPL041C N' tag pYM F	GGATAAGTGTTACACCCAAGGCA CCCTCACCAGGAACATGcgtacgctgc aggtcgac	Primer for N' tagging of gene using pYM plasmids. YPL041C
YPL041C N' tag pYM R	TCTGCAGTTGACAGGGCCTGAAG AAAAGATTCATGACAGTcatcgatgaa ttctctgtcg	Primer for N' tagging of gene using pYM plasmids. YPL041C
YPL109C N' tag CHK R	TTGGTGTCCGTAATTTTGAG	Primer for checking N' tagging of the gene. YPL109C
YPL109C N' tag pYM F	CAGAATAGAGATAAAGAACATC AGAACCATCTGGGCAATGcgtacgct gcaggtcgac	Primer for N' tagging of gene using pYM plasmids. YPL109C
YPL109C N' tag pYM R	AGTATCGCCAAGAGTTTCTATAA GCGAACTTTAAAAATGAcatcgatgaa ttctctgtcg	Primer for N' tagging of gene using pYM plasmids. YPL109C
YPR098C N' tag CHK R	CGACTTGCCAAATTCTTTAC	Primer for checking N' tagging of the gene. YPR098C
YPR098C N' tag pYM F	ACTACGCTTTACAGTCCAGTAAA CTTAACAACGAAAAATGcgtacgctgc aggtcgac	Primer for N' tagging of gene using pYM plasmids. YPR098C
YPR098C N' tag pYM R	AGGAATAAAAAAGCAAATGAGC CGTAGTTTTGACTAAACAcatcgatga attctctgtcg	Primer for N' tagging of gene using pYM plasmids. YPR098C
S4 reverse complement	cgacagagaattcatcgatg	Primer for checking N' tagging of the genes.

Yeast strains used in this study

Strain	Description	Genotype	Source or Reference	Number
Wild-type (WT)	BY4741	*MATa*; *ura3*Δ0, *leu2*Δ0, his3Δ*1*, *met15*Δ*0*	Brachmann et al., 1998	1354
Wild-type (WT)	BY4742 Δ*arg4*	MATα; *ura3*Δ0, *leu2*Δ0, his3Δ*1*, *lys2*Δ*0*, *arg4::kanMX4*	Euroscarf	2708
Wild-type (WT)	BY4741 Δ*lys2* Δ*arg4*	*MATa*; *ura3*Δ0, *leu2*Δ0, his3Δ*1*, *lys2*Δ*0*, *met15*Δ*0*, *arg4::kanMX4*	this study	3559
Wild-type (WT)	YPH499	*MAT*a; *ura3-52*, *lys2-801*, *ade2-101*, *trp1-Δ63*, *his3-Δ200*, *leu2-Δ1*	Sikorski and Hieter, 1989	1501
Wild-type (WT)	YPH499 Δ*arg4*	*MAT*a; *ura3-52*, *lys2-801*, *ade2-101*, *trp1-Δ63*, *his3-Δ200*, *leu2-Δ1*, *arg4::kanMX4*	von der Malsburg et al., 2011	2799
Wild-type (WT)	YPH499 pRS425 (empty)	YPH499 + *pRS425*	this study	4312
$Aim11_{ProtA}$	$Aim11_{ProtA}$ (chromosomal)	BY4741 *aim11::AIM11-TEV-ProtA-7HIS-kanMX6*	this study	4950
$Deg1_{ProtA}$	$Deg1_{ProtA}$ (chromosomal)	BY4741 *deg1::DEG1-TEV-ProtA-7HIS-hphNT1*	this study	5044
$Ecm4_{ProtA}$	$Ecm4_{ProtA}$ (chromosomal)	BY4741 *ecm4::ECM4-TEV-ProtA-7HIS-hphNT1*	this study	5045
$Ecm19_{ProtA}$	$Ecm19_{ProtA}$ (chromosomal)	BY4741 *ecm19::ECM19-TEV-ProtA-7HIS-hphNT1*	this study	4951
$Fmp16_{ProtA}$	$Fmp16_{ProtA}$ (chromosomal)	BY4741 *fmp16::FMP16-TEV-ProtA-7HIS-kanMX6*	this study	4952
$Fyv4_{ProtA}$	$Fyv4_{ProtA}$ (chromosomal)	BY4741 *fyv4::FYV4-TEV-ProtA-7HIS-hphNT1*	this study	4953
$Meo1_{GFP}$	$Meo1_{GFP}$ (chromosomal)	BY4741 *meo1::MEO1-γEGFP-kanMX4*	this study	4113
$Meu1_{ProtA}$	$Meu1_{ProtA}$ (chromosomal)	BY4741 *meu1::MEU1-TEV-ProtA-7HIS-hphNT1*	this study	5046
$Mlo1_{ProtA}$	$Mlo1_{ProtA}$ (chromosomal)	BY4741 *mlo1::MLO1-TEV-ProtA-7HIS-hphNT1*	this study	4954
$Mtc3_{ProtA}$	$Mtc3_{ProtA}$ (chromosomal)	BY4741 *mtc3::MTC3-TEV-ProtA-7HIS-hphNT1*	this study	4955
$Nce101_{HA}$	$Nce101_{HA}$	BY4741 *nce101::NCE101-3HA-*	this study	4956

	(chromosomal)	*kanMX6*		
$Pxp2_{ProtA}$	$Pxp2_{ProtA}$ (chromosomal)	BY4741 *pxp2::PXP2-TEV-ProtA-7HIS-hphNT1*	this study	5047
$Rdl2_{ProtA}$	$Rdl2_{ProtA}$ (chromosomal)	BY4741 *rdl2::RDL2-TEV-ProtA-7HIS-kanMX6*	this study	4957
$Rrg9_{ProtA}$	$Rrg9_{ProtA}$ (chromosomal)	BY4741 *rrg9::RRG9-TEV-ProtA-7HIS-kanMX6*	this study	4958
$Smm1_{ProtA}$	$Smm1_{ProtA}$ (chromosomal)	BY4741 *smm1::SMM1-TEV-ProtA-7HIS-hphNT1*	this study	5048
$Sua5_{ProtA}$	$Sua5_{ProtA}$ (chromosomal)	BY4741 *sua5::SUA5-TEV-ProtA-7HIS-hphNT1*	this study	5049
$Tum1_{ProtA}$	$Tum1_{ProtA}$ (chromosomal)	BY4741 *tum1::TUM1-TEV-ProtA-7HIS-hphNT1*	this study	5050
Ybl039w-b_{GFP}	Ybl039w-b_{GFP} (chromosomal)	BY4741 *ybl039w-b::YBL039W-B-γEGFP-kanMX4*	this study	4112
Ybl039w-b_{HA}	Ybl039w-b_{HA} (chromosomal)	BY4741 *ybl039w-b::YBL039W-B-3HA-kanMX6*	this study	4983
$Ybl059w_{ProtA}$	$Ybl059w_{ProtA}$ (chromosomal)	BY4741 *ybl059w::YBL059W-TEV-ProtA-7HIS-hphNT1*	this study	4959
Ybr201c-a_{ProtA}	Ybr201c-a_{ProtA} (chromosomal)	BY4741 *ybr201c-a::YBR201C-A-TEV-ProtA-7HIS-kanMX6*	this study	4960
Ybr230w-a_{ProtA}	Ybr230w-a_{ProtA} (chromosomal)	BY4741 *ybr230w-a::YBR230W-A-TEV-ProtA-7HIS-kanMX6*	this study	4961
$Ydr286c_{ProtA}$	$Ydr286c_{ProtA}$ (chromosomal)	BY4741 *ydr286c::YDR286C-TEV-ProtA-7HIS-kanMX6*	this study	4962
Ydr381c-a_{ProtA}	Ydr381c-a_{ProtA} (chromosomal)	BY4741 *ydr381c-a::YDR381C-A-TEV-ProtA-7HIS-kanMX6*	this study	4970
Ydr461c-a_{ProtA}	Ydr461c-a_{ProtA} (chromosomal)	BY4741 *ydr461c-a::YDR461C-A-TEV-ProtA-7HIS-hphNT1*	this study	4971
Yfr032c-b_{GFP}	Yfr032c-b_{GFP} (chromosomal)	BY4741 *yfr032c-b::YFR032C-B-γEGFP-kanMX4*	this study	4118
Yfr032c-b_{ProtA}	Yfr032c-b_{ProtA} (chromosomal)	BY4741 *Yfr032c-b::YFR032C-B-TEV-ProtA-7HIS-kanMX6*	this study	5054
Ygl041w-a_{ProtA}	Ygl041w-a_{ProtA} (chromosomal)	BY4741 *ygl041w-a::YGL041W-A-TEV-ProtA-7HIS-kanMX6*	this study	4972

Ygl204c$_{GFP}$	Ygl204c$_{GFP}$ (chromosomal)	BY4741 *Ygl204c::YGL204C-γEGFP-kanMX4*	this study	4117
Ygr021w$_{ProtA}$	Ygr021w$_{ProtA}$ (chromosomal)	BY4741 *ygr021w::YGR021W-TEV-ProtA-7HIS-hphNT1*	this study	4973
Ygr053c$_{ProtA}$	Ygr053c$_{ProtA}$ (chromosomal)	BY4741 *ygr053c::YGR053C-TEV-ProtA-7HIS-hphNT1*	this study	4974
Yhl018w$_{ProtA}$	Yhl018w$_{ProtA}$ (chromosomal)	BY4741 *yhl018w::YHL018W-TEV-ProtA-7HIS-kanMX6*	this study	4975
Yil002w-a$_{ProtA}$	Yil002w-a$_{ProtA}$ (chromosomal)	BY4741 *yil002w-a::YIL002W-A-TEV-ProtA-7HIS-hphNT1*	this study	4976
*yil077c*Δ	Deletion of *YIL007C* in BY4741 yeast cells	BY4741 *yil077c::kanMX4*	Euroscarf	3407
Yil077c$_{ProtA}$	Yil077c$_{ProtA}$ (chromosomal)	BY4741 *yil077c::YIL077C-TEV-ProtA-7HIS-kanMX6*	this study	4977
Yil156w-b$_{ProtA}$	Yil156w-b$_{ProtA}$ (chromosomal)	BY4741 *yil156w-b::YIL156W-B-TEV-ProtA-7HIS-kanMX6*	this study	4978
Yjl133c-a$_{ProtA}$	Yjl133c-a$_{ProtA}$ (chromosomal)	BY4741 *yjl133c-a::YJL133C-A-TEV-ProtA-7HIS-kanMX6*	this study	4979
$_{HA}$YJR085C (YPH499)	YPH499 pRS425-*$_{HA}$YJR085C*	YPH499 + *pRS425-$_{HA}$YJR085C*	this study	4378
Yjr085c$_{ProtA}$	Yjr085c$_{ProtA}$ (chromosomal)	BY4741 *yjr085c::YJR085C-TEV-ProtA-7HIS-kanMX6*	this study	4980
Ykl023c-a$_{GFP}$	Ykl023c-a$_{GFP}$ (chromosomal)	BY4741 *ykl023c-a::YKL023C-A-γEGFP-kanMX4*	this study	4114
Ykl023c-a$_{HA}$	Ykl023c-a$_{HA}$ (chromosomal)	BY4741 *ykl023c-a::YKL023C-A-3HA-kanMX6*	this study	4108
Ykl065w-a$_{GFP}$	Ykl065w-a$_{GFP}$ (chromosomal)	BY4741 *ykl065w-a::YKL065W-A-γEGFP-kanMX4*	this study	4115
Ykl065w-a$_{ProtA}$	Ykl065w-a$_{ProtA}$ (chromosomal)	BY4741 *ykl065w-a::YKL065W-A-TEV-ProtA-7HIS-hphNT1*	this study	4981
Ykl133c$_{ProtA}$	Ykl133c$_{ProtA}$ (chromosomal)	BY4741 *ykl133c::YKL133C-TEV-ProtA-7HIS-hphNT1*	this study	4982
Ylr049c$_{ProtA}$	Ylr049c$_{ProtA}$ (chromosomal)	BY4741 *ylr049c::YLR049C-TEV-ProtA-7HIS-hphNT1*	this study	4984
Ylr118c$_{ProtA}$	Ylr118c$_{ProtA}$ (chromosomal)	BY4741 *ylr118c::YLR118C-TEV-ProtA-7HIS-hphNT1*	this study	5051

Ylr281c$_{ProtA}$	Ylr281c$_{ProtA}$ (chromosomal)	BY4741 *ylr281c::YLR281C-TEV-ProtA-7HIS-hphNT1*	this study	4984
Ylr307c-a$_{ProtA}$	Ylr307c-a$_{ProtA}$ (chromosomal)	BY4741 *ylr307c-a::YLR307C-A-TEV-ProtA-7HIS-hphNT1*	this study	4986
Yml007c-a$_{ProtA}$	Yml007c-a$_{ProtA}$ (chromosomal)	BY4741 *yml007c-a::YML007C-A-TEV-ProtA-7HIS-hphNT1*	this study	4987
Ymr087w$_{ProtA}$	Ymr087w$_{ProtA}$ (chromosomal)	BY4741 *ymr087w::YMR087W-TEV-ProtA-7HIS-hphNT1*	this study	5052
Ymr130w$_{ProtA}$	Ymr130w$_{ProtA}$ (chromosomal)	BY4741 *ymr130w::YMR130W-TEV-ProtA-7HIS-hphNT1*	this study	4988
Ymr182w-a$_{GFP}$	Ymr182W-a$_{GFP}$ (chromosomal)	BY4741 *ymr182w-a::YMR182W-A-γEGFP-kanMX4*	this study	5055
Ynr040w$_{ProtA}$	Ynr040w$_{ProtA}$ (chromosomal)	BY4741 *ynr040w::YNR040W-TEV-ProtA-7HIS-hphNT1*	this study	4989
Yor020w-a$_{ProtA}$	Yor020w-a$_{ProtA}$ (chromosomal)	BY4741 *yor020w-a::YOR020W-A-TEV-ProtA-7HIS-kanMX6*	this study	4990
Yor114w$_{ProtA}$	Yor114w-a$_{ProtA}$ (chromosomal)	BY4741 *yor114w::YOR114W-TEV-ProtA-7HIS-kanMX6*	this study	5053
Ypl107w$_{ProtA}$	Ypl107w$_{ProtA}$ (chromosomal)	BY4741 *ypl107w::YPL107W-TEV-ProtA-7HIS-hphNT1*	this study	4991
Ypr010c-a$_{ProtA}$	Ypr010c-a$_{ProtA}$ (chromosomal)	BY4741 *ypr010c-a::YPR010C-A-TEV-ProtA-7HIS-kanMX6*	this study	4992
Ypr098c$_{ProtA}$	Ypr098c$_{ProtA}$ (chromosomal)	BY4741 *ypr098c::YPR098C-TEV-ProtA-7HIS-hphNT1*	this study	4993
NOP1pr-sfGFP-Aim11	NOP1pr-sfGFP-Aim11 (chromosomal)	his3Δ1 leu2Δ0 met15Δ0 ura3Δ0 hphΔn::URA3::NOP1pr-sfGFP-Aim11	this study	
NOP1pr-sfGFP-Fsf1	NOP1pr-sfGFP-Fsf1 (chromosomal)	his3Δ1 leu2Δ0 met15Δ0 ura3Δ0 hphΔn::URA3::NOP1pr-sfGFP-Fsf1	this study	
NOP1pr-sfGFP-Mmo1	NOP1pr-sfGFP-Mmo1 (chromosomal)	his3Δ1 leu2Δ0 met15Δ0 ura3Δ0 hphΔn::URA3::NOP1pr-sfGFP-Mmo1	this study	
NOP1pr-sfGFP-Mrx11	NOP1pr-sfGFP-Mrx11 (chromosomal)	his3Δ1 leu2Δ0 met15Δ0 ura3Δ0 hphΔn::URA3::NOP1pr-sfGFP-Mrx11	this study	
NOP1pr-sfGFP-Tom5	NOP1pr-sfGFP-Tom5 (chromosomal)	his3Δ1 leu2Δ0 met15Δ0 ura3Δ0 hphΔn::URA3::NOP1pr-sfGFP-Tom5	Yofe et al., 2016	
NOP1pr-sfGFP-Ybl059w	NOP1pr-sfGFP-Ybl059w (chromosomal)	his3Δ1 leu2Δ0 met15Δ0 ura3Δ0 hphΔn::URA3::NOP1	this study	

		pr-sfGFP-Ybl059w		
NOP1pr-sfGFP-Yil077c	NOP1pr-sfGFP-Yil077c (chromosomal)	his3Δ1 leu2Δ0 met15Δ0 ura3Δ0 hphΔn::URA3::NOP1pr-sfGFP-Yil077c	this study	
NOP1pr-sfGFP-Yjl127c-b	NOP1pr-sfGFP-Yjl127c-b (chromosomal)	his3Δ1 leu2Δ0 met15Δ0 ura3Δ0 hphΔn::URA3::NOP1pr-sfGFP-Yjl127c-b	this study	
NOP1pr-sfGFP-Yjr085c	NOP1pr-sfGFP-Yjr085c (chromosomal)	his3Δ1 leu2Δ0 met15Δ0 ura3Δ0 hphΔn::URA3::NOP1pr-sfGFP-Yjr085c	this study	
NOP1pr-sfGFP-Ykl133c	NOP1pr-sfGFP-Ykl133c (chromosomal)	his3Δ1 leu2Δ0 met15Δ0 ura3Δ0 hphΔn::URA3::NOP1pr-sfGFP-Ykl133c	this study	
NOP1pr-sfGFP-Ynr040w	NOP1pr-sfGFP-Ynr040w (chromosomal)	his3Δ1 leu2Δ0 met15Δ0 ura3Δ0 hphΔn::URA3::NOP1pr-sfGFP-Ynr040w	this study	
NOP1pr-sfGFP-YPR098C	NOP1pr-sfGFP-YPR098C (chromosomal)	his3Δ1 leu2Δ0 met15Δ0 ura3Δ0 hphΔn::URA3::NOP1pr-sfGFP-YPR098C	this study	
SFH5pr-sfGFP-Sfh5	SFH5pr-sfGFP-Sfh5 (chromosomal)	his3Δ1 leu2Δ0 met15Δ0 ura3Δ0 lys+ can1Δ::GAL1pr-SceI::STE2pr-SpHIS5 lyp1Δ::STE3pr-LEU2 ; SFH5pr-sfGFP-Sfh5	this study	
FMP16pr-sfGFP-Fmp16	FMP16pr-sfGFP-Fmp16 (chromosomal)	his3Δ1 leu2Δ0 met15Δ0 ura3Δ0 lys+ can1Δ::GAL1pr-SceI::STE2pr-SpHIS5 lyp1Δ::STE3pr-LEU2 ; FMP16pr-sfGFP-Fmp16	this study	
MSS116pr-sfGFP-Mss116	MSS116pr-sfGFP-Mss116 (chromosomal)	his3Δ1 leu2Δ0 met15Δ0 ura3Δ0 lys+ can1Δ::GAL1pr-SceI::STE2pr-SpHIS5 lyp1Δ::STE3pr-LEU2 ; MSS116pr-sfGFP-Mss116	this study	
YGL041W-Apr-sfGFP-Ygl041w-a	YGL041W-Apr-sfGFP-Ygl041w-a (chromosomal)	his3Δ1 leu2Δ0 met15Δ0 ura3Δ0 lys+ can1Δ::GAL1pr-SceI::STE2pr-SpHIS5 lyp1Δ::STE3pr-LEU2 ; YGL041W-Apr-sfGFP-Ygl041w-a	this study	
FYV4pr-sfGFP-Fyv4	FYV4pr-sfGFP-Fyv4 (chromosomal)	his3Δ1 leu2Δ0 met15Δ0 ura3Δ0 lys+ can1Δ::GAL1pr-SceI::STE2pr-SpHIS5 lyp1Δ::STE3pr-LEU2 ; FYV4pr-sfGFP-Fyv4	this study	
YKL018C-Apr-sfGFP-Ykl018c-a	YKL018C-Apr-sfGFP-Ykl018c-a (chromosomal)	his3Δ1 leu2Δ0 met15Δ0 ura3Δ0 lys+ can1Δ::GAL1pr-SceI::STE2pr-SpHIS5 lyp1Δ::STE3pr-LEU2 ; YKL018C-Apr-sfGFP-Ykl018c-a	this study	
FMP33pr-sfGFP-Fmp33	FMP33pr-sfGFP-Fmp33 (chromosomal)	his3Δ1 leu2Δ0 met15Δ0 ura3Δ0 lys+ can1Δ::GAL1pr-SceI::STE2pr-SpHIS5	this study	

		lyp1Δ::STE3pr-LEU2 ; FMP33pr-sfGFP-Fmp33		
LCL3pr-sfGFP-Llc3	LCL3pr-sfGFP-Llc3 (chromosomal)	his3Δ1 leu2Δ0 met15Δ0 ura3Δ0 lys+ can1Δ::GAL1pr-SceI::STE2pr-SpHIS5 lyp1Δ::STE3pr-LEU2 ; LCL3pr-sfGFP-Llc3	this study	
YLR281Cpr-sfGFP-Ylr281c	YLR281Cpr-sfGFP-Ylr281c (chromosomal)	his3Δ1 leu2Δ0 met15Δ0 ura3Δ0 lys+ can1Δ::GAL1pr-SceI::STE2pr-SpHIS5 lyp1Δ::STE3pr-LEU2 ; YLR281Cpr-sfGFP-Ylr281c	this study	
YMR252Cpr-sfGFP-Ymr252c	YMR252Cpr-sfGFP-Ymr252c (chromosomal)	his3Δ1 leu2Δ0 met15Δ0 ura3Δ0 lys+ can1Δ::GAL1pr-SceI::STE2pr-SpHIS5 lyp1Δ::STE3pr-LEU2 ; YMR252Cpr-sfGFP-Ymr252c	this study	
MNE1pr-sfGFP-Mne1	MNE1pr-sfGFP-Mne1 (chromosomal)	his3Δ1 leu2Δ0 met15Δ0 ura3Δ0 lys+ can1Δ::GAL1pr-SceI::STE2pr-SpHIS5 lyp1Δ::STE3pr-LEU2 ; MNE1pr-sfGFP-Mne1	this study	
YPL109Cpr-sfGFP-Ypl109c	YPL109Cpr-sfGFP-Ypl109c (chromosomal)	his3Δ1 leu2Δ0 met15Δ0 ura3Δ0 lys+ can1Δ::GAL1pr-SceI::STE2pr-SpHIS5 lyp1Δ::STE3pr-LEU2 ; YPL109Cpr-sfGFP-Ypl109c	this study	
YJL133C-Apr-sfGFP-Yjl133c-a	YJL133C-Apr-sfGFP-Yjl133c-a (chromosomal)	his3Δ1 leu2Δ0 met15Δ0 ura3Δ0 lys+ can1Δ::GAL1pr-SceI::STE2pr-SpHIS5 lyp1Δ::STE3pr-LEU2 ; YJL133C-Apr-sfGFP-Yjl133c-a	this study	

Plasmids used in this study

Name	Description	Source or Reference	Number
pYM1	template for amplification of *3HA-kanMX6* cassette	Knop et al., 1999	1449
pYM9	template for amplification of *TEV-ProtA-7HIS-kanMX6* cassette	Knop et al., 1999	1457
pYM10	template for amplification of *TEV-ProtA-7HIS* cassette that was cloned into pFA6a-hphNT1 vector to generate pFA6a-TEV-ProtA-7His-hphNT1 plasmid.	Knop et al., 1999	1458
pYM12	template for amplification of *γEGFP-kanMX4* cassette	Knop et al., 1999	1460
pFA6a-hphNT1	Target plasmid for TEV-ProtA-7His module (that has been amplified from pYM10 plasmid) for generation of pFA6a-TEV-ProtA-7His-hphNT1 plasmid.	Janke et al., 2004	2722
pFA6a-TEV-ProtA-7His-hphNT1	template for amplification of *TEV-ProtA-7HIS-hphNT1* cassette	this study	2723
pGEM-4Z-YJR085C	Backbone: pGEM-4Z Insert: EcoRI-YJR085C (*S. cerevisiae*)-HindIII template for in vitro synthesis of [^{35}S]Yjr085c using the TnT® Quick Coupled Transcription/ Translation System	this study	2610
pRS425	Vector used for overexpression of proteins in *S. cerevisiae*. origin of replication: 2µ yeast selectable marker: LEU2	Christianson et al., 1992	X30
pRS425-YJR085C	Backbone: pRS425 Insert: HindIII-$P_{YJR085C}$-YJR085C (*S. cerevisiae*)-$T_{YJR085C}$-BamHI	this study	2607
pRS425-$_{HA}$YJR085C	Backbone: pRS425 Insert: HindIII-$P_{YJR085C}$-1HA-YJR085C (*S. cerevisiae*)-$T_{YJR085C}$-BamHI	this study	2608
pST-N2	SWAT-GFP	Yofe et al., 2016	555
pSD-N9	Seamless-GFP	Yofe et al., 2016	561

Antibodies used in this study

Antigen	Dilution	Number	Secondary antibody
Abf2	1:200 TBS-T + 5% milk	GR B2072	anti-rabbit
Aco1	1:1000 TBS-T + 5% milk	GR945-7	anti-rabbit
Afg3	1:500 TBS-T + 5% milk	GR1551-5	anti-rabbit
Atp2	1:50 TBS-T + 5% milk	GR863 affinity purified e4	anti-rabbit
Atp4	1:250 TBS-T + 5% milk	GR1970-6	anti-rabbit
Atp5	1:250 TBS-T + 5% milk	GR1546-4	anti-rabbit
Atp17	1:250 TBS-T + 5% milk	GR1968-3	anti-rabbit
Atp20	1:250 TBS-T + 5% milk	GR1517-5	anti-rabbit
Cdc48	1:250 TBS-T + 5% milk	GR5015-4	anti-rabbit
Cor1	1:300 TBS-T + 5% milk	GR371-5	anti-rabbit
Cox1	1:400 TBS-T + 5% milk	GR1538-4	anti-rabbit
Cox2	1:250 TBS-T + 5% milk	GR1949-2	anti-rabbit
Cox4	1:1000 TBS-T + 5% milk	GR578-5	anti-rabbit
Cox5a	1:400 TBS-T + 5% milk	GR1540-5	anti-rabbit
Cox6	1:250 TBS-T + 5% milk	GR2015-2	anti-rabbit
Cox8	1:300 TBS-T + 5% milk	GR3609-5	anti-rabbit
Cox9	1:250 TBS-T + 5% milk	GR3612-3	anti-rabbit
Cox13	1:250 TBS-T + 5% milk	GR1542-4	anti-rabbit
Cta1	1:20000 TBS-T + 5% milk	12	anti-goat
Cyt1	1:750 TBS-T + 5% milk	GR541-6	anti-rabbit
Dic1	1:200 TBS-T + 5% milk	GR2054-5	anti-rabbit
Erg6	1:500 TBS-T + 5% milk	GR3034-6	anti-rabbit
Fmp10	1:500 TBS-T + 5% milk	GR3338-2	anti-rabbit
GFP	1:1000 TBS-T + 5% milk	GFP Antibody (Novus Biologicals LLC; NB600-308)	anti-rabbit
Goat IgG	1:50000 TBS-T + 5% milk	Peroxidase antibody, rabbit (Sigma-Aldrich Corp.; A8919)	–
HA	1:1000 TBS	Anti-HA-Peroxidase (F. Hoffmann-La Roche AG; 11667475001)	–
Isd11	1:250 TBS-T + 5% milk	336-7	anti-rabbit
Mdj1	1:500 TBS-T + 5% milk	GR1839-6	anti-rabbit
Mdl1	1:200 TBS-T + 5% milk	GR1518-7	anti-rabbit
Mdm38	1:1000 TBS-T + 5% milk	342-6	anti-rabbit
Mge1	1:250 TBS-T + 5% milk	GR1838-6	anti-rabbit
Mgr2	1:250 TBS-T + 5% milk	GR3121-3/4	anti-rabbit
Mia40	1:750 TBS-T + 5% milk	B315	anti-rabbit
Mic10	1:500 TBS-T + 5% milk	GR3343-2	anti-rabbit
Mic19	1:400 TBS-T + 5% milk	GR3358-2	anti-rabbit
Mic26	1:250 TBS-T + 5% milk	GR3335-2	anti-rabbit
Mic27	1:250 TBS-T + 5% milk	GR3357-2	anti-rabbit

Mic60	1:500 TBS-T + 5% milk	GR857-5	anti-rabbit
Ndi1	1:200 TBS-T + 5% milk	GR809-4	anti-rabbit
Ola1	1:1000 TBS-T + 5% milk	7173	anti-rabbit
OM14	1:500 TBS-T + 5% milk	GR3040-1	anti-rabbit
Pam16	1:200 TBS-T + 5% milk	GR750-6	anti-rabbit
Pam18	1:500 TBS-T + 5% milk	GR752-3	anti-rabbit
Pdi1	1:2000 TBS-T + 5% milk	GR1946	anti-rabbit
Pgk1	1:5000 TBS-T + 5% milk	GR753-1	anti-rabbit
Phb2	1:300 TBS-T + 5% milk	B295-10	anti-rabbit
Por1	1:500 TBS-T + 5% milk	GR3622-3	anti-rabbit
ProtA	1:200 TBS + 5% milk	Peroxidase Anti-Peroxidase Soluble Complex antibody produced in rabbit (Sigma-Aldrich Corp.; P1291)	–
Pth2	1:500 TBS-T + 5% milk	GR797-3	anti-rabbit
Qcr6	1:250 TBS-T + 5% milk	GR1054-6	anti-rabbit
Qcr8	1:5000 TBS-T + 5% milk	GR1038-1	anti-rabbit
Rcf2	1:2000 TBS-T + 5% milk	GR3113-1	anti-rabbit
Rip1	1:500 TBS-T + 5% milk	GR543-5	anti-rabbit
Rpl19	1:7000 TBS-T + 5% milk	106	anti-rabbit
Sac1	1:2500 TBS-T + 5% milk	GR1487-6	anti-rabbit
Sam50	1:500 TBS-T + 5% milk	B312-14	anti-rabbit
Scm4	1:500 TBS-T + 5% milk	GR1473-2	anti-rabbit
Sdh1	1:1000 TBS-T + 5% milk	GR1849-3	anti-rabbit
Sdh4	1:2000 TBS-T + 5% milk	GR1855-3	anti-rabbit
Sec61	1:1000 TBS-T + 5% milk	GR759-2	anti-rabbit
Ssa1	1:1000 TBS-T + 5% milk	GR1011-4	anti-rabbit
Sss1	1:100 TBS-T + 5% milk	GR787-7 / GR788-1	anti-rabbit
Tcd2	1:500 TBS-T + 5% milk	GR1396-1	anti-rabbit
Tim10	1:500 TBS-T + 5% milk 1:250 TBS-T + 5% milk	217-8 GR2041-7	anti-rabbit
Tim11	1:400 TBS-T + 5% milk	138-9	anti-rabbit
Tim12	1:250 TBS-T + 5% milk	GR906-7	anti-rabbit
Tim17	1:300 TBS-T + 5% milk	GR1845-3	anti-rabbit
Tim21	1:500 TBS-T + 5% milk	GR3899-4	anti-rabbit
Tim23	1:500 TBS-T + 5% milk	GR3878-4	anti-rabbit
Tim44	1:200 TBS-T + 5% milk	GR1836-4	anti-rabbit
Tim50	1:500 TBS-T + 5% milk	GR3881-1	anti-rabbit
Tim54	1:1000 TBS-T + 5% milk	215-6	anti-rabbit
Tom7	1:250 TBS-T + 5% milk	230-9	anti-rabbit
Tom20	1:5000 TBS-T + 5% milk	GR3225	anti-rabbit
Tom22	1:5000 TBS-T + 5% milk	GR3227	anti-rabbit
Tom40	1:500 TBS-T + 5% milk	168-4	anti-rabbit
Tom70	1:500 TBS-T + 5% milk	GR657-4	anti-rabbit
Yil077c (Rci37)	1:250 TBS-T + 5% milk	GR3731-5	anti-rabbit

Yme1	1:400 TBS-T + 5% milk	GR1435-3	anti-rabbit

SUPPLEMENTAL REFERENCES

Brachmann, C.B., Davies, A., Cost, G.J., Caputo, E., Li, J., Hieter, P., and Boeke, J.D. (1998). Designer deletion strains derived from Saccharomyces cerevisiae S288C: a useful set of strains and plasmids for PCR-mediated gene disruption and other applications. Yeast *14*, 115–132.

Christianson, T.W., Sikorski, R.S., Dante, M., Shero, J.H., and Hieter, P. (1992). Multifunctional yeast high-copy-number shuttle vectors. Gene *110*, 119–122.

Cox, J., and Mann, M. (2008). MaxQuant enables high peptide identification rates, individualized p.p.b.-range mass accuracies and proteome-wide protein quantification. Nat. Biotechnol. *26*, 1367–1372.

Cox, J., Neuhauser, N., Michalski, A., Scheltema, R.A., Olsen, J.V., and Mann, M. (2011). Andromeda: a peptide search engine integrated into the MaxQuant environment. J. Proteome Res. *10*, 1794–1805.

Delmotte, N., Lasaosa, M., Tholey, A., Heinzle, E., and Huber, C.G. (2007). Two-dimensional reversed-phase x ion-pair reversed-phase HPLC: an alternative approach to high-resolution peptide separation for shotgun proteome analysis. J. Proteome Res. *6*, 4363–4373.

Dubaquié, Y., Looser, R., Fünfschilling, U., Jenö, P., Rospert, S. (1998). Identification of in vivo substrates of the yeast mitochondrial chaperonins reveals overlapping but non-identical requirement for hsp60 and hsp10. EMBO J. *17*, 5868-5876.

Fin, R.D., Clements, J., Arndt, W., Miller, B.L., Wheeler, T.J., Schreiber, F., Bateman, A., and Eddy, S.R. (2015). HMMER web server: 2015 update. Nucleic Acids Res. *43*, W30–W38.

Fukasawa, Y., Tsuji, J., Fu, S.-C., Tomii, K., Horton, P., and Imai, K. (2015). MitoFates: improved prediction of mitochondrial targeting sequences and their cleavage sites. Mol. Cell. Proteomics *14*, 1113–1126.

Gietz, R.D., and Woods, R.A. (2002). Transformation of yeast by lithium acetate/single-stranded carrier DNA/polyethylene glycol method. Meth. Enzymol. *350*, 87–96.

Huxley, C., Green, E.D., and Dunham, I. (1990). Rapid assessment of S. cerevisiae mating type by PCR. Trends Genet. *6*, 236.

Janke, C., Magiera, M.M., Rathfelder, N., Taxis, C., Reber, S., Maekawa, H., Moreno-Borchart, A., Doenges, G., Schwob, E., Schiebel, E., et al. (2004). A versatile toolbox for PCR-based tagging of yeast genes: new fluorescent proteins, more markers and promoter substitution cassettes. Yeast *21*, 947–962.

Knop, M., Siegers, K., Pereira, G., Zachariae, W., Winsor, B., Nasmyth, K., and Schiebel, E. (1999). Epitope tagging of yeast genes using a PCR-based strategy: more tags and improved practical routines. Yeast *15*, 963–972.

Kushnirov, V.V. (2000). Rapid and reliable protein extraction from yeast. Yeast 16, 857–860.

Lasaosa, M., Delmotte, N., Huber, C.G., Melchior, K., Heinzle, E., and Tholey, A. (2009). A 2D reversed-phase x ion-pair reversed-phase HPLC-MALDI TOF/TOF-MS approach for shotgun proteome analysis. Anal. Bioanal. Chem. *393*, 1245–1256.

Longtine, M.S., McKenzie, A., Demarini, D.J., Shah, N.G., Wach, A., Brachat, A., Philippsen, P., and Pringle, J.R. (1998). Additional modules for versatile and economical PCR-based gene deletion and modification in Saccharomyces cerevisiae. Yeast *14*, 953–961.

Meisinger, C., Sommer, T., and Pfanner, N. (2000). Purification of Saccharomcyes cerevisiae mitochondria devoid of microsomal and cytosolic contaminations. Anal. Biochem. *287*, 339–342.

Sikorski, R.S., and Hieter, P. (1989). A system of shuttle vectors and yeast host strains designed for efficient manipulation of DNA in Saccharomyces cerevisiae. Genetics *122*, 19–27.

Smith, J.E., Alvarez-Dominguez, J.R., Kline, N., Huynh, N.J., Geisler, S., Hu, W., Coller, J., Baker, K.E. 2014. Translation of Small Open Reading Frames within Unannotated RNA Transcripts in Saccharomyces cerevisiae. Cell Rep. 7, 1858-1866.

Tyanova, S., Temu, T., Sinitcyn, P., Carlson, A., Hein, M.Y., Geiger, T., Mann, M., and Cox, J. (2016). The Perseus computational platform for comprehensive analysis of (prote)omics data. Nat. Methods *13*, 731–740.

von der Malsburg, K., Müller, J.M., Bohnert, M., Oeljeklaus, S., Kwiatkowska, P., Becker, T., Loniewska-Lwowska, A., Wiese, S., Rao, S., Milenkovic, D., et al. (2011). Dual role of mitofilin in mitochondrial membrane organization and protein biogenesis. Dev. Cell *21*, 694–707.

Wiśniewski, J.R., Ostasiewicz, P., Duś, K., Zielinska, D.F., Gnad, F., and Mann, M. (2012). Extensive quantitative remodeling of the proteome between normal colon tissue and adenocarcinoma. Mol. Syst. Biol. *8*, 611.

Wysocki, R., Roganti, T., Van Dyck, E., de Kerchove D'Exaerde, A., Foury, F. 1999. Disruption and basic phenotypic analysis of 18 novel genes from the yeast Saccharomyces cerevisiae. Yeast 15, 165–171.